

THESIS

STRUCTURAL SYSTEMS WITH SUSPENDED AND SELF-CENTERED FLOOR SLABS
FOR EARTHQUAKE RESISTANCE

Submitted by

Akshat Chulahwat

Department of Civil and Environmental Engineering

In partial fulfillment of the requirements

For the Degree of Master of Science

Colorado State University

Fort Collins, Colorado

Summer 2013

Master's Committee:

Advisor: Hussam Mahmoud

Bogusz Beinkiewicz
Darrell Whitley

Copyright by Akshat Chulahwat 2013

All Rights Reserved

ABSTRACT

STRUCTURAL SYSTEMS WITH SUSPENDED AND SELF-CENTERED FLOOR SLABS FOR EARTHQUAKE RESISTANCE

The purpose of this study is to develop a novel structural system for mitigating the effects of earthquakes on buildings by suspending the concrete floor slabs, which act as Tune Mass Dampers (TMDs) to reduce the response of the structural system. Each slab is suspended using hanger rods and steel links are added between the bottom face of the suspended slab and the beam below the slab and to be used as energy dissipaters during an earthquake. Moreover, post-tensioned cables are installed adjacent to the steel links to provide a self-centering capability to the floor slab and eliminate residual drift after a seismic event. The Suspended Slab (SS) system is analyzed by constructing suitable theoretical models, from which mathematical equations describing the response of the system are developed and analyzed. The location and number of suspended slabs and energy dissipation links needs to be carefully chosen for optimum performance of the system.

To obtain the optimized condition, the simple optimization approach of Numerical Search is used. The optimization identifies the best locations, damping ratio and the frequency ratio of the slabs. The approach is suitable for short structures, however with increase in number of floors the algorithm becomes time costly. A new combinatorial approach of optimization is implemented that uses Nelder Mead algorithm and Covariance Matrix Adaptation Evolution Strategy. The new optimization is modified and tested to assess its effectiveness.

Finally, three structures are utilized in a case study to evaluate the effectiveness of the suspended slab system using the combinatorial optimization approach. The earthquake is modeled as a stationary white noise and Kanai – Tajimi Spectrum is used as excitation input to obtain the Root Mean Square response, which is considered as the performance evaluation parameter. From the results of this study it is concluded that the suspended slab system can be quite an effective strategy for earthquake mitigation.

ACKNOWLEDGEMENTS

I would like to thank my supervisor, Dr. Hussam Mahmoud, for not only his technical guidance but also for the insightful lessons he taught me over the past 2 years, without which I would not have gained so much.

I want to thank Dr. Bogusz Beinkiewicz for his great lectures on ‘Vibration Theory’ that laid the foundation to my work. I would like to thank Dr. Darrell Whitley for that one suggestion that allowed me to finish the thesis.

I would like to thank my parents for their unconditional love and support, without whom I would have never made it this far. Finally, I would like to thank a special friend for enduring and staying beside me for all this time.

TABLE OF CONTENTS

TABLE OF CONTENTS.....	v
LIST OF FIGURES	ix
NOMENCLATURE	xii
CHAPTER 1 INTRODUCTION AND LITERATURE REVIEW	1
1.1 Problem Statement.....	1
1.2 Motivation of the Study	1
1.3 Proposed System.....	3
1.4 Organization of Thesis.....	5
1.5 Performance of Moment Resisting frames under Seismic Loading	8
1.6 Isolation Systems	10
1.6.1 Base Isolation.....	11
1.6.2 Tuned Mass Dampers	13
1.6.2.1 Passive Translational Tuned Mass Damper.....	14
1.6.2.2 Passive Pendulum Tuned Mass Damper.....	15
1.6.2.3 Active Tuned Mass Damper	15
1.6.2.4 Semi Active Tuned Mass Damper (SATMD)	17
1.6.2.5 Multi – Tuned Mass Damper	18
1.7 Suspended Systems.....	19
CHAPTER 2 THEORETICAL DEVELOPMENT OF PROPOSED SYSTEM.....	22
2.1 Introduction.....	22
2.2 A Single Suspended Slab (SSS) Model	23
2.2.1 System Idealization.....	23
2.2.2 Simplification.....	25
2.3 Response Transfer Functions.....	28
2.3.1 System Behavior	31
2.3.2 Numerical Example	35
2.3.2.1 Composite Slab Frame.....	37
2.3.2.2 Suspended Slab Frame.....	37
2.4 Multi Suspended Slab (MSS) Model	40
2.4.1 System Idealization.....	42
2.4.2 Equations of Motion	42
2.4.3 Response Equations	47
2.4.4 System Behavior	51
2.4.5 Benchmark Example.....	54
2.4.5.1 Suspended Slab Frame.....	55
CHAPTER 3 OPTIMIZATION APPROACH	58
3.1 Introduction.....	58
3.2 Numerical Search (NS) Pattern Algorithm.....	59

3.2.1	Introduction.....	59
3.2.1.1	Implementation	60
3.3	Combinatorial Algorithm.....	62
3.3.1	Nelder Mead Algorithm.....	63
3.3.1.1	Introduction.....	63
3.3.1.2	Procedure	64
3.3.2	Covariance Matrix Adaptation Evolution Strategy (CMA-ES).....	71
3.3.2.1	Introduction.....	71
3.3.2.2	Sampling	74
3.3.2.3	Selection and Recombination	77
3.3.2.4	Adaptation.....	78
3.3.2.5	Step Size (σ).....	81
3.3.2.6	Process Flowchart	83
3.3.3	Numerical Testing.....	83
3.3.3.1	Introduction.....	84
3.3.3.2	Elitist Selection (Elitism).....	85
3.3.3.3	Flatness Recovery	86
3.3.3.4	Cases Considered.....	88
CHAPTER 4 SYSTEM RESPONSE to generated white noise EARTHQUAKE excitations.....		96
4.1	Stationary White Noise	96
4.2	Kanai-Tajimi Filter	97
4.3	Fast Fourier Transform (FFT) and Power Spectral Density Function (PSDF)	
	99	
4.4	Analysis Procedure	100
4.5	Numerical Examples.....	103
4.5.1	4 Story 2 Bay	106
4.5.2	7 Story 3 Bay	107
4.5.3	10 Story 5 Bay	108
4.5.4	Results.....	109
CHAPTER 5 DESIGN CONSIDERATIONS		112
5.1	Design Considerations	112
5.1.1	Design of Energy Dissipation Links	112
5.1.2	Design of Post – Tension (PT) Links.....	113
CHAPTER 6 CONCLUSIONS AND FUTURE WORK.....		116
6.1	Conclusions.....	116
6.2	Future Work	117
REFERENCES		118
APPENDIX A RESPONSE EQUATIONS DERIVATION FOR MSS MODEL		125

LIST OF TABLES

Table 2-1 Commonly Used Parameters for TMDs	27
Table 2-2 Definition of response parameters.....	29
Table 2-3 Structural Properties of 4 Story 1 Bay Frame	38
Table 2-4 Transfer Function Values and SS system parameters for different Optimizations	39
Table 2-5 List of response parameters for MSS model	48
Table 2-6 Structural Properties of 4 Story 2 Bay Frame	54
Table 2-7 Transfer Function Values and SS system parameters for Optimization w.r.t. Steel Frame Top Floor Displacement Amplitude	55
Table 2-8 Transfer Function Values and SS system parameters for Optimization w.r.t. Steel Frame Top Floor Acceleration Amplitude.....	56
Table 2-9 Transfer Function Values and SS system parameters for Optimization w.r.t. Top Floor SS Displacement Amplitude	56
Table 2-10 Transfer Function Values and SS system parameters for Optimization w.r.t. Top Floor SS Acceleration Amplitude	57
Table 3-1 List of important parameters for Adaptation process in CMA-ES.....	82
Table 3-2 Structural Properties of 10 Story 2 Bay Frame	84
Table 3-3 Probability values for different step - lengths	88
Table 4-1 Parameters of Kanai – Tajimi Model for Near Fault and Far Fault Earthquakes.....	101
Table 4-2 Structural Properties of 4-Story 1-Bay Frame.....	104
Table 4-3 Structural Properties of 7-Story 3-Bay Frame.....	104
Table 4-4 Structural Properties of 10-Story 5-Bay Frame.....	105

Table 4-5 Transfer Function Values and SS system optimized parameters for different Optimizations	111
Table 5-1 List of parameters for PT links	114

LIST OF FIGURES

Figure 1.1 Elevation view of the proposed structural system and its components	4
Figure 1.2 Fractured Connection in 1994 Northridge Earthquake	8
Figure 1.3 Yield and Buckling pattern in a Reduced Beam Section	10
Figure 1.4 The suspended West Coast Transmission building in Vancouver, Canada.....	20
Figure 2.1 System Representation and Idealization of a Single Suspended Slab System	23
Figure 2.2 Simplified SDOF Model.....	26
Figure 2.3 Effect of Mass Ratio on Response Displacement Amplitude of Steel Frame for $\alpha = 1$ and constant Damping Ratio	32
Figure 2.4 Effect of Damping Ratio on Response Displacement Amplitude of Steel Frame for α $= 1$	32
Figure 2.5 Variation of Response Displacement Amplitude of Steel Frame with Excitation Frequency $\alpha = 1$	33
Figure 2.6 Variation in Response Displacement Amplitude for Steel Frame with Input Excitation Frequency and Mass Ratio.....	34
Figure 2.7 Variation in Response Displacement Amplitude for Steel Frame with Input Excitation Frequency and Frequency Ratio	35
Figure 2.8 Analysis Procedure.....	36
Figure 2.9 Optimized Amplitudes for different type of Optimizations for SSS Model	39
Figure 2.10 Multi Suspended Slabs (MSS) System Representation.....	40
Figure 2.11 Idealization of the MSS System	42
Figure 2.12 Physical Representation of Variable C_n	44

Figure 2.13 Effect of Mass Ratio on Response Displacement Amplitude	52
Figure 2.14 Variation in Optimum Frequency Ratio with Mass Ratio.....	52
Figure 2.15 Variation in Optimum Damping Ratio with Mass Ratio.....	53
Figure 2.16 Variation of Optimum Frequency Ratio with Number of SS.....	53
Figure 2.17 Optimized Amplitudes for different type of Optimizations for MSS model.....	57
Figure 3.1 Surface plot of Numerical Search Pattern	62
Figure 3.2 Covergence Pattern of N – M Algorithm for Solution on Initial Assumption (on vertex)	65
Figure 3.3 Covergence Pattern of N – M Algorithm for Solution outside Initial Assumption (outside).....	65
Figure 3.4 Covergence Pattern of N – M Algorithm for Solution inside Initial Assumption (inside).....	66
Figure 3.5 Covergence Pattern of N – M Algorithm for an Optimal Initial Assumption chosen	66
Figure 3.6 (i) Reflection (ii) Expansion (iii) Outside Contraction (iv) Inside Contraction (v) Shrink	69
Figure 3.7 Flowchart of Nelder – Mead Algorithm.....	70
Figure 3.8 Schematic of Data Movement Pattern of CMA-ES Algorithm.....	73
Figure 3.9 Projection Method	75
Figure 3.10 Unbiased Nature of Sampling Function	76
Figure 3.11 CMA – ES Procedure Flowchart.....	83
Figure 3.12 Elitist Strategy Modifications.....	86
Figure 3.13 Boxplot of Case I Convergence.....	90
Figure 3.14 Box plot of Case II Convergence	91

Figure 3.15	Box plot of Case III Convergence	92
Figure 3.16	Change in Step – Length for Case IV.....	94
Figure 3.17	Case IV Convergence and Accuracy.....	95
Figure 3.18	Box – Plot of Case IV Convergence.....	95
Figure 4.1	An Example of a White Noise Signal.....	97
Figure 4.2	Typical Shape of Kanai – Tajimi Spectrum	98
Figure 4.3	Average Power Spectrum for Near Fault Earthquakes.....	101
Figure 4.4	Average Power Spectrum for Far Fault Earthquakes	101
Figure 4.5	Performance of Steel Frame for Near and Far Fault Earthquakes.....	106
Figure 4.6	Performance of Top Floor Suspended Slab for Near and Far Fault Earthquakes	106
Figure 4.7	Performance of Steel Frame for Near and Far Fault Earthquakes.....	107
Figure 4.8	Performance of Top Floor Suspended Slab for Near and Far Fault Earthquakes	107
Figure 4.9	Performance of Steel Frame for Near and Far Fault Earthquakes.....	108
Figure 4.10	Performance of Top Floor Suspended Slab for Near and Far Fault Earthquakes ..	108
Figure 5.1	Schematic of Post – tensioned links	114

NOMENCLATURE

TMD	Tuned mass damper
TTMD	Translational tuned mass damper
PTMD	Pendulum tuned mass damper
SATMD	Semi-active tuned mass damper
ATMD	Active tuned mass damper
APTMD	Active pendulum tuned mass damper
MTMD	Multi tuned mass damper
DTMD	Distributed tuned mass damper
SS	Suspended Slab
c_{links}	Damping coefficient of energy dissipation links
c_d	Viscous damping coefficient of Suspended Slab
k_d	Total stiffness of Suspended Slab
k_{links}	Stiffness of Post – tensioned links
a_g	Magnitude of ground excitation
K_S	Structure stiffness constant [N/m]
C_S	Viscous damping coefficient of Steel Frame
M_S	Structure mass [slugs]
m_d	Mass of suspended slab [kg]
μ_d	Mass ratio of suspended slab system [kg]
α	Input excitation frequency ratio
L	Length of cables used for suspending slab [in]

RMS	Root mean square
SDOF	Single degree of freedom
SSS	Single suspended slab
MDOF	Multi degree of freedom
MSS	Multi suspended slabs
PSDF	Power spectral density function
X_S	Displacement amplification factor of steel frame for SSS model
X_d	Displacement amplification factor of suspended slab for SSS Model
u_S	Steel frame horizontal displacement [in]
u_d	Suspended slab horizontal displacement [in]
\ddot{u}_S	Steel frame horizontal acceleration [in]
$\ddot{\theta}$	Pendulum angular acceleration of suspended slab [rad/s ²]
\ddot{u}_d	Suspended slab horizontal acceleration [in]
α	Excitation frequency ratio
β_d	Frequency ratio
γ_{HS}	Phase difference of steel frame displacement [rad]
γ_{Hd}	Phase difference of suspended slab displacement [rad]
γ_{AS}	Phase difference of steel frame acceleration [rad]
γ_{Ad}	Phase difference of suspended slab acceleration [rad]
ξ_S	Damping ratio of bare steel frame
ξ_d	Damping ratio of suspended slabs
ω_S	Natural frequency of steel frame [rad/s]
ω_d	Natural frequency of suspended slabs [rad/s]

ω	Input excitation frequency [rad/s]
$ H_S $	Displacement response amplitude of steel frame for top floor of SSS model
$ A_S $	Acceleration response amplitude of steel frame for top floor
$ H_d $	Displacement response amplitude of top floor suspended slab
$ A_d $	Acceleration response amplitude of top floor suspended slab
C_n	Control parameter of n^{th} floor
N	Total number of floors in SS system
M	Total number of suspended slabs on each floor
n	Floor id number
m_n	Mass of n^{th} floor
k_n	Stiffness of n^{th} floor
c_n	Damping coefficient of n^{th} floor
m_E	Effective mass of steel frame in MSS model
k_E	Effective stiffness of steel frame in MSS model
c_E	Effective damping coefficient of steel frame in MSS model
u_n	Horizontal displacement of n^{th} Floor
c_{dnj}	Damping coefficient of n^{th} Floor j^{th} suspended Slab
k_{dnj}	Stiffness of n^{th} Floor j^{th} suspended slab
u_{dnj}	Horizontal displacement of n^{th} floor j^{th} suspended slab [in]
\ddot{u}_{dnj}	Suspended slab horizontal acceleration of j^{th} SS on n^{th} floor [in/s ²]
ϕ_{in}	i^{th} mode shape of n^{th} Floor
P	Modal matrix

v_n	Modal coordinates of n^{th} Floor
Γ_e	Modal Participation Factor
q_n	Mode Shape Ratio
$ H_N $	Displacement response amplitude of Top floor Steel Frame for MSS Model
$ A_N $	Acceleration response amplitude of Top floor Steel Frame for MSS Model
$ H_{a_{Nj}} $	Displacement response amplitude of j^{th} Suspended Slab for top floor
$ A_{a_{Nj}} $	Acceleration response amplitude of j^{th} Suspended Slab for top floor
NS	Numerical Search
CMA-ES	Covariance Matrix Adaptation Evolution Strategy
B	Best Vertex
G	Good Vertex
W	Worst Vertex
M	Mid - Point
R	Reflection
E	Expansion
C	Contraction
S	Shrinking
x_k^g	Sampled Data Point for k^{th} member of population of g^{th} Generation
m^g	Mean for g^{th} Generation
σ^g	Step Length for g^{th} Generation
C^g	Covariance Matrix for g^{th} Generation
$N(m,C)$	Normalized Distribution with Mean m and Covariance C
σ	Step Length Starting Value

λ	Size of Population
w_i	Weight of I^{th} index
μ	Number of Members Selected From Population
n	Number of Floors excluding Top Floor
p_c	Evolution Path of Covariance Matrix
p_σ	Evolution Path of Step – Length
c_μ	Learning Rate for Rank – μ Update for Covariance Matrix
c_1	Learning Rate for Rank – One Update for Covariance Matrix
c_c	Inverse Backward Time Horizon of Evolution Path p_c
c_σ	Inverse Backward Time Horizon of Evolution Path p_σ
d_σ	Damping parameter
$E\ N(m,C)\ $	Expectation Value of Euclidian Norm of a Distribution $N(m,C)$
$\Phi(Z)$	Standard Normal Cumulative Distribution Function
$S_{KT}(\omega)$	Kanai Tajimi Spectrum
S_0	Ground intensity
ξ_g	Ground damping ratio
ω_g	Ground frequency
$x(t)$	time history
A	Amplitude of fourier amplitude spectrum
T	Total duration of time history
S_E	Power spectrum density function
ω_0	Cut – off frequency
Num	No. of records considered

Ψ	RMS acceleration
ω_c	Central frequency
δ	Shape factor
λ_n	n^{th} spectral moment
$\sqrt{\sigma^2}$	RMS response
I	Improvement factor
k_{total}	Total stiffness of suspended slab
k_d	Stiffness of suspended slab only due to PT links
k_{in}	Inherent stiffness of suspended slab
X_{max}	Maximum displacement of suspended slab
h_s	Spacing between suspended slab and beam
s_p	Horizontal spacing between the two ends of a PT link
θ	Horizontal angle PT link for maximum displacement of slab
F_{PV}	Vertical force of PT link
F_{PH}	Horizontal force of PT link
F_P	Net force of PT link
n_{PT}	Number of PT links

CHAPTER 1

INTRODUCTION AND LITERATURE REVIEW

1.1 Problem Statement

1.2 Motivation of the Study

On January 17th, 1994, an earthquake generated in Los Angeles, California of Moment magnitude 6.7 lasting for about 10 – 20 seconds, caused an estimate damage of about \$20 billion dollars. The earthquake is labelled as the Northridge earthquake and is considered to be one of the costliest natural disasters in U.S. history. The Northridge although had a death toll of 57 persons but the damage to the infrastructure was in a magnitude of its own. Although steel buildings have a capacity to withstand large seismic events without collapse, the cost of repair is not so forgiving. These repair costs can sometimes be on the order of billions of dollars, which imposes huge financial constraints on post-disaster recovery and economic growth.

In the earlier stages of earthquake engineering the designs were based on Direct Design approach in which the main aim was to satisfy the performance objectives, which included immediate occupancy, damage control, and collapse prevention. Due to the high investment cost, the design procedure shifted to a more economical approach called the Capacity Design, whose main objective is to prevent structural collapse with an acceptable level of damage. Soon the drawbacks of this approach were realized, especially after Northridge, and the focus was shifted to minimizing structural loss without compromising on performance. Therefore, it is necessary to develop new structural systems that satisfy higher performance goals and can be easily repaired with minimal

cost after major seismic events. In light of this, various systems have been developed such as - base isolation and floor isolation systems, damping devices, rocking frames with fuses and many more. The concept behind such systems is to concentrate the damage on specific repairable/replaceable elements and/or limit the residual drift. Numerous studies have been done on these systems and have demonstrated promising results both in terms of cost and performance.

Amongst these new developments are Tuned Mass Dampers (TMDs) with numerous types of configurations developed over the years. A TMD, or harmonic absorber, is a passive system (although active version also exists) which can be modeled with a mass, a spring, and a damper. The TMD is tuned to a ratio of the structures natural frequency (or another modal frequency). When the structure is excited at the tuned frequency, the damper resonates out-of-phase with the point of connection to the structure (Setareh at al. 2006). Vibration energy is dissipated from the structure via dissipative elements (dampers) that are a part of the TMD system. There have been a lot of popular applications, such as the Taipei 101, among others. It has been found that the performance of all TMD's is proportional to the mass used in the system (Li, 2000). Usually the mass used in the TMD's is not more than 1.5 % of that of the main structure (Feng & Mita, 1995), which leads to the expectation that the performance of TMD should improve if the mass were to be increased. The limitation on the weight of TMDs is due to the fact that if TMDs with larger masses are used, the sizes of the beams and columns of the main building will have to increase, which can lead to uneconomical design. In light of this a new system is proposed in which the floor slab are suspended from the beams above using hanger rods. The suspended slab is expected to act like a TMD and due to the high mass of the slab the whole system is expected to show an elevated performance than usual TMDs.

One of the main drawbacks of implementing the TMD system is that it needs to be tuned for optimal performance so there is a risk of getting detuned. In response to problem a new type of TMD system known as the MTMD was inquired, where instead of a single TMD on the top floor a certain number of TMD's are placed. It is seen that using multiple TMDs tend to reduce the system's detuning possibility (Li, 2000). Based on the same principle the proposed system can be implemented as a MTMD system, by selectively suspending few slabs, thereby making it a robust system. The TMD systems have another limitation that they require extra space and as a result are generally avoided below the top floors. So an inherent TMD system would prove to be far more economical and easy to implement, such as the Suspended Slab system.

1.3 Proposed System

The proposed structural system consists of hanging the floor slabs by the beam above using cables or rods. The Suspended slabs tend to act as a typical PTMD. In order to ensure a controlled motion of the slabs they are connected to the beam below by a couple of links. These links are categorized into two types – Post – Tensioned (PT) links and Energy Dissipation (ED) links. The PT links are responsible to provide the necessary stiffness to control the motion of slabs without yielding and to ensure zero residual drift once the effect of excitation fades away. These are similar to the self-centering cables used in the rocking frame (Eatherton et al., 2008). The ED links are the other set of links which are designed in such a way to dissipate energy in these links, thus act as damping devices. As a result of this combined mechanism the only part that needs to be replaced would be the ED links, which are not only economical but also easy to replace. Thus the combination of these two links would ensure that the motion of the suspended slab would tend to act as a TMD

system; thereby reducing the motion of the primary steel frame. The proposed system is shown in Figure 1.1.

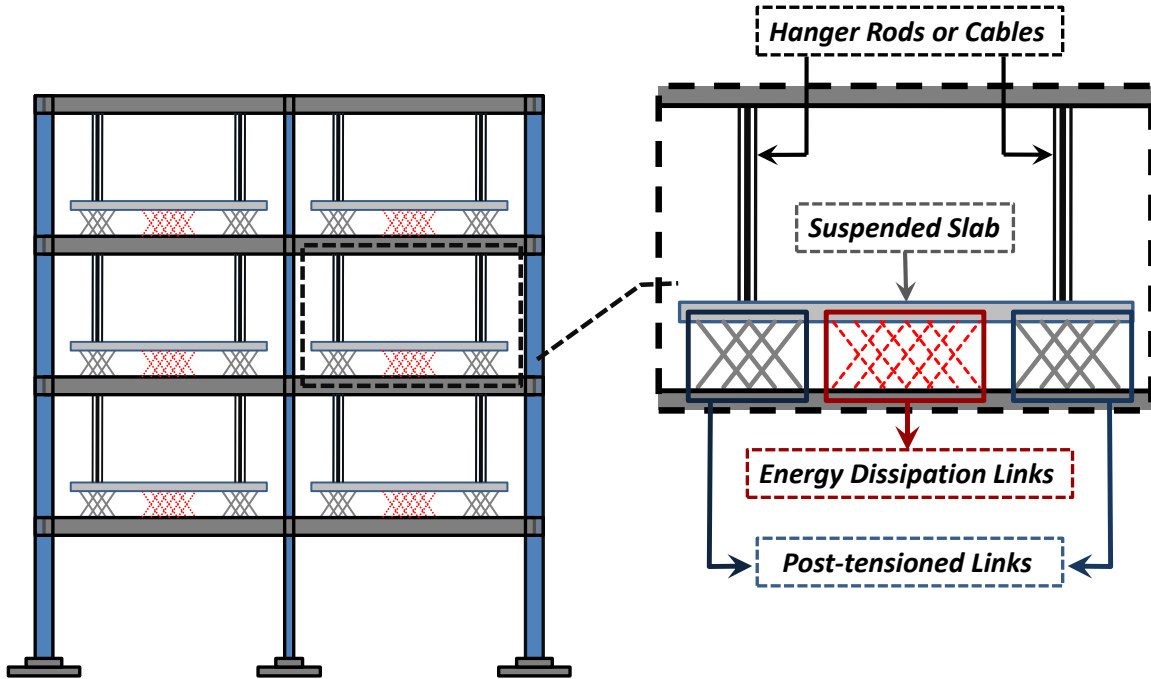


Figure 1.1 Elevation view of the proposed structural system and its components

The performance of the SS system is a function of 3 things:

1. The mass ratio (μ_d), which is the ratio of the mass of a suspended slabs to the mass of remainder of the frame (non-suspended slabs & steel skeleton)
2. The damping ratio of the energy dissipation links (ξ_d) and;
3. The ratio of natural frequency of the slab to the steel frame (β_d)

The design of typical TMD systems includes optimum selection of these 3 parameters. Based on the mass ratio obtained the mass of the isolator is chosen accordingly, thus the mass ratio play a vital role in the design. However, in case of the SS system, the size of slabs will be decided before the design of the suspension systems. Thus, in case of SS system, the mass ratio cannot be

considered as a variable during the analysis. The design or as usually called ‘The Tuning’ of the system, depends on the other two factors - ξ_d and β_d of each slab. TMD’s have been found to be most effective when placed at the top floor (Connor, 2003) so the location of TMD’s have not been put into much question. However in case of SS system the location plays a vital role as it directly affects the performance. Based on the location, the equations of motion for the system changes, so the position and number of TMDs is also considered a variable for the system.

Suitable optimization algorithms are used to solve for these variables to get the optimal performance. As discussed, the location of suspended masses, which is generally not a source of concern in general TMD’s, plays a vital role in the SS system thus separate optimization algorithms are used for it. Unlike usual TMDs, the slabs in the SS system can be placed on any floors without any space limitation. As a result the SS system comprises of multiple suspended masses (or slabs) not on just the top floor but also on the other floors.

1.4 Organization of Thesis

The thesis has been organized as follows:

- CHAPTER 2: This chapter evaluates the features of different types of TMD’s ranging from passive to active. This chapter mainly draws out a performance comparison between each type by pointing out their advantages and limitations.
- CHAPTER 3: This chapter investigates the steps involved in theoretically studying and subsequently developing the SS system. First, a simplified Pendulum Tune Mass Damper (PTMD)

model is considered, which comprises of a PTMD attached to a Single Degree-of-Freedom (SDOF) frame. Eventually a more complex model is developed to represent the system, which comprises of multiple TMD's attached to a Multi- Degree-of-Freedom (MDOF) frame. Dynamics and vibration theories are used to analyze these models, and finally response relations are obtained to describe the performance and behavior of the SS system. These response relations are optimized in a conventional way to obtain the necessary design parameters – β_d (Frequency Ratio) and ξ_d (Damping ratio of TMD), for tuning the corresponding SS system. Finally, a numerical example is considered to bring out the performance difference between the SS system and a Composite steel frame.

- CHAPTER 4: This chapter examines different optimization methods and assess their effectiveness with regard to the developed system. Initially, the '*Numerical Search*' method is looked into in detail. Numerical Search or Linear Search is seen to be too time costly to be implemented on tall structures (suggested but not limited to number of story < 9). In light of this, 2 separate algorithms are implemented in combination to develop a much more efficient strategy for optimization. The two algorithms used are Nelder –Mead algorithm and Covariance Matrix Adaptation Evolution Strategy (CMA-ES). The performance of the '*Combinatorial optimization*' evaluated and few modifications are made to improve its efficiency, both in terms of time and accuracy.

- CHAPTER 5: This chapter mainly concerned with performance comparison between the SS system and a conventional composite slab frame. The performance comparison is conducted using the frequency domain method of analysis. The earthquake is modeled as a stationary noise

and the model used for it is a commonly used Spectrum known as the 'Kanai-Tajimi Spectrum'. It is used to model 2 sets of earthquakes - Near-fault earthquakes and Far-fault earthquakes. The performance comparison is drawn out using the Root Mean Square response of the two systems for these 2 sets of earthquakes.

- CHAPTER 6: This chapter looks into some of the important design aspects of the SS system that are required for the design. The design of PT and ED links are looked into which play a vital role in optimizing the performance of the SS system.
- CHAPTER 7: The Final chapter highlights the important features of the SS system and proposes the scope for future research. This thesis addresses the performance aspects of the developed system; however for proper development of the SS system, detailed design of the various components and connections is required as well.

1.5 Performance of Moment Resisting frames under Seismic Loading

The integrity of fully-welded connections in the beam-to-column joints of steel frames under earthquake loading has come under question as many steel and composite buildings suffered severe damage in connections during the Northridge (1994) and Hyogo-ken Nanbu (1995) earthquakes. Forensic investigations following the earthquake identified failed welded beam-column connections in more than 200 buildings in moment resisting frames (Whitaker, Gilani, & Bertero, 1998). The failure was attributed to poor connection detailing practices and inadequate weld material properties that were common prior to the earthquake (SAC Joint Venture 2000). The backing bars and weld runoff tabs used to make the groove welds connecting the beams to the columns were normally left in place after completion of the weld. The existence of backing bars or weld tabs created a lack-of-fusion defect, which was large enough to originate crack growth which propagated in the heat affected zone of the weld metal and in the column flange as shown in Figure 1.2.



Figure 1.2 Fractured Connection in 1994 Northridge Earthquake

Subsequently, other design alternatives were investigated to reduce the risk of connection failure during earthquakes. One of such alternatives for the design of special moment frames is to include the reduced beam section (RBS) detail (also known as dog-bone connection), which has shown to exhibit stable hysteretic loops and sufficient ductility during numerous laboratory tests and has gained rapid acceptance worldwide (Chen et al. 1996; Plumier 1997; Engelhardt and Winneberger et al. 1998; Zekioglu et al. 1997). The concept behind the reduced beam section detail is to trim the width of the beam flange for a particular length of the beam and force inelastic deformation and energy dissipation to occur along the reduced flange portion of the beam. One of the main advantages of using a RBS detail in moment frames is that it results in a smaller moment at the column face, which limits demand on the connection and reduces the likelihood of brittle fracture in the connection. In addition, the RBS detail helps satisfy the “strong column - weak beam” seismic design requirements. However, one of the behavioral disadvantages of the RBS detail is the need to account for the increased probability of web buckling and lateral-torsional buckling caused by reduction in flange stiffness (Chi & Uang, 2002). Another shortcoming of using such detail is the large cost associated with material replacement and repair downtime resulting from the large inelasticity in the beam. With the recent trend pointing towards sustainable engineering, the need for investigating alternative safe, cost-effective, and environmentally friendly design approaches for steel frames is ever pressing. As previously discussed, rocking of frames is one approach by which damaged in the steel building can be controlled and easily repaired. Another approach is base isolation, which although an effective approach in reducing seismic demand, its high cost and complexity associated with isolating an entire structure can be a discouraging. Figure 1.3 shows the deformation of an RBS connection after high inelastic demand.

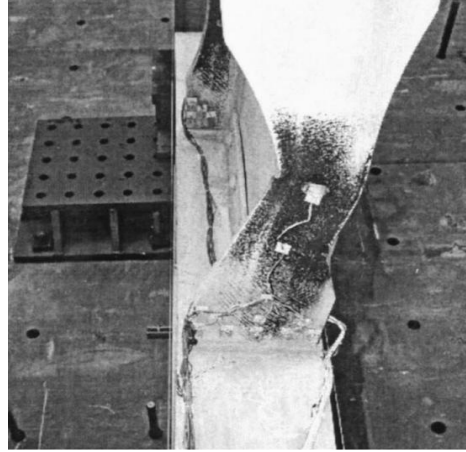


Figure 1.3 Yield and Buckling pattern in a Reduced Beam Section

1.6 Isolation Systems

The concept of base isolation is considered to be one of the most promising developments in the field of earthquake engineering. In addition to limiting damage to the main structural component of a building, the importance of base isolation lays in the fact that the majority of the value of the building is in its contents and nonstructural components. In early 1970's, various studies were conducted on base isolation systems with focus on elastomeric and friction-type bearings. In the 1980s and early 1990s, attention was shifted towards active control device-based hybrid system (Taghavi & Miranda, 2003). However, the practical use of active control-based hybrid systems in large structures has been restricted due to problems, including instability, reliability, and, power consumption. As a result, researchers shifted their focus towards the feasibility of semi-active control devices (Kelly, Leitmann, & Soldatos, 1987; Reinhorn & Riley, 1994), which can be both adaptable and stable, while maintaining low external power requirements (S. P. Chang et al. 2002). Following initial studies on semi- active control devices, smart structural control system, of the

same type, employing MR fluid dampers was proposed and studied (Ramallo, Johnson, & Spencer, B. F., 2002; Yoshioka, Ramallo, & Spencer, B. F., 2002).

However, the considerably high cost and complexity associated with the practical application of such system on an entire structure can be source of concern. Shape Memory Alloy has found application in different fields and has been tested and incorporated in civil structures for earthquake mitigation including SMA wire re-centering devices (Dolce, Cardone, & Marnetto, 2001), SMA spring isolation system (Khan & Lagoudas, 2002; Mayes, Lagoudas, & BK., 2001) and SMA tendon isolation system for multi degree of freedom shear frame structure (Corbi, 2003). SMA wires were also used as a bracing. The mentioned studies, among others, demonstrated the effectiveness of base isolation for earthquake mitigation.

1.6.1 Base Isolation

Base Isolation (BI) is considered to be one of the biggest and most popular isolation methods implemented in the field of earthquake engineering. It has turned out to be quite an economical and effective approach for mitigating the effects of earthquakes over the past two decades. The fundamental concept of base isolation is to decouple the main structure from the earthquake induced ground motion. By decoupling, the ground motion transferred to the main structure is reduced thereby reducing the damage incurred by the main structure. Base isolation has not only been used to isolate structures but has also been used to isolate specific floors containing fragile and sensitive equipment.

A typical base isolation system comprises of lead-rubber bearings placed at the foundation level which tends to introduce flexibility to the main structure and at the same time dissipates energy in the damping elements. The isolated structure tends to vibrate like a rigid body with large deformations taken by the bearings. This not only reduces the lateral forces experienced but also reduces them uniformly over the floors. The lead-rubber bearings have been vastly researched on and have been shown to be quite effective (F.Y. Chen et al. 2008; Islam and Ahmad 2010)

Significant research has been done with regards to base isolation systems over a few decades. Seismic isolation for multi-story buildings has been also well evaluated and reviewed (Hong and Kim 2004; Matsagar and Jangid 2004; Komodromos 2008; Lu and Lin 2008; Spyrakos et al. 2009). Base isolator with hardening behavior under increasing loading has been developed for medium-rise buildings (up to four stories) and sites with moderate earthquake risk (Pocanschi & Phocas, 2007). Resonant behavior of base-isolated high-rise buildings under long-period ground motions was evaluated by Ariga et al. (2006) and long period building responses by Olsen et al. (2008). Deb (2004), Dicleli and Buddaram (2007), Di Egidio and Contento (2010) have also given effort in progresses of isolated system. Komodromos et al. (2007), Kilar and Koren (2009) focused the seismic behavior and responses through dynamic analyses of isolated buildings.

Base Isolation has been particularly popular because of its easy to implement and easy to maintain; however it has its share of limitations as well. The BI system is only suitable for structures with short periods (Maldonado-mercado, 1995) as the BI system tends to elongate the period of the main structure. The more the difference in time periods between the isolated and the non-isolated structures the more efficient is the BI system. In case the non-isolated structure has long period

then the elongation in period of the isolated structure would be negligible thereby making the BI system ineffective. The BI system therefore is not effective on soils that produce long periods. The BI system is also seen to be ineffective against wind loads, as they act above the foundation level thereby rendering the isolation aspect useless. Further, the BI system requires an isolation gap to allow for the free lateral displacement of the isolators (Maldonado-mercado, 1995). Lead-rubber bearings tend to deteriorate over time but not much is known about the effects of aging and long term creep and how the chemical and physical properties change over time (Villaverde, 1990). Other limitations include the inability to measure the coefficient of friction with certainty after a long period of inactivity (Villaverde, 1990).

1.6.2 Tuned Mass Dampers

A Tuned Mass Damper is a device that comprises of a mass, a damper and a spring, that is used to reduce the response of the structure to dynamic loading. The TMDs are designed such that their natural frequency matches the frequency of the predominant mode of the main structure. Under these conditions, the TMDs are said to be optimally tuned and are considered to give the best performance. The TMD's have been quite widely studied for wind loading and earthquake loading. The concept of TMD was first applied by Frahm (1909) to reduce the rolling motion of ships as well as ship hull vibrations.

1.6.2.1 Passive Translational Tuned Mass Damper

Passive TMDs are absent of any external source of energy to control the motion of the mass. As a result these systems are entirely mechanical and entirely dependent on the initial settings. Consequently, they are susceptible to detuning (Setareh & Hanson, 1992) and are thus unreliable than its counterparts. The effectiveness of the TMDs tends to be within a narrow bandwidth around the natural frequency of the structure thus it becomes highly necessary to tune the TMDs (Roffel, Lourenco, Narasimhan, and Yarusevych, 2011). Even small deviations from the optimal tuning frequency can deteriorate the performance significantly. Despite these significant limitations, passive TMD systems are still considered to be the primary choice as they are relatively inexpensive systems. Furthermore the absence of an external actuator or energy source means that there are no additional operational costs once the system is installed.

One of the most common type of passive tuned mass dampers are the translational TMDs (Connor, 2003). These can be further classified into unidirectional or bidirectional system (Connor, 2003). In unidirectional systems, the motion of the TMD mass is restricted to a single direction, often by placing the mass on a set of rails or roller bearings. In bidirectional systems, the mass can move along both coordinate axes. In either topology a set of springs and dampers are placed between the TMD mass and the supporting structure which is fixed to the structure. Translational TMD systems have been implemented in large scale structures for over 40 years (Kareem, Kijewski, and Tamura, 2007). Some prominent examples of structures incorporated with translational TMD systems include, the Washington National Airport Tower in in Arlington County, Virginia; the John Hancock Tower, in Boston, MA, and the Chiba Port Tower in Chiba Prefecture, Japan.

1.6.2.2 Passive Pendulum Tuned Mass Damper

In this type, the translational spring and damper system are replaced with a pendulum, which consists of a mass supported by a cable that pivots about a point, similar to a pendulum. It is proven analytically that for small angular oscillations the PTMDs can be considered equivalent to a translational TMD (Connor, 2003) and can be modeled identically. However PTMDs have certain advantages over translational TMDs such as they do not require any bearings, which are quite expensive and susceptible to wear and tear.

Numerous researches have been conducted regarding PTMD systems and different systems have been developed. A bidirectional homogeneous PTMD has been developed that can be tuned for different frequencies in the two directions (Almazán, De la Llera, Inaudi, López-García, and Izquierdo, 2007). Lourenco (2011) developed an adaptive PTMD that increased the robustness of the passive system. PTMD systems are one of the most widely used in the world. Almost half of the structures in Japan utilize PTMD systems (Kareem et al., 2007). Some of the prominent examples are the Crystal Tower in Osaka, Japan; Higashimiyama Sky Tower in Nagoya, Japan; and Taipei 101 in Taipei, Taiwan (Connor, 2003).

1.6.2.3 Active Tuned Mass Damper

Active systems contain an external energy source, often in the form of an actuator. In comparison to passive systems, which operate without an energy source and utilize an open loop control, active systems utilize sensors to measure system conditions and employ a closed loop control.

An Active Tuned Mass Damper (ATMD) system comprises of an actuator which drives the motion of either the TMD mass or an auxiliary mass connected to the TMD mass. By actively controlling the motion of an external mass, the ATMD can control the forces exerted on the structure. There are two advantages in this design. First, the performance of an ATMD system will outperform an equivalent passive TMD under detuning conditions, since any detuning is compensated by feedback control (e.g. Nishimura et al. 1992; Nagashima 2001). Secondly, an ATMD system is capable of optimizing its transient performance. This is particularly useful for impact loads, such as earthquake loads (Connor, 2003). As a result ATMD systems have been implemented to reduce the lateral response of structures when induced by earthquake loads. For, example the Kyobashi Seiwa Building in Tokyo, Japan contains two ATMDs to mitigate structural vibration induced by frequent earthquakes (Spencer and Sain, 1997). The installed system reduces the lateral displacement by approximately 67%.

Several studies have been performed on the use and performance of ATMDs. These studies generally focus on an optimal control algorithm used to improve the ATMDs performance. Nishimura et al. (1992) compared the performance of an ATMD using a set of optimized parameter equations to a passive TMD system, observing an 80% improvement at the peak frequency. Nagashima (2001) presented an optimal displacement feedback control law for an ATMD system on a SDOF system. Although ATMDs can outperform their passive counterparts, they have some drawbacks. The added design, manufacturing, and instrumentation complexity results in significantly higher financial costs over passive systems. Furthermore, the addition of an actuator significantly increases the energy requirements of the system. To reduce energy demands, active systems can be converted into hybrid systems (Connor, 2003). In hybrid systems the ATMD acts

as a passive system under typical loading conditions. Once the structure reaches a certain threshold, the active system is turned on. An example of a hybrid system is the Ando Nishikicho Building in Tokyo, Japan, which uses a hybrid system containing an 18 tonne passive TMD and two auxiliary actuated masses weighing a combined 3.6 tonnes.

1.6.2.4 Semi Active Tuned Mass Damper (SATMD)

ATMD systems provide improved vibration suppression performance at the cost of added complexity, maintenance, and energy requirements (Connor, 2003). As a result, active systems are usually employed in structures that are exposed to significant dynamic loading. PTMD systems are fairly simple systems, which provide excellent vibration suppression when accurately tuned and when the structure is excited by narrowband dynamic loading (Setareh et al 2006). Their lack of robustness to multiple-frequency narrowband excitations and structural detuning limit their performance. SATMD systems combine the advantages of both passive and active systems. These systems provide active control of either the stiffness or dampening components of the TMD system, instead of driving the system itself. The power requirements to control these components are orders of magnitude lower than the power required to drive the TMD mass for active systems (e.g. Lin et al 2010; Nagarajaiah, S., and Varadarajan 2005; Chey et al 2010). Since SATMDs do not supply mechanical energy to the structure they are considered passive systems. Hence, they preserve system stability. By providing active control of the TMD components at lower energy costs, they provide improved performance over passive TMD systems while mitigating the negative attributes of ATMD systems. There are numerous methods of providing active control to TMD components. (Nagarajaiah and Sonmez 2007; Nagarajaiah and Varadarajan 2005) utilized

a semi-active variable stiffness TMD for the suppression of wind induced vibrations for a building model. The TMD system allows for adjustment in stiffness via the motion of a linear actuator. Setareh (2002 and 2007) proposed dampening control for a PTMD via a magneto rheological damper. The magneto rheological damper is a magnetically responsive fluid containing magnetisable particles, which in the presence of a magnetic field will affect the fluid's viscosity. Chey (2007 and 2010) conducted an analytical study of a SATMD using a resettable device in the form of a non-linear pneumatic spring. The conclusions common to each of these studies is that the semi-active design outperforms the equivalent passive design while providing superior performance for detuned testing conditions.

1.6.2.5 Multi – Tuned Mass Damper

As the name implies, multiple TMD systems uses several smaller TMD systems to reduce structural vibrations instead of using a single large mass tuned to the structures natural frequency (Chen and Wu, 2001). Multiple TMD systems are innately passive systems; however their design allows them to be more robust to detuning conditions than traditional passive TMD designs. In structures with limited space the use of several smaller TMDs can allow for greater mass ratios (Sun et al 1992). For example, if one large TMD system (tuned to the structures natural frequency) is divided into several smaller TMD systems (also tuned to the structures natural frequency) with an equivalent mass to the original TMD system, then both systems will have an equivalent dynamic response (Sun et al 1992).

Generally, multiple TMD designs contain individual TMD systems tuned to different frequencies. There are two approaches to this implementation. The first is to utilize multiple TMD systems tuned to multiple structural modal frequencies. This is a commonly used approach in real structures. For example, the antennae sitting atop the Canadian National Tower in Toronto, Canada contains two twenty tons pendulum type dampers tuned to the structure's second and fourth vibration modes (Connor, 2003). The second approach is to utilize multiple TMD systems tuned to frequencies distributed around the structure's natural frequency. Igusa and Xu (1994) demonstrated that the optimal approach is to distribute the tuned frequencies of the individual TMD systems about the natural frequency. It was concluded that the optimized designed multiple TMD system is more robust and effective than the equivalent mass optimized single TMD system. Lin and Cheng (2001) evaluated the use of an optimized multiple TMD system to reduce the buffeting response and increase the critical wind speed of long spanning bridges. The results show that multiple TMD systems, once optimized, perform better and are more robust against wide frequency bandwidth wind excitation than the equivalent mass optimized passive TMD system. Chen and Wu (2001) made similar observations for structures induced by seismic loading.

1.7 Suspended Systems

The concept of suspending a whole structural system is not new in design and construction of buildings against wind and seismic forces. The idea of suspending the structural system is to suspend the floors from a concrete core tower using hanger straps draped over the core as shown in Figure 1.4 The suspended West Coast Transmission building in Vancouver, Canada. An energy dissipating device, typically steel rods, are installed between the floor and the concrete cores and

are left to fracture while the system is allowed to freely sway during an earthquake (Goodno, 1975). Although the suspension systems offer some quite promising attributes with respect to earthquake engineering, it still has not been developed to its full potential (Demetriades et al 1992). Thus, there is a need to further explore the possible application of the concept and conduct research in the area of resistance using suspended systems. Some examples of suspended structures include the West Coast Transmission building, built in 1969 in Vancouver, Canada (Figure 1.4 The suspended West Coast Transmission building in Vancouver, Canada) the OCBC Centre, built in 1976 in Singapore, Singapore; and the Administrative Center for the State of Minas Gerais, built in 2007 in Minas Gerais, Brazil, which is known as the world's largest suspended structure. In the US, the use of suspension mechanism has also been explored. Examples of such include the suspended structure developed by International Environmental Dynamics (IED), San Jose, California; the eleven story pacific trade Center, San Pedro; the Great Western Savings and Loan Building, Berkeley, California; the Sherman building in San Jose, California; and the Marshall building in San Mateo, California.

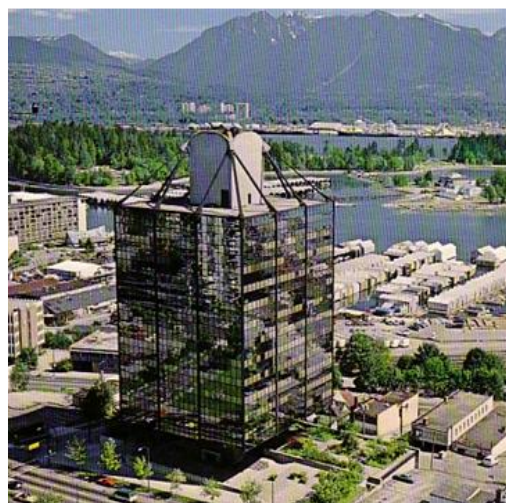


Figure 1.4 The suspended West Coast Transmission building in Vancouver, Canada

Isolated floor systems are gaining acceptance in various applications to protect nonstructural components that can be moved and located anywhere on the floor or specific rooms—instead of isolating single equipment or the entire building. One example is where the floor isolation system consists of a raised platform which is isolated using friction-pendulum bearings and damped by the friction and/or by viscous dampers (Demetriades et al 1992). Other similar systems have also been studied, such as the use of a special kind of bidirectional spring units (Shenlei Cui, M., 2010) and wire-rope isolators (Lambrou, V. and Constantinou, 1994) instead of friction bearings to provide stiffness, damping and self-centering capabilities to the isolated floor. An advantage of these modified systems over traditional friction pendulum bearing system is that the vertical and horizontal force transfer mechanisms are uncoupled so that a wide range of isolated periods can be achieved by tuning them. Moreover, the friction bearing system experiences high stress concentrations at the contact of the bearing and the concave dish that results in formation of grooves, which could hinder the motion of the bearing during subsequent earthquakes events. There have been other studies investigating the performance and reliability of passive and semi-active equipment isolation systems located on the upper levels of multi-story structures (Alhan 2005; Gavin, H.P. and Zaicenco 2007). Some other systems have also been developed, such as ball in cone isolators. Floor isolation systems have also been investigated and implemented internationally over the past 15 years. Among the various analytical investigations, an experimental study was conducted on three dimensional floor isolation systems in Japan (Kaneko et al 1995).

CHAPTER 2

THEORETICAL DEVELOPMENT OF PROPOSED SYSTEM

2.1 Introduction

In 1928, Ormondroyd and Den Hartog presented the theory on TMD, followed by a detailed discussion of optimal tuning and damping parameters in Den Hartog's book on mechanical vibrations (J. P. Den Hartog, 1940). Since then, significant contributions have been made in terms of analytical studies on TMDs, for example - Randall et al. (1981), Warburton and Ayorinde (1980), H.C. and Lin G.C. (1993) and many more. A number of new TMD systems have been developed and evaluated, ranging from passive type systems, such as Multi – Tuned Mass Dampers (MTMD) and Distributed Tuned Mass Dampers (DTMD), to active and semi-active types. Based on the vast repertoire of knowledge on TMDs, the proposed SS system can be considered as an analogue to a MTMD, and it is therefore analyzed in a similar manner.

2.2 A Single Suspended Slab (SSS) Model

2.2.1 System Idealization

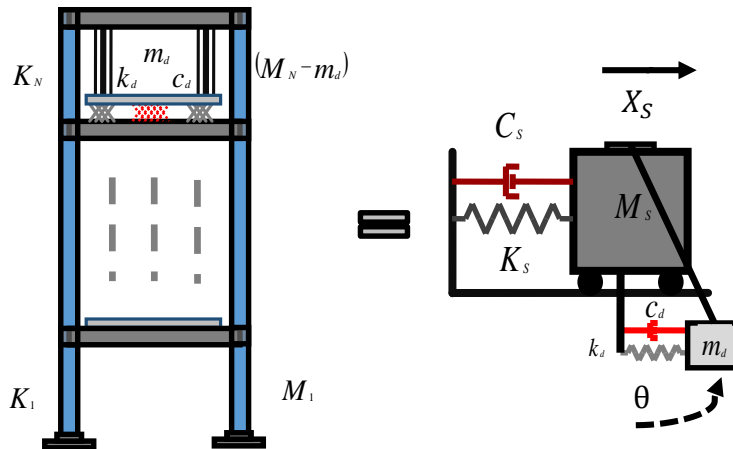


Figure 2.1 System Representation and Idealization of a Single Suspended Slab System

A simplified analytical model (SSS model) is developed to understand and analyze the behavior of the SS system. The reference system considered is a 4 – story 1 – bay structure with single suspended slab on the 4th floor. The system is analyzed as a 2 DOF system, where the steel frame is represented by a single degree of freedom (X_S) and the slab by another (θ) (Figure 2.1). The proposed analytical model can be considered similar to a typical PTMD system. As discussed earlier, a PTMD system comprises of mass suspended by cables at particular location(s) (which is mostly the top floor). Similarly in the SS system the slabs are suspended using cables or hanger rods. The PTMD system also comprises of some stiffness and damping to keep the motion of the pendulum mass within acceptable limit.

In the SSS system, the stiffness is provided by the post-tensioned links and the damping by the energy dissipation links. Thus, the two systems are quite similar in nature, and so the proposed analytical model for the SSS system is exactly the same as that of a PTMD system. The model comprises of a mass ' M_S ' that represents the mass of the 4 story structure excluding the mass of the suspended slab, and mass ' m_d ' represents the suspended slab's mass. The damping (C_S) and stiffness (K_S) of mass M_S represent the structure's total stiffness and damping, excluding that of the suspended slab, and for mass m_d the stiffness (k_d) and damping (c_d) represent the slab's properties. As discussed earlier, the suspended slab is connected to the beams below them by 2 set of links – the PT and the ED links. So k_d is actually the stiffness provided by the PT and c_d is the damping provided by the ED links.

As mentioned earlier there are two degrees of freedom used to describe the motion of the complete system. The main steel frame's displacement is described by ' X_S ' and the motion of the suspended slab is described by ' θ '. The equations of motions to describe the behavior of this analytical model are derived using the Euler Lagrange method of energy conservation (Tedesco, McDoughal, & Ross, 1999). The Lagrange's equation is given by Equation 3.1, which is a derivative of the principle of conservation of energy. The L is known as the 'Lagrange' and is the difference between the total Kinetic Energy (K) and the total Potential energy (U) of the system. The generalized coordinates of the respective system is represented by q_j while the work done by the non-potential forces is represented by Q_j . Equations 3.2 and 3.3 represent the kinetic energy of our respective components of the model - M_S and m_d . Equations 3.4 and 3.5 give the potential energy of these components. The final equations of motion derived using the Lagrange equation are shown below in Equations 3.8 and 3.9.

$$Q_j = \frac{d}{dt} \left(\frac{\partial L}{\partial \dot{q}_j} \right) - \frac{\partial L}{\partial q_j} \quad \text{and} \quad L = K - U \quad (2.1)$$

$$K_{M_s} = \frac{1}{2} M_s (\dot{X}_s)^2 \quad (2.2)$$

$$K_{m_d} = \frac{1}{2} m_d \left(\frac{d}{dt} (X_s + L \sin \theta) \right)^2 + \frac{1}{2} m_d \left(\frac{d}{dt} (L \cos \theta) \right)^2 = \frac{1}{2} m_d (\dot{X}_s + L \cos \theta \dot{\theta})^2 + \frac{1}{2} m_d (-L \sin \theta \dot{\theta})^2 \quad (2.3)$$

$$U_{M_s} = \frac{1}{2} K_s (X_s)^2 \quad (2.4)$$

$$U_{m_d} = \frac{1}{2} K_d (L \sin \theta)^2 + m_d g L (1 - \cos \theta) \quad (2.5)$$

$$K_{Total} = \frac{1}{2} M_s (\dot{X}_s)^2 + \frac{1}{2} m_d (\dot{X}_s + L \cos \theta \dot{\theta})^2 + \frac{1}{2} m_d (-L \sin \theta \dot{\theta})^2 \quad (2.6)$$

$$U_{Total} = \frac{1}{2} K_s (X_s)^2 + \frac{1}{2} K_d (L \sin \theta)^2 + m_d g L (1 - \cos \theta) \quad (2.7)$$

1st Equation of motion:

$$(m_d + M_s) \ddot{X}_s + m_d L \ddot{\theta} \cos \theta - m_d L \dot{\theta}^2 \sin \theta + K_s X_s + C_s \dot{X}_s = -(m_d + M_s) a_g \quad (2.8)$$

2nd Equation of motion:

$$(m_d L^2) \ddot{\theta} + m_d L \ddot{X}_s \cos \theta + m_d g L \sin \theta + k_d L^2 \cos \theta \sin \theta + c_d (L \cos \theta)^2 \dot{\theta} = -(m_d L) a_g \quad (2.9)$$

2.2.2 Simplification

As previously discussed, the concept of the SS system can be considered parallel to the principle of a typical PTMD. Thus, to describe the behavior of the SSS system, equations similar to that of PTMDs are used. The relations describing the PTMD system can be converted to a much simpler

form. It has been shown that for small oscillations the PTMD system can be considered equivalent to a TTMD (Connor, 2003). Under small oscillations the assumptions (Equation 3.10) tend to be true, as a result the equations of motion (Equations 3.8 and 3.9) can be converted to TTMD equations using the assumptions shown in Equation 3.10.

$$\cos \theta \approx 1 \quad \sin \theta \approx 0 \quad \theta \approx X_d L \quad (\dot{\theta})^2 \approx 0 \quad (2.10)$$

The SS system is intended to be designed in a way that ensures that the suspended slabs move within a small range and since it is considered equivalent to a PTMD, the SSS system can be analyzed as a TTMD system instead of a PTMD system. The simplified analytical model is shown in Figure 2.2. The suspended slab is represented by a block as it has been converted to a translational degree of freedom with displacement ‘ X_d ’. This simplification makes it easier to solve the equations of motion and interpret the results.

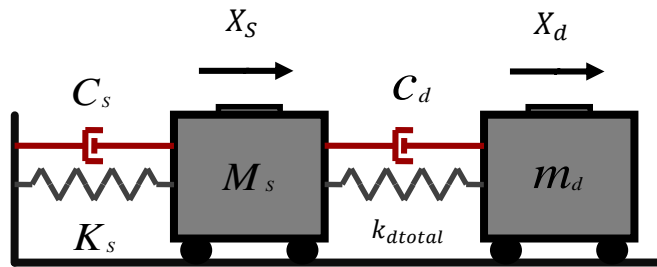


Figure 2.2 Simplified SDOF Model

The new set of equations of motion are in terms of 2 degrees of freedom - X_s (Roof Displacement of Steel Frame) and X_d (Displacement of Slab). The equations of motion of both the components are a function of their respective damping ratio, mass, stiffness and the length of the cable from which the slab is suspended. Generally, the equations of TMD are represented in terms of

commonly used variables as showed in Table 2-1. The final equations obtained for the simplified SSS model are given by Equations 3.11 and 3.12.

Table 2-1 Commonly Used Parameters for TMDs

ω_s	$\sqrt{\frac{K_s}{M_s}}$	Natural frequency of structure without the suspended slab
ξ_s	$\frac{c_s}{2M_s\omega_s}$	Bare steel frame damping
k_{dtotal}	$\frac{m_d g}{L} + k_d$	Total Stiffness of Suspended Slabs
ω_d	$\sqrt{\frac{k_{dtotal}}{M_d}}$	Natural frequency of suspended slab
α	$\frac{\omega}{\omega_s}$	Excitation Frequency Ratio
ξ_d	$\frac{c_d L}{2m_d \omega_d L}$	Suspended Slab Damping Ratio
β_d	$\frac{\omega_d}{\omega_s}$	Tuned Frequency Ratio
μ_d	$\frac{m_d}{M_s}$	Mass Ratio

$$\ddot{u}_s + 2\xi_s \omega_s \dot{u}_s + \omega_s^2 u_s - 2\omega_d \mu_d \xi_d \dot{u}_d - \mu_d \omega_d^2 u_d = -a_g \quad (2.11)$$

$$\ddot{u}_d + 2(1+\mu_d)\xi_d \omega_d \dot{u}_d + (1+\mu_d)\omega_d^2 u_d - 2\xi_s \omega_s \dot{u}_s - \omega_s^2 u_s = -a_g \quad (2.12)$$

2.3 Response Transfer Functions

The solution to differential equations is comprised of a homogenous and a non-homogenous solution. The homogenous solution, or the transient response, diminishes after a finite time at a rate dependent on the internal dampening of the system (Franklin, Fowell, & Emami-Naeini, 2009). The non-homogenous solution, or steady state response, persists as long as the input excitation is provided to the system. In terms of analysis, the homogenous solution is generally ignored since the system is incapable of controlling the transient response (Tedesco et al., 1999). In practice, the engineers are generally interested in the structure's steady state response, so the homogeneous response is ignored in the analysis.

The 2nd order differential equations (Equations 3.11 and 3.12), which are obtained from the previous section, are solved simultaneously using the complex frequency response approach to acquire the respective response amplitude transfer functions for both – the steel frame and the slab.

It is considered that the system is excited by a ground excitation of the form (Equation 3.13). The displacement response to this forcing function can be considered as a harmonic motion for both, the steel frame and the suspended slab (Equations 3.13 and Equation 3.14) and the acceleration response can be assumed to satisfy Equations 3.16 for steel frame and Equation 3.17 for the suspended slab. The displacement equations are used to transform the differential equations to a linear form, which are further solved to obtain the respective displacements amplitudes of the two components. The derived displacement amplitudes are further used to obtain the acceleration amplitudes using Equations 3.16 and 3.17. Below are given the derived response amplitudes

(displacement and acceleration) for the steel frame and the suspended slab, along with their corresponding phase angles. The phase angles are the phase difference between the input excitation and the response parameter (displacement or acceleration) of the frame or slab. Table 2-2 gives the clear definitions of the terminology used.

$$a_g = \tilde{a}_g e^{-i(\alpha t)} \quad (2.13)$$

Table 2-2 Definition of response parameters

Variable	Definition
X_s	Harmonic response of steel frame
X_d	Harmonic response of suspended slab
H_s	Displacement amplitude of steel frame
γ_{HS}	Phase angle for steel frame
H_d	Response amplitude of suspended slab
γ_{Hd}	Phase angle for suspended slab
A_s	Acceleration amplitude of steel frame
γ_{AS}	Phase angle for steel frame
A_d	Acceleration amplitude of suspended slab
γ_{AS}	Phase angle for suspended slab

$$X_s = H_s e^{-i(\alpha t - \gamma_s)} \quad (2.14)$$

$$X_d = H_d e^{-i(\alpha t - \gamma_d)} \quad (2.15)$$

$$\ddot{X}_s + a_g = A_s e^{-i(\alpha - \gamma_s)} \quad (2.16)$$

$$\ddot{X}_d + a_g = A_d e^{-i(\alpha - \gamma_d)} \quad (2.17)$$

$$|H_s| = \sqrt{\frac{\left((1 + \mu) \beta_d^2 - \alpha^2 \right)^2 + \left(2 \xi_d \beta_d \alpha (1 + \mu) \right)^2}{\left((\beta_d^2 - \alpha^2)(1 - \alpha^2) - \mu \beta_d^2 \alpha^2 - 4 \xi_d \xi_d \beta \alpha^2 \right)^2 + \left(2 \alpha \xi (\beta_d^2 - \alpha^2) + 2 \xi_d \beta_d \alpha (1 - \alpha^2 (1 + \mu)) \right)^2}} \quad (2.18)$$

$$\gamma_{HS} = \tan^{-1} \left(\frac{2 \xi_d \beta_d \alpha (1 + \mu)}{(1 + \mu) \beta_d^2 - \alpha^2} \right) - \tan^{-1} \left(\frac{2 \alpha \xi (\beta_d^2 - \alpha^2) + 2 \xi_d \beta_d \alpha (1 - \alpha^2 (1 + \mu))}{(\beta_d^2 - \alpha^2)(1 - \alpha^2) - \mu \beta_d^2 \alpha^2 - 4 \xi_d \xi_d \beta \alpha^2} \right) \quad (2.19)$$

$$|H_d| = \sqrt{\frac{1 + (2 \xi \alpha)^2}{\left((\beta_d^2 - \alpha^2)(1 - \alpha^2) - \mu \beta_d^2 \alpha^2 - 4 \xi_d \xi_d \beta \alpha^2 \right)^2 + \left(2 \alpha \xi (\beta_d^2 - \alpha^2) + 2 \xi_d \beta_d \alpha (1 - \alpha^2 (1 + \mu)) \right)^2}} \quad (2.20)$$

$$\gamma_{Hd} = \tan^{-1}(2 \xi \alpha) - \tan^{-1} \left(\frac{2 \alpha \xi (\beta_d^2 - \alpha^2) + 2 \xi_d \beta_d \alpha (1 - \alpha^2 (1 + \mu))}{(\beta_d^2 - \alpha^2)(1 - \alpha^2) - \mu \beta_d^2 \alpha^2 - 4 \xi_d \xi_d \beta \alpha^2} \right) \quad (2.21)$$

$$|A_s| = a_g \sqrt{\frac{\left((\beta_d^2 - \alpha^2)(1 - \alpha^2) - \mu \beta_d^2 \alpha^2 - 4 \xi_d \xi_d \beta \alpha^2 + \alpha^2 \left((1 + \mu) \beta_d^2 - \alpha^2 \right) \right)^2 + \left(2 \alpha \xi (\beta_d^2 - \alpha^2) + 2 \xi_d \beta_d \alpha \right)^2}{\left((\beta_d^2 - \alpha^2)(1 - \alpha^2) - \mu \beta_d^2 \alpha^2 - 4 \xi_d \xi_d \beta \alpha^2 \right)^2 + \left(2 \alpha \xi (\beta_d^2 - \alpha^2) + 2 \xi_d \beta_d \alpha (1 - \alpha^2 (1 + \mu)) \right)^2}} \quad (2.22)$$

$$\gamma_{sA} = \tan^{-1} \left(\frac{2 \alpha \xi (\beta_d^2 - \alpha^2) + 2 \xi_d \beta_d \alpha}{(\beta_d^2 - \alpha^2)(1 - \alpha^2) - \mu \beta_d^2 \alpha^2 - 4 \xi_d \xi_d \beta \alpha^2 + \alpha^2 \left((1 + \mu) \beta_d^2 - \alpha^2 \right)} \right) - \tan^{-1} \left(\frac{2 \alpha \xi (\beta_d^2 - \alpha^2) + 2 \xi_d \beta_d \alpha (1 - \alpha^2 (1 + \mu))}{(\beta_d^2 - \alpha^2)(1 - \alpha^2) - \mu \beta_d^2 \alpha^2 - 4 \xi_d \xi_d \beta \alpha^2} \right) \quad (2.23)$$

$$|A_d| = a_g \sqrt{\frac{\left((\beta_d^2 - \alpha^2)(1 - \alpha^2) - \mu \beta_d^2 \alpha^2 + \alpha^2 - 4 \xi_d \xi_d \beta \alpha^2 \right)^2 + \left(2 \alpha \xi \beta_d^2 + 2 \xi_d \beta_d \alpha (1 - \alpha^2 (1 + \mu)) \right)^2}{\left((\beta_d^2 - \alpha^2)(1 - \alpha^2) - \mu \beta_d^2 \alpha^2 - 4 \xi_d \xi_d \beta \alpha^2 \right)^2 + \left(2 \alpha \xi (\beta_d^2 - \alpha^2) + 2 \xi_d \beta_d \alpha (1 - \alpha^2 (1 + \mu)) \right)^2}} \quad (2.24)$$

$$\gamma_{dA} = \tan^{-1} \left(\frac{2 \alpha \xi (\beta_d^2 - \alpha^2) + 2 \xi_d \beta_d \alpha}{(\beta_d^2 - \alpha^2)(1 - \alpha^2) - \mu \beta_d^2 \alpha^2 - 4 \xi_d \xi_d \beta \alpha^2 + \alpha^2 \left((1 + \mu) \beta_d^2 - \alpha^2 \right)} \right) - \tan^{-1} \left(\frac{2 \alpha \xi (\beta_d^2 - \alpha^2) + 2 \xi_d \beta_d \alpha (1 - \alpha^2 (1 + \mu))}{(\beta_d^2 - \alpha^2)(1 - \alpha^2) - \mu \beta_d^2 \alpha^2 - 4 \xi_d \xi_d \beta \alpha^2} \right) \quad (2.25)$$

2.3.1 System Behavior

In the previous section, transfer functions for the performance parameters of SSS system are obtained. These functions depend on the parameters - α , β_d , ξ_d , ξ and μ_d . By plotting these parameters the fundamental characteristics of the system behavior can be evaluated. To study the behavior in detail the parameters are varied one at a time and plotted against the steel frame roof amplitude assess the SS system's behavior. Figure 2.3 shows a plot of how the roof transfer function varies with mass ratio for different values of β_d while the structure is under resonance condition ($\alpha = 1$) and the damping ratio is kept constant. From the plot it is seen that as the mass ratio increases the roof displacement amplitude decreases thereby indicating an improvement in performance. This is logically correct as higher the mass higher the opposing force generated by the Suspended slab. Also, the pattern in performance is seen to be true for a wide range of values of β_d thus a high mass ratio can be considered advantageous for a TMD. Normally TMDs have an upper limit to the mass ratio that can be used practically. The mass ratio chosen for most TMDs is generally below 0.05, however this limitation is not applicable to the SSS system since in this system the slab is suspended which constitutes for a high percentage of mass as a result the mass ratio obtained can be as high as 0.20, which improves the performance of the system notably.

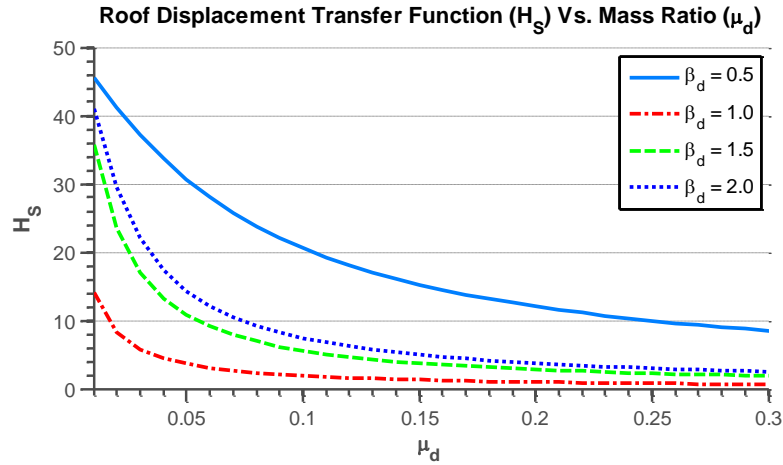


Figure 2.3 Effect of Mass Ratio on Response Displacement Amplitude of Steel Frame for $\alpha = 1$ and constant Damping Ratio

Figure 2.4 shows the variation in performance with respect to the damping ratio of the Suspended slabs for different mass ratios at resonance condition. From the plot it is seen that the increasing the damping of the suspended slab seems to affect the performance of the main structure adversely. As the damping of the suspended slab increases its ability to move gets restrained, as a result the opposing force generated by the slabs is reduced.

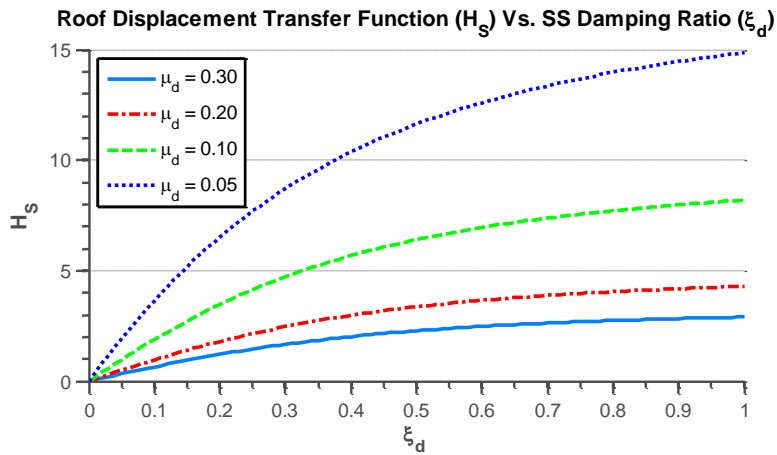


Figure 2.4 Effect of Damping Ratio on Response Displacement Amplitude of Steel Frame for $\alpha = 1$

The tuned frequency ratio, β_d , is a function of the ratio of the stiffness of the suspended slabs to that of the main structure. This parameter tends to control the motion of the slab, which suggests a correlation to the performance of the main structure. Figure 2.5 shows the variation of the transfer function with β_d for different damping ratios that vary from 0.05 to 0.30 at the resonance condition. From the plot it is evident that there exists only a single value of β_d for which the performance is minimum for a particular value of damping and mass ratio. This frequency at which maximum performance is seen is termed as the ‘Tuned frequency’ and varies with other parameters - μ_d and ξ_d .

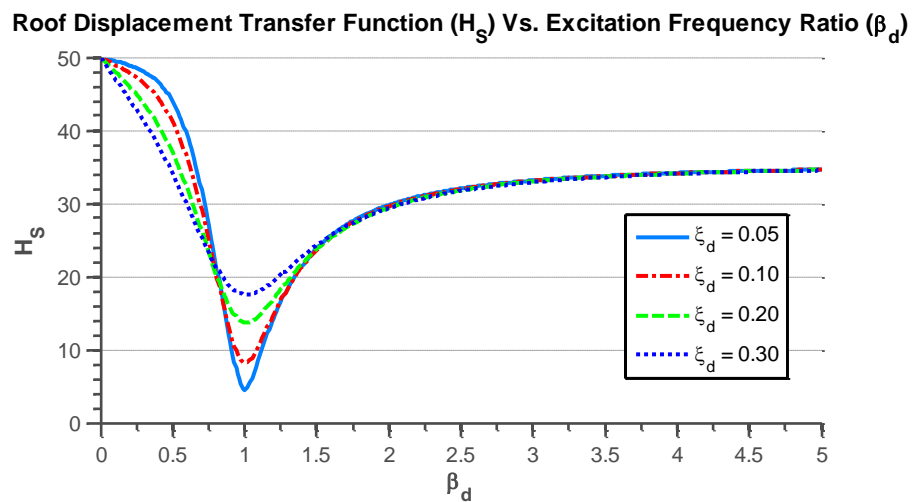


Figure 2.5 Variation of Response Displacement Amplitude of Steel Frame with Excitation Frequency $\alpha = 1$

Thus far, the behavior of the system is evaluated under the influence of different parameters, under the same input excitation frequency ratio where $\alpha = 1$ (i.e. under resonance condition). Figure 2.6 and Figure 2.7 evaluate the behavior of the system over a range of input frequency ratios. From both plots it is seen that the performance is optimum when the two peaks tend to have the same height (J. P. Den Hartog, 1940). So the optimal performance or the ‘Tuning condition’ is obtained

when the system acquires particular value for all parameters. In Figure 2.6 the optimal configuration is seen for mass ratio 0.20 and in Figure 2.7 for frequency ratio of 0.77. A point to note is that although from the figure it seems that the response for $\mu = 0.30$ is almost equal, if not less, but the main point of this section not to point out variation in response with the mass ratio. Instead the key point here is to highlight the fact that when the tuning condition is achieved the two peaks tend to align at the same level.

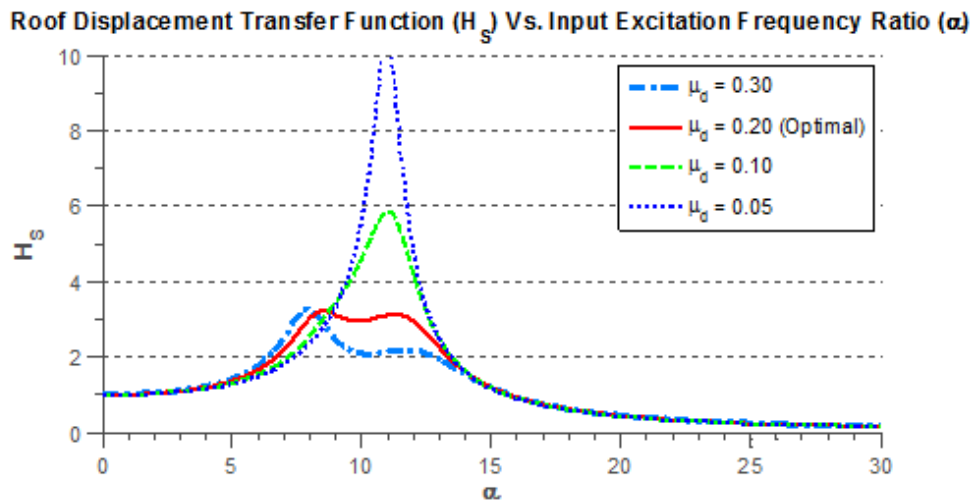


Figure 2.6 Variation in Response Dispalcement Amplitude for Steel Frame with Input Excitation Frequency and Mass Ratio

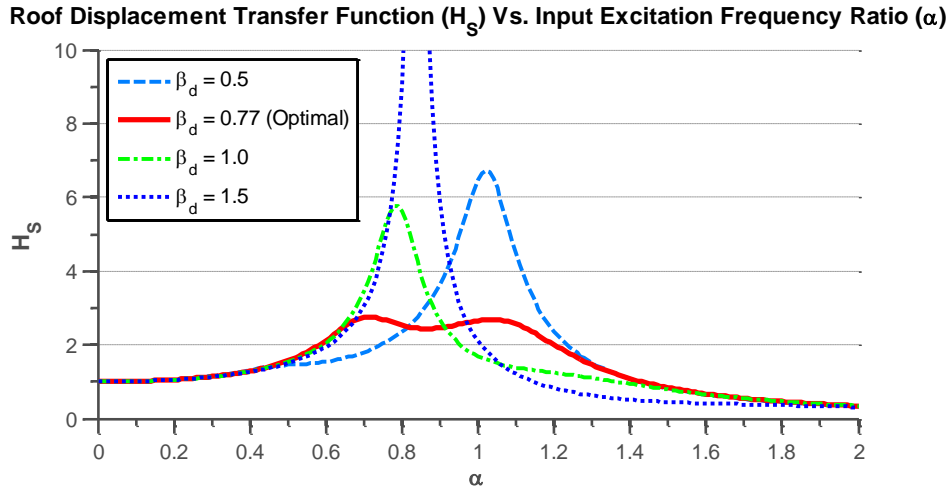


Figure 2.7 Variation in Response Displacment Amplitude for Steel Frame with Input Excitation Frequency and Frequency Ratio

2.3.2 Numerical Example

A Numerical example is presented to assess the effectiveness of the SSS system against a standard composite slab frame. The example comprises of a reference system same as considered earlier, a 4-story frame with a suspended slab at the top floor. The system is represented by one DOF for steel structure and one DOF for suspended slab, similar to the one described analytically. The response parameters are calculated based on the equations derived in the previous sections. The analysis procedure follows the flowchart shown in Figure 2.8.

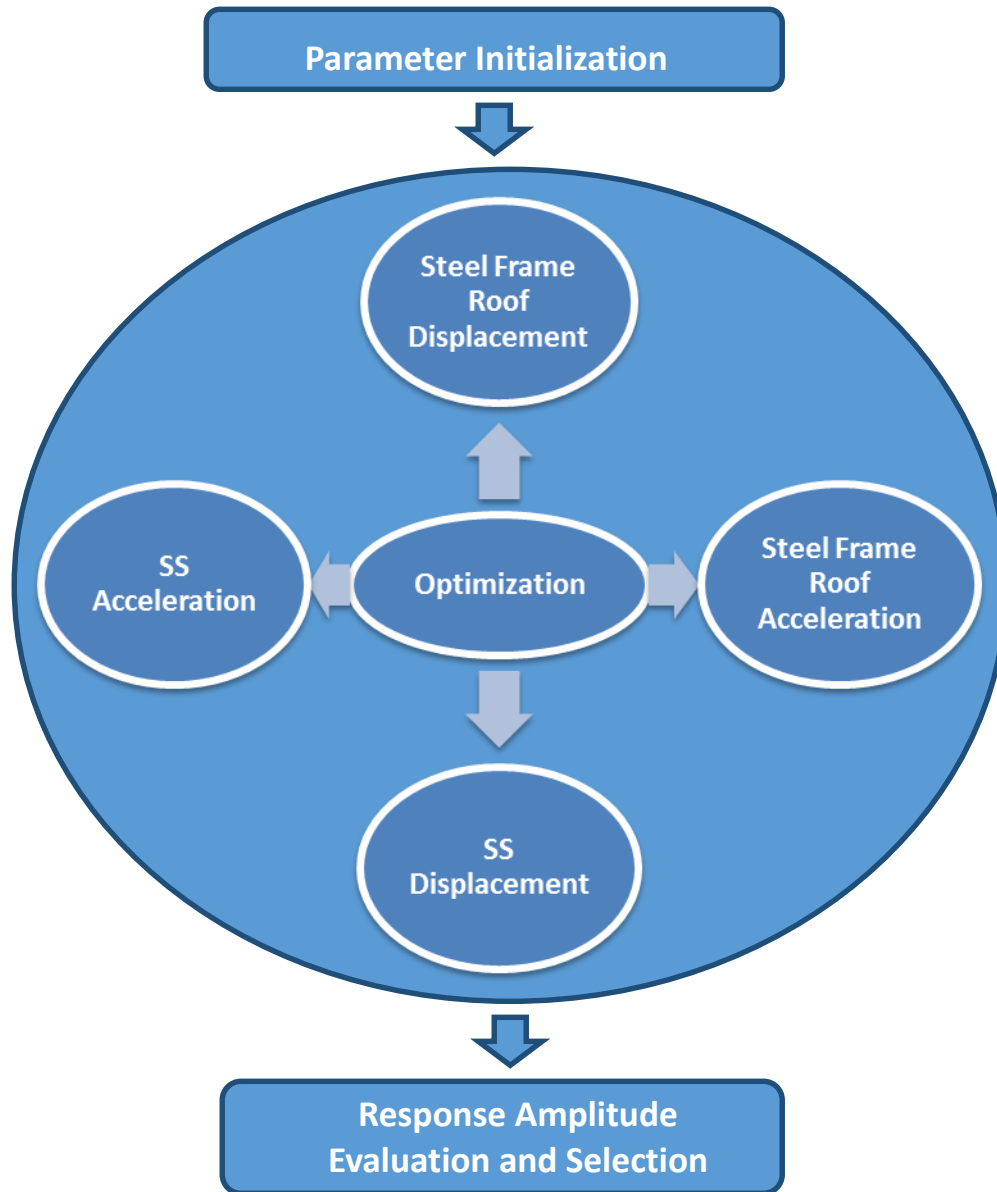


Figure 2.8 Analysis Procedure

Values are assigned to known variables such as the mass ratio, damping of steel frame, input excitation frequency, etc. Next step is to obtain the set of optimal parameters for the system using a suitable optimization algorithm. The details on this part are discussed in the next chapter (CHAPTER – 4). The numerical optimization involves minimizing the maximum response of the SS system for different input excitation frequencies

2.3.2.1 Composite Slab Frame

A 4-story 1-bay frame is considered for the composite slab steel frame in this example. The damping of the frame is chosen to be quite small (1%); normally, in conventional steel frames under large seismic demand, it is considered to be 5%. The main focus of developing the SS system is to avoid dissipation of energy in the main steel frame thus it is important to evaluate the performance of the structure while considering little or no energy dissipation in the main structure; hence the low damping. The response amplitude for a composite slab frame is given by Equation (3.26) in vibration theory under the assumption that the harmonic response is given by Equation 3.27. Equation 3.28 represents the phase difference between the input ground excitation and the steel frame's response.

$$|H_{cs}| = \frac{1}{\sqrt{\left((1-\alpha^2)\right)^2 + \left(2\xi_d \alpha\right)^2}} \quad (2.26)$$

$$X_s = |H_{cs}| e^{-i(\alpha t - \gamma_{cs})} \quad (2.27)$$

$$\gamma_{cs} = \tan^{-1} \left(\frac{2\xi_d \alpha}{(1-\alpha^2)} \right) \quad (2.28)$$

2.3.2.2 Suspended Slab Frame

A 4-story 1-bay steel frame with a slab suspended from the 4th floor, is considered for the SS system. The structural properties are the same as the composite frame as given in Table 2-3. To

keep consistency in comparison, the properties of the steel frame and the slabs, such as their material properties, dimensions, etc. are kept the same as the composite slab frame.

Table 2-3 Structural Properties of 4 Story 1 Bay Frame

Floor No.	Mass (slugs)	Stiffness (kips/inch)
1	0.309	37.6
2	0.304	37.6
3	0.304	37.6
4	0.274	37.6

The equations derived in the previous sections are used to obtain the amplitudes of the performance parameters. As discussed earlier the steps undertaken for the design process have been showed in Figure 2.8. The SSS system is first tuned to optimum conditions by using a ‘Mini-max’ approach. In this approach the maximum response is calculated for a range of input frequencies (ω) for a controlled set of TMD parameters. From the set of maximum responses, the minimum value is chosen and the parameters corresponding to it are considered as the ‘Optimal Tuning Parameters’. It is important to note that for the optimization, the parameter about which mini – max is applied is the input excitation frequency (α). The approach is applied to optimize the system based on 4 performance parameters – steel frame roof displacement and acceleration, and top floor suspended slab displacement and acceleration. Table 2-4 shows the optimized response parameters with their corresponding tuning parameters for different optimizations. Based on the performance parameter chosen for optimization the response of the SSS system changes accordingly. The displacement

amplitude response of the composite frame is seen to be 50, which is quite high compared to the SSS system. Thus, the SSS system out performs the composite slab frame.

Table 2-4 Transfer Function Values and SS system parameters for different Optimizations

Optimization Variable	μ	ξ_d	β_d	$ U _s$	$ A _s$	$ U _d$	$ A _d$
$ U _s$	0.198	0,17	0.80	2.2552	2.3270	7.6181	4.9331
$ A _s$	0.198	0.17	0.82	2.4491	2.1318	7.7650	4.8510
$ U _d$	0.198	0.40	0.72	4.4990	4.1153	6.7541	4.6852
$ A _d$	0.198	0.40	0.86	5.0938	4.3394	6.8029	4.5864

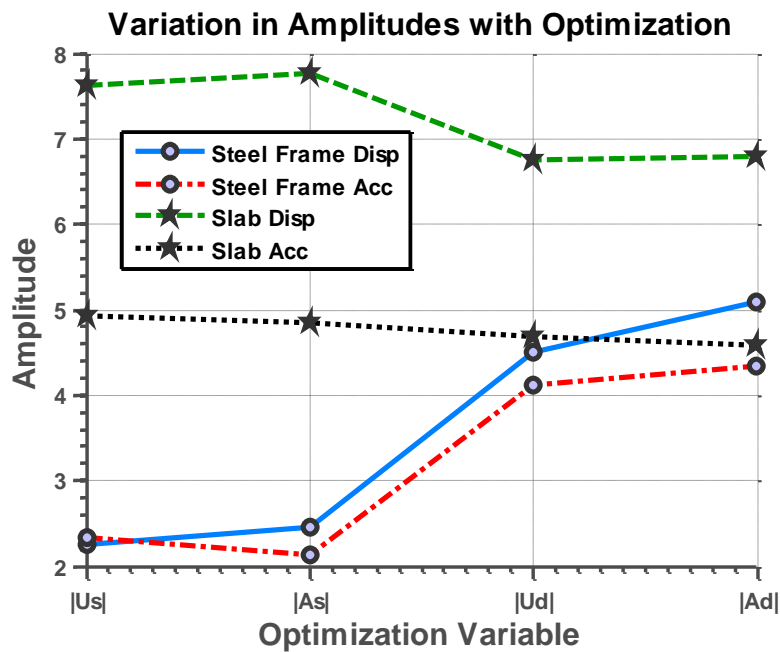


Figure 2.9 Optimized Amplitudes for different type of Optimizations for SSS Model

2.4 Multi Suspended Slab (MSS) Model

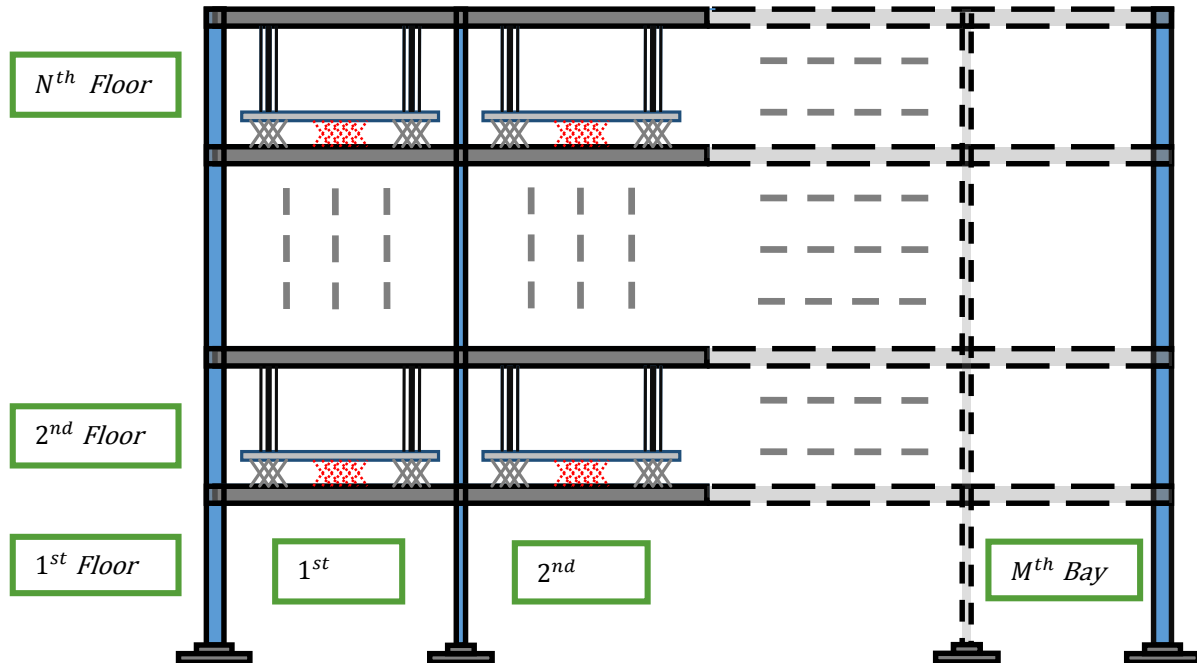


Figure 2.10 Multi Suspended Slabs (MSS) System Representation

TMDs are usually incorporated at the top floor of the structures as their performance is optimum when placed at the point of maximum lateral displacement. Initial systems of TMD used a single mass at the top floor, however further developments in this field have led to the use of multiple small masses. The use of multiple TMDs has popularly known to be called as MTMDs, as discussed before. Many researchers have looked into this field such as Kareem and Klein (1995), Abe and Igusa (1995). Yamaguchi and Harnpornchai (1993) evaluated the fundamental characteristics of horizontally distributed MTMDs in comparison to single TMDs. The study suggested that the optimum MTMD is more effective and robust than the optimum single TMD and using a larger number of TMDs tend to increase the effectiveness of the system.

Compared with the research on the horizontal distribution of MTMDs, vertical distribution of MTMDs has been less intensely investigated. Bergman et al. (1989) presented the effectiveness of vertically distributed MTMDs using a cantilever beam building model having a maximum of three TMDs distributed from the top to three-fifths the building height. K. Moon (2005) presented an extensive work on vertical distribution of TMDs that showed an elaborate design procedure for tuning vertically distributed TMDs to different modes. The analysis highlighted the effectiveness of vertically distributing TMDs both in terms of architectural constraint and performance.

To simulate a more realistic presentation of the intended SS system a Multi Suspended Slabs (MSS) model is developed as an analogue to a simultaneous, vertically and horizontally distributed TMD system. The proposed analytical system in this study not only accounts for vertical distribution, but also horizontal distribution. The equations formulated tends to account for variation in the properties of each slab, unlike previous studies. K. Moon (2005) presented the response for vertically and horizontally distributed TMD's, however his equations assumed a uniformity in the properties of TMD's. Also, the equations in this study are able to incorporate the effect of variation in the placement of suspended slabs. This is achieved using a parameter we would refer to as the - 'Control Parameter (C_n)', and would be discussed in detail in the sections below.

(NOTE: Although the equation in this study can account for variation in the properties of TMD's (or slabs) but in the scope of this study the properties of all slabs are assumed to be the same. This has been done to simplify the analysis and to reduce the optimization variables.)

2.4.1 System Idealization

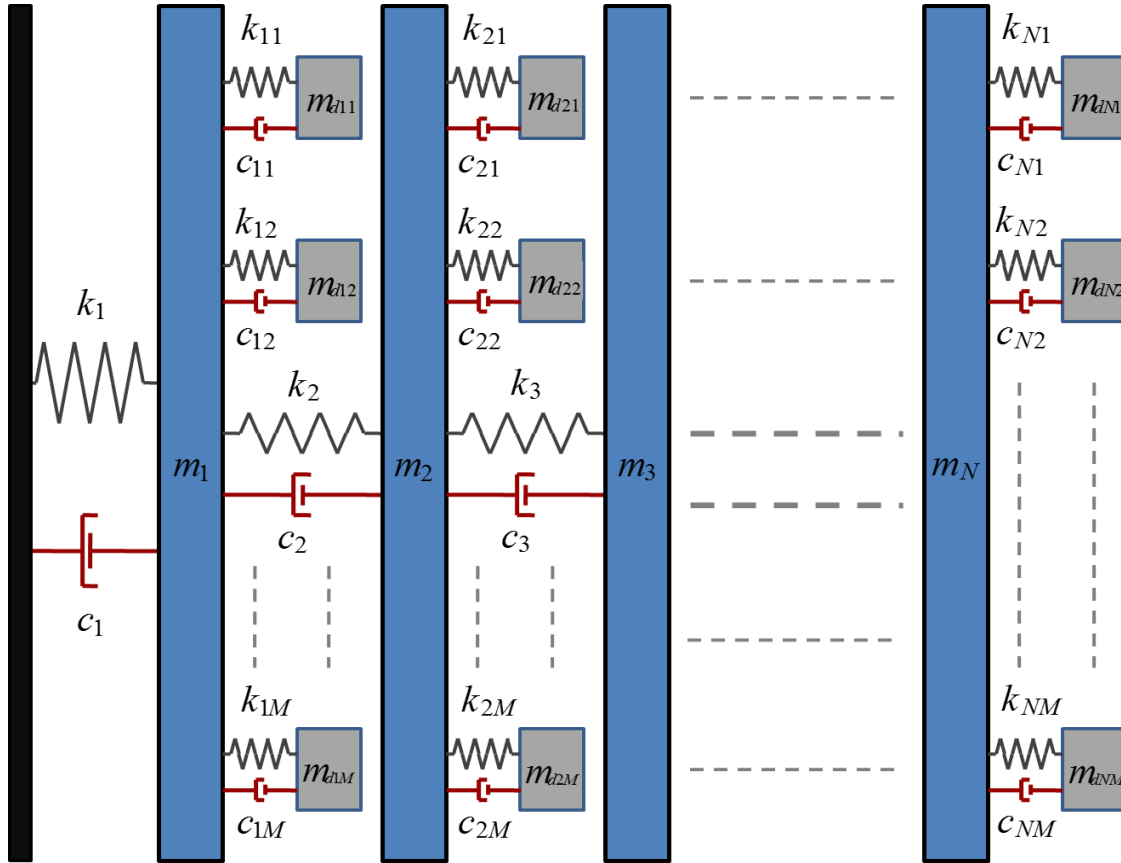


Figure 2.11 Idealization of the MSS System

2.4.2 Equations of Motion

The governing equations for the MSS system takes into account the restoring forces due to all the suspended slabs present in the system. The equation for MSS model is obtained by the same principle as the SSS model except it takes into account the contribution of each floor's suspended slabs based on a term defined as 'modal ratios (q_n)'. The modal ratio is the ratio of mode shape for a particular floor (ϕ_n) to the mode shape of the top floor (ϕ_N). To show the procedure for

development of the equations of motion, a reference system is considered initially from which the generalized equations are be obtained. A 4-story 2-bay SS system is considered as the reference system. Equations (3.30 – 3.33) are the dynamic equilibrium equations for the 4-story structure with unspecified number of suspended slabs on each floor. Since the slabs are not suspended necessarily on all floors, a Control parameter, C_n , is used to indicate the presence or absence of suspended slabs on a given floor. As shown by Equation 3.29, C_n takes only binary values, thus the SS system can be physically represented in the form shown in Figure 2.12 Physical Representation of Variable C_n .

By representing C_n in the form of a matrix it not only gives a physical outlook to C_n , but also aids in the optimization procedure. This aspect would be discussed in detail in the section ‘*Numerical Search*’ of Chapter – 4. It is worth noting that in the MSS system it is assumed that for any case there will be no slab suspended at the bottom floor ($C_1 = 0$), since it would not make sense in terms of civil engineering application. In addition, it is assumed that every MSS system will have at least SSs on the top floor ($C_N = 1$), since it has been proved by earlier researches that TMD’s are most effective when placed at top (Connor, 2003). This way we are able to reduce 2 variables for optimization.

$$C_n = \begin{cases} 0 & (\text{if Slab Suspended}) \\ 1 & (\text{if Slab not Suspended}) \end{cases} \quad (2.29)$$

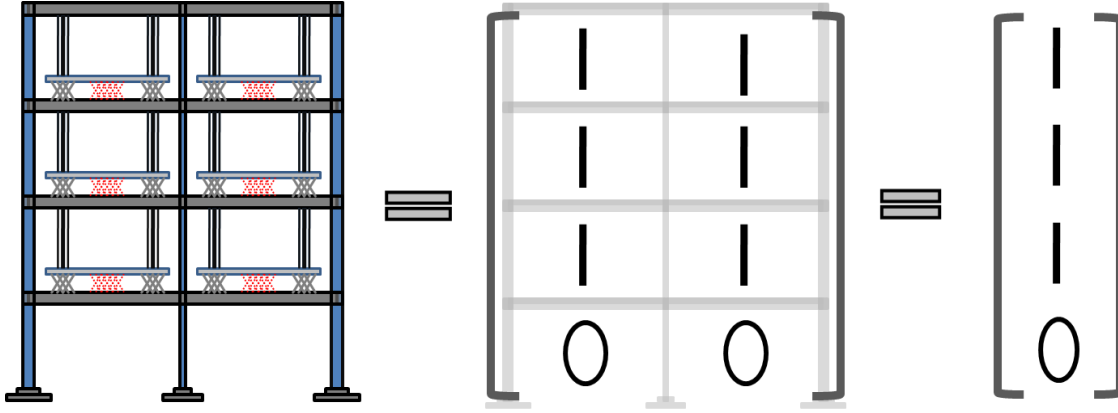


Figure 2.12 Physical Representation of Variable C_n

The equations 3.30 – 3.33 represent the equations of motion for the 4 stories. These are formulated by balancing the forces experienced by each story of the structure. The Left hand side terms in each equation represents the force generated in the steel frame due to inertia, damping and stiffness. The 1st term on the right ($-m_n a_g$) is the force generated due to ground acceleration and the other term is the pull generated by the suspended slab(s), due to its motion.

$$m_1 \ddot{u}_1 + c_1 \dot{u}_1 + k_1 u_1 - c_2 (\dot{u}_2 - \dot{u}_1) - k_2 (u_2 - u_1) = -m_1 a_g + \sum_{j=1}^2 [C_1 (c_{d1j} \dot{u}_{d1j} + k_{d1j} u_{d1j})] \quad (2.30)$$

$$m_2 \ddot{u}_2 + c_2 (\dot{u}_2 - \dot{u}_1) + k_2 (u_2 - u_1) - c_3 (\dot{u}_3 - \dot{u}_2) - k_3 (u_3 - u_2) = -m_2 a_g + \sum_{j=1}^2 [C_2 (c_{d2j} \dot{u}_{d2j} + k_{d2j} u_{d2j})] \quad (2.31)$$

$$m_3 \ddot{u}_3 + c_3 (\dot{u}_3 - \dot{u}_2) + k_3 (u_3 - u_2) - c_4 (\dot{u}_4 - \dot{u}_3) - k_4 (u_4 - u_3) = -m_3 a_g + \sum_{j=1}^2 [C_3 (c_{d3j} \dot{u}_{d3j} + k_{d3j} u_{d3j})] \quad (2.32)$$

$$m_4 \ddot{u}_4 + c_4 (\dot{u}_4 - \dot{u}_3) + k_4 (u_4 - u_3) = -m_4 a_g + \sum_{j=1}^2 [C_4 (c_{d4j} \dot{u}_{d4j} + k_{d4j} u_{d4j})] \quad (2.33)$$

Similar to the steel frame the general equations for the SSs are obtained and given by the Equations 3.34 and 3.35. The former is for the top floor SSs and the latter is for the rest of the floors, which in this case is 1st – 3rd floors.

$$m_{d4j} \ddot{u}_{d4j} + c_{d4j} \dot{u}_{d4j} + k_{d4j} u_{d4j} + m_{d4j} \ddot{u}_4 = -m_{d4j} a_g \quad (2.34)$$

$$m_{dnj} \ddot{u}_{dnj} + c_{dnj} \dot{u}_{dnj} + k_{dnj} u_{dnj} + m_{dnj} \ddot{u}_n = -m_{dnj} a_g, \text{ where } n = 1 - 3 \text{ and } j = 1 - 2 \quad (2.35)$$

The equations of motion for respective floors of the main steel frame are combined into a single equation shown in Equation (3.36) by using matrix notation. In order to solve this equation ‘Mode Summation’ method is implemented, which is based on the superposition of modes. The response of the system is considered as the sum of contribution of each mode as shown in Equation 3.37. Usually in the scope of civil engineering, engineers are concerned with just the 1st 2 modes, thus the response of the system can be shown by Equation 3.38, where ϕ_{in} are the mode shapes for i^{th} mode and n^{th} story, and v_i are the modal coordinates for i^{th} mode.

$$M_s \ddot{U}_s + C_s \dot{U}_s + K_s U_s = - \begin{bmatrix} m_1 \\ m_2 \\ m_3 \\ m_4 \end{bmatrix} a_g + \begin{bmatrix} C_1 \\ C_2 \\ C_3 \\ C_4 \end{bmatrix} \begin{bmatrix} \sum_{j=1}^2 [c_{d1} \dot{u}_{d1} + k_{d1} u_{d1}] \\ \sum_{j=1}^2 [c_{d2} \dot{u}_{d2} + k_{d2} u_{d2}] \\ \sum_{j=1}^2 [c_{d3} \dot{u}_{d3} + k_{d3} u_{d3}] \\ \sum_{j=1}^2 [c_{d4} \dot{u}_{d4} + k_{d4} u_{d4}] \end{bmatrix} \quad (2.36)$$

$$U_s = [P][v], \quad \text{where } [P] = \begin{bmatrix} \left[\begin{matrix} \phi_{11} \\ \phi_{12} \\ \phi_{13} \\ \phi_{14} \end{matrix} \right] & \left[\begin{matrix} \phi_{21} \\ \phi_{22} \\ \phi_{23} \\ \phi_{24} \end{matrix} \right] \end{bmatrix} \quad (2.37)$$

$$U_s = \phi_{1n} v_1 + \phi_{2n} v_2 \quad (2.38)$$

Equation 3.37 is substituted in 3.36 to get Equation 3.39 which is converted into modal coordinates by multiplying with $[P]^T$ and using assumptions from Equations 3.41. m_i , k_i and c_i are known as

the modal mass, stiffness and damping of the structure for i^{th} mode. Equation (3.39) is broken down 2 separate modal equations (Equations 3.42 and 3.43).

$$\left[M_s \right] \left[P \right] \left[\ddot{v} \right] + \left[C_s \right] \left[P \right] \left[\dot{v} \right] + \left[K_s \right] \left[P \right] \left[v \right] = - \begin{bmatrix} m_1 \\ m_2 \\ m_3 \\ m_4 \end{bmatrix} a_g + \begin{bmatrix} C_1 \\ C_2 \\ C_3 \\ C_4 \end{bmatrix} \begin{bmatrix} \sum_{j=1}^2 [c_{d1j} \dot{u}_{d1j} + k_{d1j} u_{d1j}] \\ \sum_{j=1}^2 [c_{d2j} \dot{u}_{d2j} + k_{d2j} u_{d2j}] \\ \sum_{j=1}^2 [c_{d3j} \dot{u}_{d3j} + k_{d3j} u_{d3j}] \\ \sum_{j=1}^2 [c_{d4j} \dot{u}_{d4j} + k_{d4j} u_{d4j}] \end{bmatrix} \quad (2.39)$$

$$\left[P \right]^T \left[M_s \right] \left[P \right] \left[\ddot{v} \right] + \left[P \right]^T \left[C_s \right] \left[P \right] \left[\dot{v} \right] + \left[P \right]^T \left[K_s \right] \left[P \right] \left[v \right] = \left[P \right]^T \left(- \begin{bmatrix} m_1 \\ m_2 \\ m_3 \\ m_4 \end{bmatrix} a_g + \begin{bmatrix} C_1 \\ C_2 \\ C_3 \\ C_4 \end{bmatrix} \begin{bmatrix} \sum_{j=1}^2 [c_{d1j} \dot{u}_{d1j} + k_{d1j} u_{d1j}] \\ \sum_{j=1}^2 [c_{d2j} \dot{u}_{d2j} + k_{d2j} u_{d2j}] \\ \sum_{j=1}^2 [c_{d3j} \dot{u}_{d3j} + k_{d3j} u_{d3j}] \\ \sum_{j=1}^2 [c_{d4j} \dot{u}_{d4j} + k_{d4j} u_{d4j}] \end{bmatrix} \right) \quad (2.40)$$

$$\tilde{m}_i = \phi_i^T M_s \phi_i, \quad \tilde{k}_i = \phi_i^T K_s \phi_i, \quad \tilde{c}_i = \phi_i^T C_s \phi_i \quad (2.41)$$

$$\tilde{m}_1 \ddot{v}_1 + \tilde{c}_1 \dot{v}_1 + \tilde{k}_1 v_1 = -a_g \sum_{j=1}^4 m_j \phi_{1j} + C_4 \phi_{14} \sum_{j=1}^2 [k_{d4j} u_{d4j} + c_{d4j} \dot{u}_{d4j}] + \sum_{n=1}^3 \left[C_n \phi_{1n} \left[\sum_{j=1}^2 (k_{dnj} u_{dnj} + c_{dnj} \dot{u}_{dnj}) \right] \right] \quad (2.42)$$

$$\tilde{m}_2 \ddot{v}_2 + \tilde{c}_2 \dot{v}_2 + \tilde{k}_2 v_2 = -a_g \sum_{j=1}^4 m_j \phi_{2j} + C_4 \phi_{24} \sum_{j=1}^2 [k_{d4j} u_{d4j} + c_{d4j} \dot{u}_{d4j}] + \sum_{n=1}^3 \left[C_n \phi_{2n} \left[\sum_{j=1}^2 (k_{dnj} u_{dnj} + c_{dnj} \dot{u}_{dnj}) \right] \right] \quad (2.43)$$

The response for mode 1 is generally considered to be the governing case for TMD systems, thus for the purpose of analysis we would consider only its contribution (Equation 3.44). The modal equation for 1st mode is converted back into real coordinates by using Equation 3.44. Equation 3.45 is divided by the mode shape of the top floor to obtain the equation of motion, which is given

by Equation (3.46). m_E , k_E and c_E are known as the effective mass, stiffness and damping of the steel frame.

$$\mathbf{u}_n \approx \boldsymbol{\phi}_{1n} v_1 \quad v_1 \approx \frac{u_4}{\phi_{14}} \quad (2.44)$$

$$\left(\frac{\tilde{m}_1}{\phi_{14}^2} \right) \ddot{u}_4 + \left(\frac{\tilde{c}_1}{\phi_{14}^2} \right) \dot{u}_4 + \left(\frac{\tilde{k}_1}{\phi_{14}^2} \right) u_4 = -a_g \left(\frac{\sum_{j=1}^4 m_j \phi_{1j}}{\phi_{14}} \right) + C_4 \sum_{j=1}^2 [k_{d4j} u_{d4j} + c_{d4j} \dot{u}_{d4j}] + \sum_{n=1}^3 \left[C_n \frac{\phi_{1n}}{\phi_{14}} \left[\sum_{j=1}^2 (k_{dnj} u_{dnj} + c_{dnj} \dot{u}_{dnj}) \right] \right] \quad (2.45)$$

$$\tilde{m}_E \ddot{u}_4 + \tilde{c}_E \dot{u}_4 + \tilde{k}_E u_4 = -a_g \Gamma_e + C_4 \sum_{j=1}^2 [k_{d4j} u_{d4j} + c_{d4j} \dot{u}_{d4j}] + \sum_{n=1}^3 \left[C_n \frac{\phi_{1n}}{\phi_{14}} \left[\sum_{j=1}^2 (k_{dnj} u_{dnj} + c_{dnj} \dot{u}_{dnj}) \right] \right] \quad (2.46)$$

2.4.3 Response Equations

In the previous section the equations of motion have been derived for a 4-story 2-bay frame, however a general set of equations is needed. The procedure to derive the response equations is almost the same as for the SSS model. The response equations for MSS system's performance are derived from the system's equation of motion (Equation 3.46). Since the earthquake is considered as a harmonic excitation, the required responses are also assumed to be harmonic. These are substituted in the primary equations of motion, which are then solved for the response amplitudes of different components of the MSS system. The reference system is solved first and the derivation has been shown in APPENDIX A. The response equations obtained from the reference system are used to infer the generalized response equations for the MSS model.

Only the steady state solution is considered for the analysis of this model. From Equation 3.51, the response of other floors is related to the top floor, and therefore the response of others floors can also be obtained. The response relations for suspended slabs on floors other than the top have not been derived as they would be less than the top floor's slabs. In addition, since the parameters (β , ξ and μ) of all suspended slabs are considered the same, so the response of all suspended slabs on top floor would be given by the same set of equations. The response amplitudes for respective components of the MSS system have been shown below, where Equation (3.52) and (3.53) show the main frame's top floor displacement and acceleration. Equation (3.64) and (3.65) show the top floor's MSS displacement and acceleration. Table 2-5 shows the definition for the variables used to represent the response equations.

Table 2-5 List of response parameters for MSS model

Variable	Definition
u_N	Harmonic response of steel frame top floor
u_n	Harmonic response of steel frame n^{th} floor
u_{dnj}	Harmonic response of j^{th} suspended slab of top floor
H_N	Displacement amplitude of steel frame top floor
H_{dnj}	Displacement amplitude of j^{th} suspended slab on top floor
A_N	Acceleration amplitude of steel frame top floor
A_{dnj}	Acceleration amplitude j^{th} suspended slab on top floor
q_n	Mode shape ratio for n^{th} floor

$$u_N = H_4 e^{-i\alpha x} \quad (2.47)$$

$$u_{dNj} = H_{dNj} e^{-i\alpha x} \quad (2.48)$$

$$\ddot{u}_N + a_g = A_N e^{-i\alpha x} \quad (2.49)$$

$$\ddot{u}_{dNj} + a_g = A_{dNj} e^{-i\alpha x} \quad (2.50)$$

$$u_n = q_n u_N \quad (2.51)$$

$$|H_N| = \frac{\sqrt{(NUM_{RN})^2 + (NUM_{IN})^2}}{\sqrt{(DEN_{RN})^2 + (DEN_{IN})^2}} \quad (2.52)$$

$$|A_N| = \frac{\sqrt{(DEN_{RN} + \alpha^2 NUM_{RN})^2 + (DEN_{IN} + \alpha^2 NUM_{IN})^2}}{\sqrt{(DEN_{RN})^2 + (DEN_{IN})^2}} \quad (2.53)$$

where,

$$NUM_{RN} = \left[\Gamma_e + \sum_{n=1}^{N-1} \left[C_n q_n \sum_{j=1}^M \left[(\text{Re}_{Hdnj}) \mu_{dnj} \right] \right] + C_N \sum_{j=1}^M \left[(\text{Re}_{HdNj}) \mu_{dNj} \right] \right] \quad (2.54)$$

$$NUM_{IN} = \left[\sum_{n=1}^{N-1} \left[C_n q_n \sum_{j=1}^M \left[(\text{Im}_{Hdnj}) \mu_{dnj} \right] \right] + C_N \sum_{j=1}^M \left[(\text{Im}_{HdNj}) \mu_{dNj} \right] \right] \quad (2.55)$$

$$DEN_{RN} = \left[(\text{Re}_{Hs}) - \sum_{n=1}^{N-1} \left[C_n q_n^2 \sum_{j=1}^M \left[(\text{Re}_{Hdnj}) \mu_{dnj} \alpha^2 \right] \right] - C_N \sum_{j=1}^M \left[(\text{Re}_{HdNj}) \mu_{dNj} \alpha^2 \right] \right] \quad (2.56)$$

$$DEN_{IN} = \left[(\text{Im}_{Hs}) - \sum_{n=1}^{N-1} \left[C_n q_n^2 \sum_{j=1}^M \left[(\text{Im}_{Hdnj}) \mu_{dnj} \alpha^2 \right] \right] - C_N \sum_{j=1}^M \left[(\text{Im}_{HdNj}) \mu_{dNj} \alpha^2 \right] \right] \quad (2.57)$$

And

$$\operatorname{Re}_{H_s} = -2\xi_s \alpha^2 \quad (2.58)$$

$$\operatorname{Re}_{H_s} = 1 - \alpha^2 \quad (2.59)$$

$$\operatorname{Re}_{H_{dnj}} = \frac{\beta_{dnj}^2 (\beta_{dnj}^2 - \alpha^2) + 4 (\xi_{dnj} \beta_{dnj} \alpha)^2}{(\beta_{dnj}^2 - \alpha^2)^2 + 4 (\xi_{dnj} \beta_{dnj} \alpha)^2} \quad (2.60)$$

$$\operatorname{Re}_{H_{d4j}} = \frac{\beta_{d4j}^2 (\beta_{d4j}^2 - \alpha^2) + 4 (\xi_{d4j} \beta_{d4j} \alpha)^2}{(\beta_{d4j}^2 - \alpha^2)^2 + 4 (\xi_{d4j} \beta_{d4j} \alpha)^2} \quad (2.61)$$

$$\operatorname{Im}_{H_{dnj}} = \frac{2 \xi_{dnj} \beta_{dnj} \alpha^3}{(\beta_{dnj}^2 - \alpha^2)^2 + 4 (\xi_{dnj} \beta_{dnj} \alpha)^2} \quad (2.62)$$

$$\operatorname{Im}_{H_{d4j}} = \frac{2 \xi_{d4j} \beta_{d4j} \alpha^3}{(\beta_{d4j}^2 - \alpha^2)^2 + 4 (\xi_{d4j} \beta_{d4j} \alpha)^2} \quad (2.63)$$

$$|H_{dNj}| = \left(\frac{NUM_{RdNj} + i NUM_{IdNj}}{DEN_{RdNj} + i DEN_{IdNj}} \right) \quad (2.64)$$

$$|A_{dNj}| = \frac{\sqrt{(DEN_{RdNj} + \alpha^2 NUM_{RdNj})^2 + (DEN_{IdNj} + \alpha^2 NUM_{IdNj})^2}}{\sqrt{(DEN_{RdNj})^2 + (DEN_{IdNj})^2}}, \text{ where} \quad (2.65)$$

$$NUM_{RdNj} = \alpha^2 NUM_{RN} - DEN_{RN} \quad (2.66)$$

$$NUM_{IdNj} = \alpha^2 NUM_{IN} - DEN_{IN} \quad (2.67)$$

$$DEN_{RdNj} = Re_{HS} DEN_{IN} + Im_{HS} DEN_{RN} \quad (2.68)$$

$$DEN_{RdNj} = DEN_{RN} Re_{HS} - DEN_{IN} Im_{HS} \quad (2.69)$$

The parameters NUM_{IN} , DEN_{IN} , NUM_{RN} , DEN_{RN} , Re_{HS} , Im_{HS} are the same ones derived for the response of the steel frame.

2.4.4 System Behavior

While analyzing the SSS model the response functions were plotted against different variables to develop an idea of the behavior of the system. The performance functions derived in the previous sections are plotted against different parameters in this section. Figure 2.13 shows a plot of how the steel frame's roof displacement transfer function varies with mass ratio for different number of slabs suspended, while the structure is under resonance condition ($\alpha = 1$) and the TMD parameters correspond to 'Tuned parameters'. The performance of the system is seen to improve with increase in the mass ratio and this can be attributed to the same logic as the SSS model. However, now variation with number of suspended slabs is also considered. As expected with increase in the number of slabs suspended there is increase in performance as well, which can be explained in terms of increase in the mass ratio. As more slabs are suspended the mass of the main frame tends to reduce, as a result the mass ratio increases and thereby the performance.

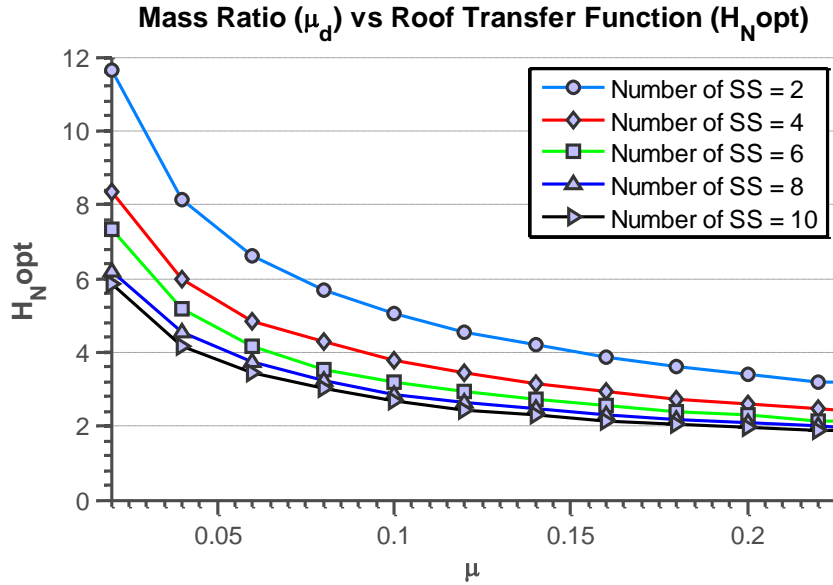


Figure 2.13 Effect of Mass Ratio on Response Displacement Amplitude

Further plots of other TMD parameters against the mass ratio showed that as the mass ratio increased the optimum tuned frequency ratio (β_d) decreased (Figure 2.14) and the optimum damping ratio increased (Figure 2.15). A similar trend for both the parameters is seen with an increase in the number of suspended slabs as well (Figure 2.16).

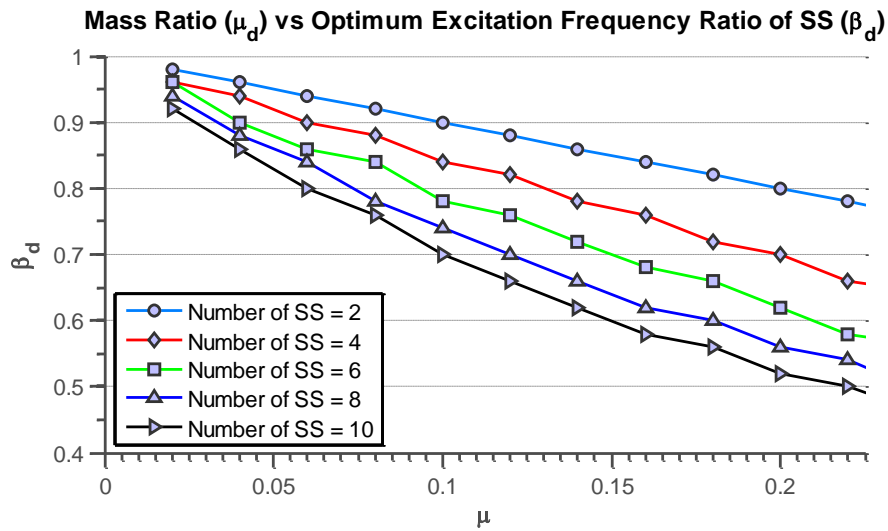


Figure 2.14 Variation in Optimum Frequency Ratio with Mass Ratio

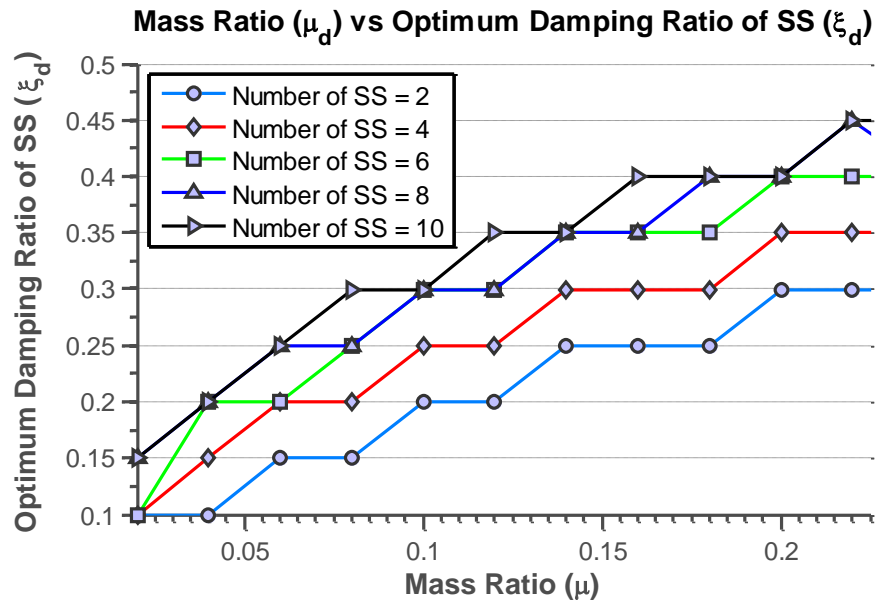


Figure 2.15 Variation in Optimum Damping Ratio with Mass Ratio

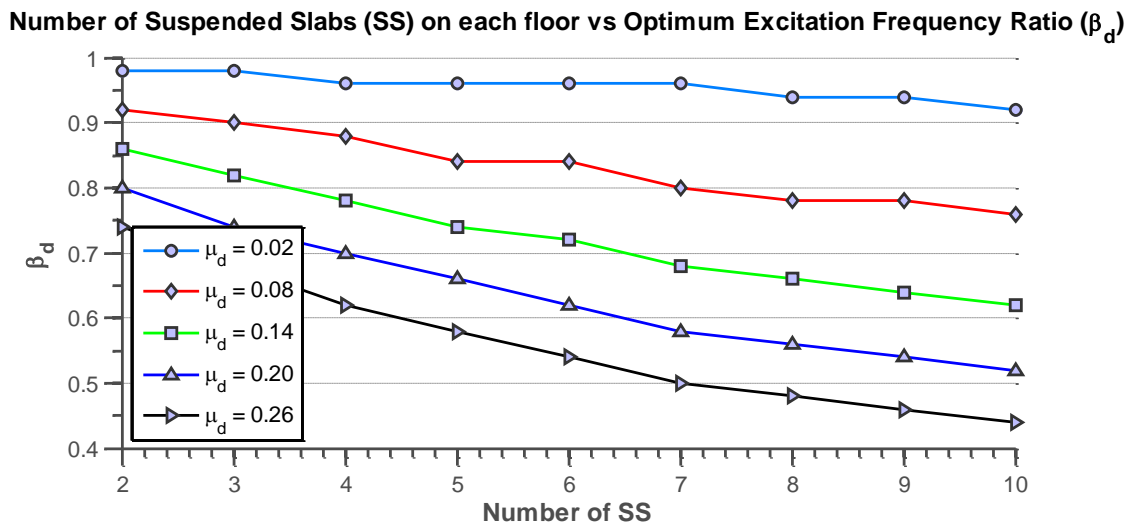


Figure 2.16 Variation of Optimum Frequency Ratio with Number of SS

2.4.5 Benchmark Example

The reference structure considered for this example is a 4 story 2 bay structure and its structural properties are given by Table 2-6. The location of the SSs are not predefined since the location parameter (C_n) is also considered as a variable. The analysis steps followed are to first Input the known frame and suspended slab parameters. Then a suitable Optimization methodology is used to obtain the location and the parameters of the suspended slabs. Unlike SSS model, now the location of suspended slabs is unknown, so the Optimization method adopted also finds the Optimum location i.e. C_n values. Two different optimization strategies were adopted, which are discussed in detail in ‘CHAPTER – 4’. Once the tuning parameters are obtained they are used to get the response amplitudes for the steel frame and the SSs.

Table 2-6 Structural Properties of 4 Story 2 Bay Frame

Floor No.	Mass (slugs)	Stiffness (kips/inch)
1	0.618	75.3
2	0.608	75.3
3	0.608	75.3
4	0.547	75.3

2.4.5.1 Suspended Slab Frame

Table 2-7 Transfer Function Values and SS system parameters for Optimization w.r.t. Steel Frame Top Floor

Displacement Amplitude

Steel Frame Top Floor Displacement Amplitude Optimization								
M	μ_d	ξ_d	β_d	$ H_N $	$ A_N $	$ H_{dNj} $	$ A_{dNj} $	C_n
1	0.2393	0.10	0.82	6.9998	8.2723	25.2145	17.4840	[0 0 1 1]
1	0.3121	0.20	0.74	4.6792	5.1803	13.0041	8.4388	[0 1 1 1]
1	0.3121	0.30	0.695	4.2849	4.2793	9.0052	6.1663	[0 1 1 1]
2	0.2393	0.10	0.60	7.8057	9.0579	29.7768	13.4079	[0 0 1 1]
2	0.2393	0.20	0.60	4.7710	5.1797	14.7943	7.5858	[0 0 1 1]
2	0.2393	0.30	0.5975	3.9126	3.8711	9.9610	5.4175	[0 0 1 1]
2	0.2393	0.40	0.61	3.7604	3.5134	7.4938	4.0117	[0 0 1 1]

Table 2-8 Transfer Function Values and SS system parameters for Optimization w.r.t. Steel Frame Top Floor

Acceleration Amplitude

Steel Frame Top Floor Acceleration Amplitude Optimization								
M	μ_d	ξ_d	β_d	$ H_N $	$ A_N $	$ H_{dNj} $	$ A_{dNj} $	C_n
1	0.3121	0.10	0.83	9.9565	5.8196	26.5475	13.6787	[0 1 1 1]
1	0.3121	0.20	0.82	6.0196	3.7884	13.6598	7.1411	[0 1 1 1]
1	0.3121	0.30	0.81	5.1171	3.6196	9.5446	5.3505	[0 1 1 1]
2	0.3121	0.10	0.6225	16.2830	4.6883	36.6992	8.3440	[0 1 1 1]
2	0.3121	0.20	0.5975	8.7245	2.7615	18.0701	4.0219	[0 1 1 1]
2	0.3121	0.30	0.59	6.4336	2.2547	11.9632	3.0887	[0 1 1 1]
2	0.3121	0.40	0.57	5.3490	2.2157	9.0587	2.5913	[0 1 1 1]

Table 2-9 Transfer Function Values and SS system parameters for Optimization w.r.t. Top Floor SS

Displacement Amplitude

Top Floor Suspended Slab Displacement Amplitude Optimization								
M	μ_d	ξ_d	β_d	$ H_N $	$ A_N $	$ H_{dNj} $	$ A_{dNj} $	C_n
1	0.3121	0.10	0.75	9.6970	11.0699	23.7966	20.5774	[0 0 1 1]
1	0.3121	0.20	0.74	6.9620	7.5360	12.3748	12.6778	[0 0 1 1]
1	0.3121	0.30	0.67	5.3799	5.5079	8.6633	7.4650	[0 1 1 1]
2	0.3121	0.10	0.86	17.1154	8.1951	26.2015	12.0281	[0 0 1 1]
2	0.3121	0.20	0.68	5.6979	6.2339	13.0367	9.4323	[0 1 0 1]
2	0.3121	0.30	0.66	5.3468	5.4825	8.7847	7.4065	[0 1 0 1]
2	0.3121	0.40	0.65	5.5749	5.3362	7.3417	6.3423	[0 1 0 1]

Table 2-10 Transfer Function Values and SS system parameters for Optimization w.r.t. Top Floor SS

Acceleration Amplitude

Top Floor Suspended Slab Acceleration Amplitude Optimization								
M	μ_d	ξ_d	β_d	$ H_N $	$ A_N $	$ H_{dNj} $	$ A_{dNj} $	C_n
1	0.3121	0.10	0.79	8.5469	6.8828	25.6921	12.9829	[0 1 1 1]
1	0.3121	0.20	0.81	5.8197	3.9435	13.4524	6.9814	[0 1 1 1]
1	0.3121	0.30	0.82	5.2964	3.7331	9.6493	5.2812	[0 1 1 1]
2	0.3121	0.10	0.53	12.6702	6.8183	39.2665	8.6576	[0 1 1 1]
2	0.3121	0.20	0.56	7.7655	3.4320	18.4777	4.4572	[0 1 1 1]
2	0.3121	0.30	0.585	6.3582	2.3617	11.9558	3.0347	[0 1 1 1]
2	0.3121	0.40	0.60	5.7786	2.4064	8.9546	2.4534	[0 1 1 1]

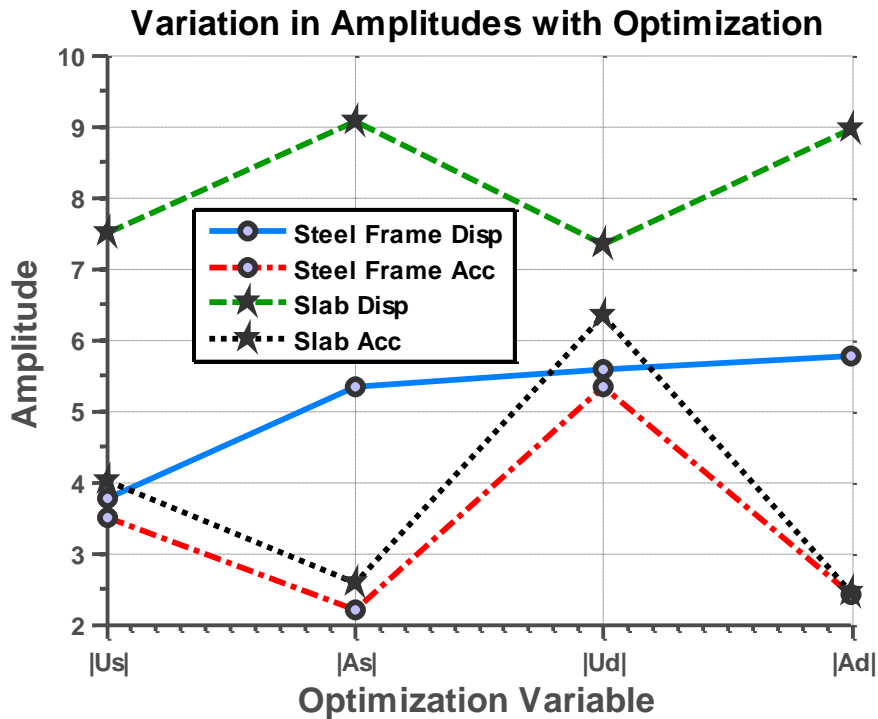


Figure 2.17 Optimized Amplitudes for different type of Optimizations for MSS model

CHAPTER 3

OPTIMIZATION APPROACH

3.1 Introduction

In the previous chapter the response relations are found for a single suspended slab and a multi suspended slabs model. These relations are seen to be a function of some variables, which governed the response of the system. In order to get the best response, these variables need to be optimized, which is refer to as the ‘Tuned Condition’. As a start the optimization approach adopted for the SSS model is first investigated.

The performance of the SSS system is found to be a function of α, μ_d, β_d and ξ_d . An approach known popularly as the Mini – Max approach is used to optimize the response transfer functions to obtain the parameters of the SS system. The Mini - Max approach states that the optimum response should be the minimum value amongst the maximum response obtained for a range of α . Basically, first the transfer function is calculated for different values of α and the maximum value is chosen so that we are considering the worst case possible. In civil or any other engineering, the approach adopted is always the conservative one in order to increase the reliability of the system. This is repeated for different values of β_d, ξ_d and a list of maximum transfer function values are noted. Amongst these maximum values the minimum value is considered to be the most optimum one. The mini – max approach is incorporated for the SS system in the optimization procedures that are discussed further down in this chapter.

As previously discussed, in the case of the MSS model a new variable, called the control parameter (C_n) is added . It affects the complete configuration of the system and thereby affects the values of α and μ_d . For the MSS model the approach adopted for SSS model is extended to incorporate the new variable. Now the variables are inter – dependent so a 2 level optimization is implemented (i.e. an optimization within another one). The outer optimization sends the input to the inner one, which calculates the response and sends it back to the outer one, which finally optimizes based on Mini – Max approach to get the final optimized results. The inner optimization takes care of the variables β_d and ξ_d , whereas the outer optimization takes care of the control parameter (C_n) for each floor.

In this chapter, two algorithms that are used for optimization are discussed. The first is the ‘Numerical Search (NS) Pattern’, and the second is a combination of two independent approaches - Nelder-Mead and the Covariance Matrix Adaptation Scheme Strategy (CMA-ES). The second approach is developed as an alternative to the NS for instances with large number of variables.

3.2 Numerical Search (NS) Pattern Algorithm

3.2.1 Introduction

Numerical Search (NS) is a basic optimization algorithm used extensively in every field of optimization. It belongs to a family of optimization which does not require the optimization of the variables’ gradient and is thus easy to implement. The basic principle of NS is that each variable is varied at a time in order of a particular magnitude and all the cases are compared to get the optimum solution. Although an easy to implement method, however it has its limitations. Since it

linearly scans through the entire domain it is required that the domain should be finite and not too expansive in nature, as the latter effects the cost of computation. Thus, numerical search cannot be applied to complex problems; however it can be used as a preliminary tool to provide a general sense for the values of the optimized parameters.

3.2.1.1 Implementation

For the SSS model, as discussed earlier, the NS approach is applied in a very simple manner. The variables α , β_d and ξ_d are varied in a finite domain to get a set of response values, from which the optimized value was chosen using the Mini – Max approach. A MATLAB code was written to implement this method.

For the MSS model a new variable is added, the position of the suspended slabs (C_n). Similar to the SSS model the code considers a range for the parameters β_d and ξ_d as the search space however to account for C_n some modification has to be made. The Control Parameter ' C_n ' takes only binary values – 0 or 1 so to implement the NS approach on C_n , a function is used to generate matrices of all possible combinations of 0s and 1s. The function takes in the number of floors of the structure and the number of slabs to be suspended, and in turn generates a matrix with dimensions [N x Pm]. N is the number of floors of the SS system and Pm is the number of permutations possible. Equation (4.1) shows an example of the function for a 3 story SS system, where number of floors (N) = 3 and the number of slabs to be suspended (M) = 1. A loop is used to vary the variable M, as a result all possible permutations and combinations of the variable C_n

are obtained. Equations (4.1 – 4.3) show all possible combinations and permutations of C_n generated for 3 story SS system.

The rows of these matrices are considered one at a time as an input for variable C_n and based on it, the code evaluates other properties of the frame such as natural frequency, mode shapes, etc. Once initial conditions for the SS system are obtained the code moves onto the second level of numerical search, which optimizes the variables β_d and ξ_d . The second level optimization is performed in the same manner as for the SSS model. It optimizes the system for every possible combination of C_n and stores the values. The code finally selects the best case based on the response calculated and the parameters corresponding to it are the optimized parameters. Figure 3.1 shows the response plot of SS system with variation in β_d and ξ_d , and also the optimal solution.

$$N = 3 \quad \text{and} \quad M = 1 \quad \xrightarrow{\text{yields}} \begin{bmatrix} 1 & 0 & 0 \\ 0 & 1 & 0 \\ 0 & 0 & 1 \end{bmatrix} \quad (3.1)$$

$$N = 3 \quad \text{and} \quad M = 2 \quad \xrightarrow{\text{yields}} \begin{bmatrix} 1 & 1 & 0 \\ 0 & 1 & 1 \\ 1 & 0 & 1 \end{bmatrix} \quad (3.2)$$

$$N = 3 \quad \text{and} \quad M = 3 \quad \xrightarrow{\text{yields}} [1 \quad 1 \quad 1] \quad (3.3)$$

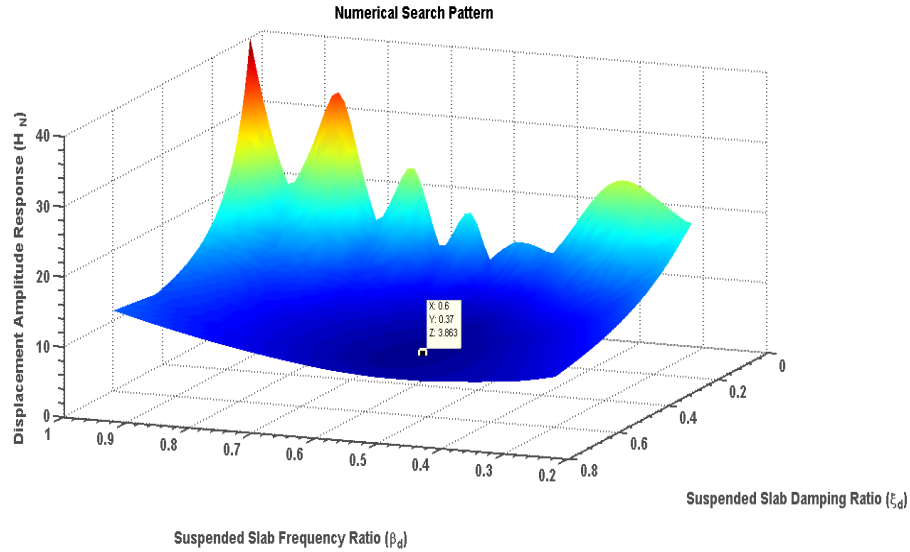


Figure 3.1 Surface plot of Numerical Search Pattern

3.3 Combinatorial Algorithm

In the previous section, the implementation of numerical search pattern to optimize the MSS model is discussed. It is seen that the numerical search pattern is quite effective, however it has its limits. As the number of stories increase, the time cost of the code increases rapidly to a point where the numerical search becomes infeasible to implement. In light of high computation cost a new optimization algorithm is implemented, which utilizes a combination of 2 algorithms – Nelder Mead and Covariance Matrix Adaptation Scheme Strategy (CMA-ES). The former is used for the inner optimization (i.e. to find the optimal β_d and ξ_d values) and the latter is used for outer optimization, which deals with optimizing the location of the Suspended Slabs (C_n). Evolutionary algorithms such as Genetic algorithm and Bee – Swarm optimization have also been successfully implemented to find the optimum variables of TMD (Farshidianfar & Soheili, 2011; D. Hartog, Although, & Namara, 1998; Mohebbi, Shakeri, Ghanbarpour, & Majzoub, 2012).

3.3.1 Nelder Mead Algorithm

3.3.1.1 Introduction

The Nelder – Mead Algorithm, also known as the Amoeba Method, was developed by John Nelder and Roger Mead (Nelder & Mead, 1965). This optimization algorithm is a type of ‘Simplex Method’ for finding the local minima of a function for several variables. A ‘Simplex’ is referred to a polytope of N+1 side for N dimensions, for example: Simplex for 2-Dimensions is a triangle and for 3-Dimensions a tetrahedron. A polytope is geometric shape with flat sides for a given number of dimensions. Examples of polytope are – polygon is a polytope in 2 dimensions and polyhedron a polytope in 3 dimensions. The Nelder Mead method was chosen as it is quite efficient for problems which are convex in nature. From Figure 3.1, it can be seen that the response of the SS system is convex with respect to β_d and ξ_d .

The algorithm is a pattern search method that compares function value at the vertices of the polytope and ranks them in order of their performance. Once the worst vertex is identified it is then modified to a better value, thereby generating a new polytope. The process is repeated to form a number of polytopes till the three vertices tend to converge to a single point or get within a tolerance limit. The final convergence point is considered as the optimal solution. The procedure is discussed in the next section in detail.

3.3.1.2 Procedure

The case considered for this thesis is a 2 dimensional problem so a triangle is used as a simplex. The evaluation function used are the response parameters of the SS system - $|H_N|$, $|A_N|$, $|H_{dNj}|$ and $|A_{dNj}|$. The algorithm starts with an initial guess to form the three vertices of the triangle. The worst vertex is then modified by a series of steps as discussed below.

Initial Assumption

The procedure starts with an initial assumption for the three vertices of the triangle. The choice of these vertices is supposedly random however the aim is to minimize the time cost, so some thought has to be given while choosing the initial vertices. 3 cases are considered to see the effects of initial assumption on the processing time for a 10 story 2 bay SS system. The first case considered is when one of the vertices is actually the optimum solution. Second, when the optimal solution is outside the initial triangle and finally, when the solution lies inside the initial triangle. Figure 3.2 - Figure 3.4 shows the respective convergence pattern for each case along with the time taken for convergence. The best case is seen when the solution lies on the triangle, followed by when it is on the outside. Since the 1st case is quite unlikely, a triangle away from the optimal solution should be considered. Based on experience, it can be said that the optimal parameters for the SS system would most likely lie in the range of 0.50 – 0.90 for β_d , and 0.10 – 0.50 for ξ_d . Considering this domain, the initial assumption is considered as (0.50, 0.10), (0.50, 0.50) and (0.50, 0.80). Figure 3.5 shows the time convergence for this assumption which is seen to be quite cost effective as expected.

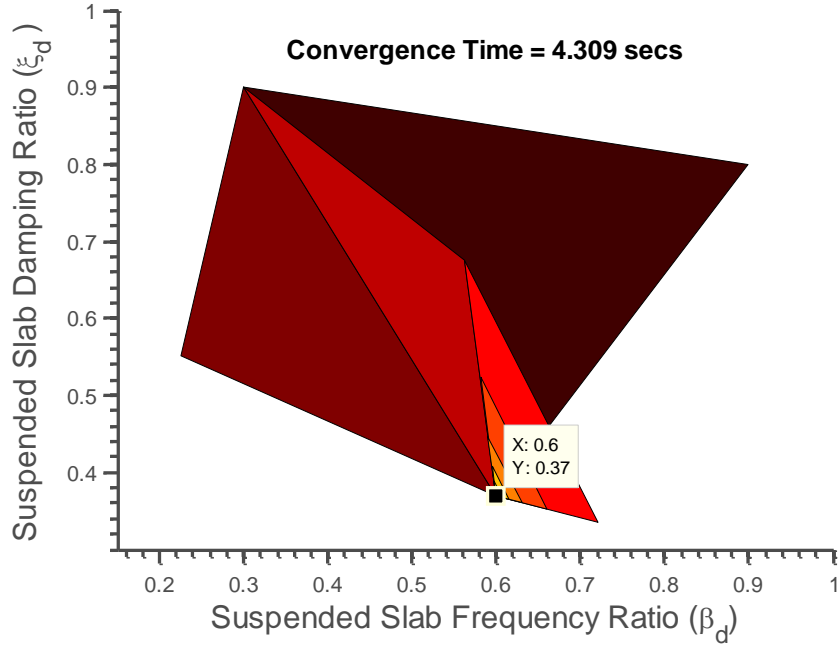


Figure 3.2 Coverage Pattern of N – M Algorithm for Solution on Initial Assumption (on vertex)

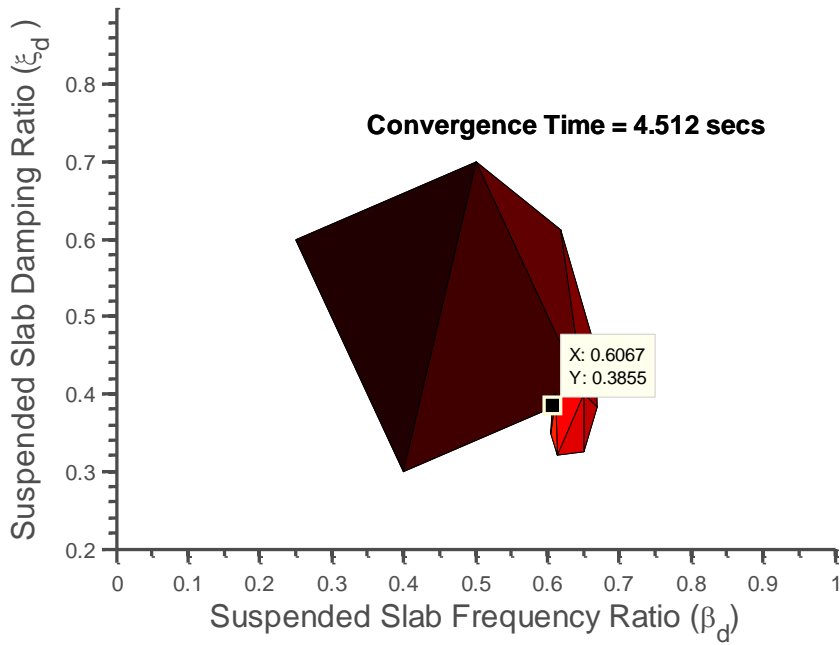


Figure 3.3 Coverage Pattern of N – M Algorithm for Solution outside Initial Assumption (outside)

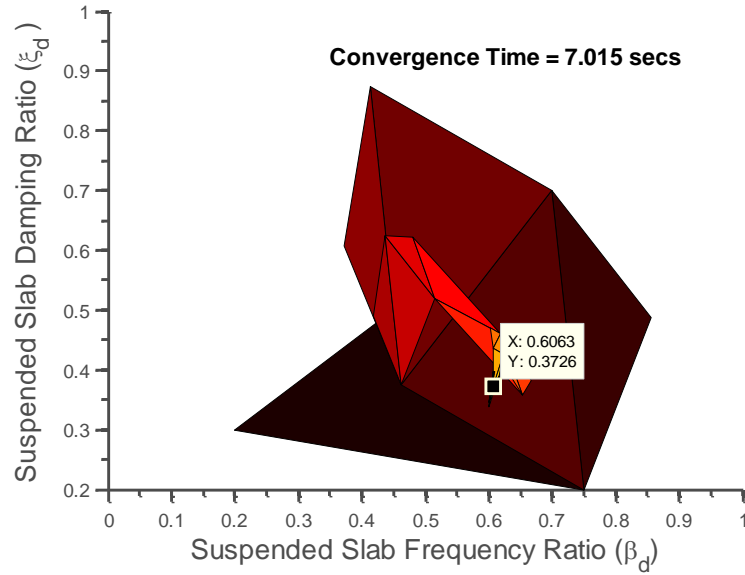


Figure 3.4 Coverage Pattern of N – M Algorithm for Solution inside Initial Assumption (inside)

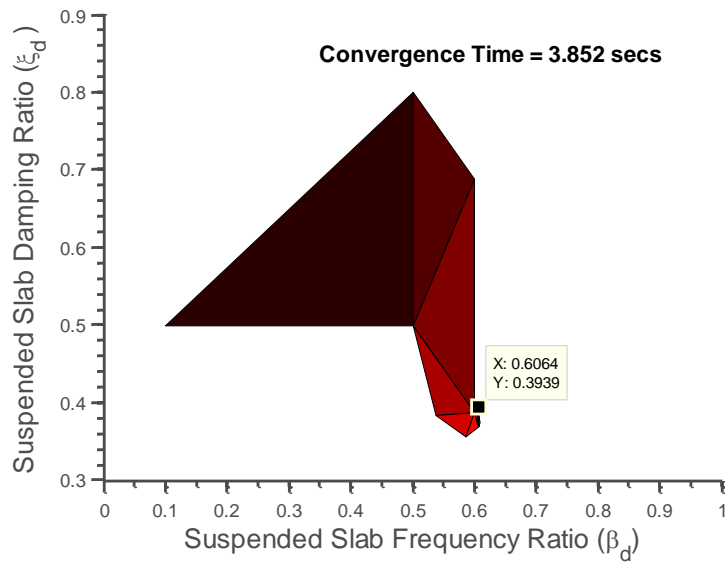


Figure 3.5 Coverage Pattern of N – M Algorithm for an Optimal Initial Assumption chosen

The three vertices assumed are substituted in the evaluation function to obtain their respective fitness values. Based on their fitness the vertices are arranged in increasing order and assigned to suitable variable. Point ‘B’ refers to the Best point, ‘G’ refers to the 2nd best (i.e., Good), and ‘W’

refer to the Worst point. The respective variables are assigned according to the assumption given by Equation 4.4.

$$F(\beta_{d1}, \xi_{d1}) < F(\beta_{d2}, \xi_{d2}) < F(\beta_{d3}, \xi_{d3}) \quad (3.4)$$

$$\mathbf{B} = (\beta_{d1}, \xi_{d1}) \quad \mathbf{G} = (\beta_{d2}, \xi_{d2}) \quad \mathbf{W} = (\beta_{d3}, \xi_{d3}) \quad (3.5)$$

Midpoint (M)

The Midpoint of the line joining B and G is considered quite important as it plays a key role in the steps ahead. The term given to this point is ‘M’ and it is simply the mid-point of the best and the 2nd best vertex (Equation 4.6).

$$\mathbf{M} = \frac{(\mathbf{B} + \mathbf{G})}{2} \quad (3.6)$$

Reflection (R)

Considering the triangle formed by the three vertices above, it is clear that the fitness value would increase as we go from B to W or G to W. Therefore there is a possibility that the fitness value may be better further away from point W (i.e. exactly opposite of the line BG) as shown in Figure 3.6. A new point ‘R’, which is the mirror opposite of point W about BG, is chosen and its fitness value is calculated and this step is known as Reflection. This reflection is taken by using equation (4.7).

$$\mathbf{R} = \mathbf{M} + \alpha_R(\mathbf{M} - \mathbf{W}) \quad (3.7)$$

Where, α_R is a constant whose conventional value is taken to be as 1, and for the purpose of this study, the value is kept the same. Equation (4.7) therefore reduces to Equation (4.8).

$$R = 2M - W \quad (3.8)$$

Expansion (E)

Once R is obtained and if its fitness value turns out to be better than W then, then the assumption made is correct. However, there is another possibility that a smaller value can be found further away from R. Therefore, the line passing through M and R is extended to a new point named 'E' (Figure 3.6). The location of E is obtained by equation (4.9), where γ_E is a constant whose value is generally considered to be 2.

$$E = M + \gamma_E(M - W) \quad (3.9)$$

Contraction (C)

The next logical possibility is that if the fitness does not improve at R or E then we consider two new points C_1 and C_2 (Figure 3.6). C_1 is the mid-point of M-R line segment and C_2 the mid-point of W-M. The fitness value for each is calculated using Equations 4.10 and 4.11 and the one with better fitness is termed as point 'C'.

$$C_1 = M + \rho_C(M - R) \quad (3.10)$$

$$C_2 = M + \rho_C(M - W) \quad (3.11)$$

where ρ_C is a constant whose value is generally taken to be -1/2.

Shrinking (S)

If the fitness value at C is not better than W then the last option remains is to shift the points G and W to M and S (Figure 3.6), where M is the mid-point of line segment joining B and G and S is the mid-point of line segment between B and W. Point S is calculated using Equation (4.12).

$$S = W + \sigma_s(B - W) \quad (3.12)$$

where σ_s is a constant whose value is generally taken to be 1/2.

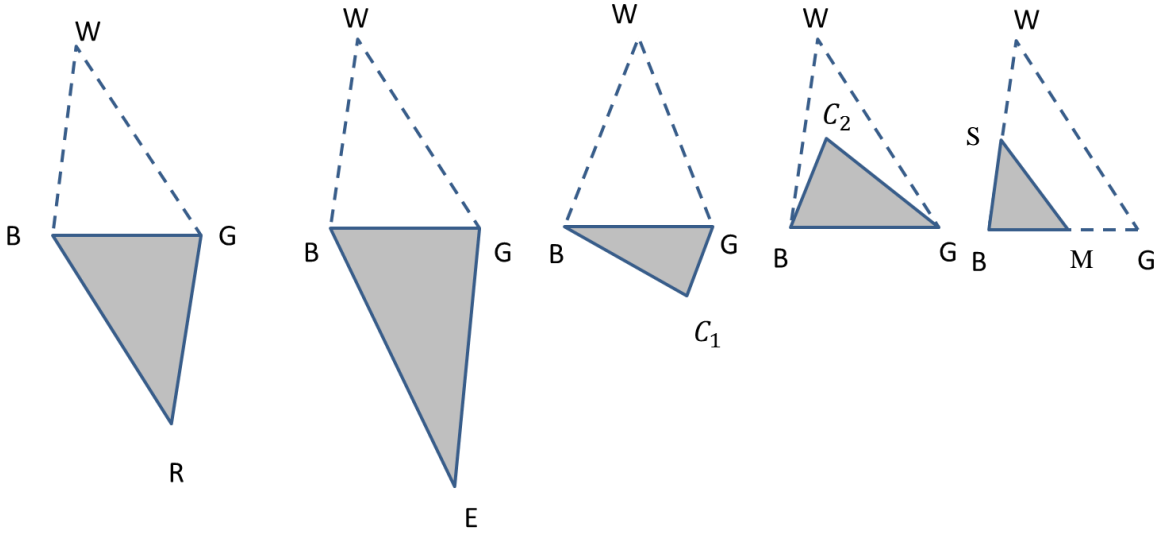


Figure 3.6 (i) Reflection (ii) Expansion (iii) Outside Contraction (iv) Inside Contraction (v) Shrink

The basic outline of the procedure adopted in the Nelder-Mead algorithm can be condensed into the steps discussed. For each iteration, the above steps are followed and the iterations are continued till the 3 vertices of the triangle tend to converge to a particular point or till they reach a certain tolerance limit. In reality exact convergence to a common point is highly unlikely, so the latter case is adopted. The final optimum point is considered to be the average of all the 3 vertices. The final procedure is best explained as shown in the flow diagram below (Figure 3.7).

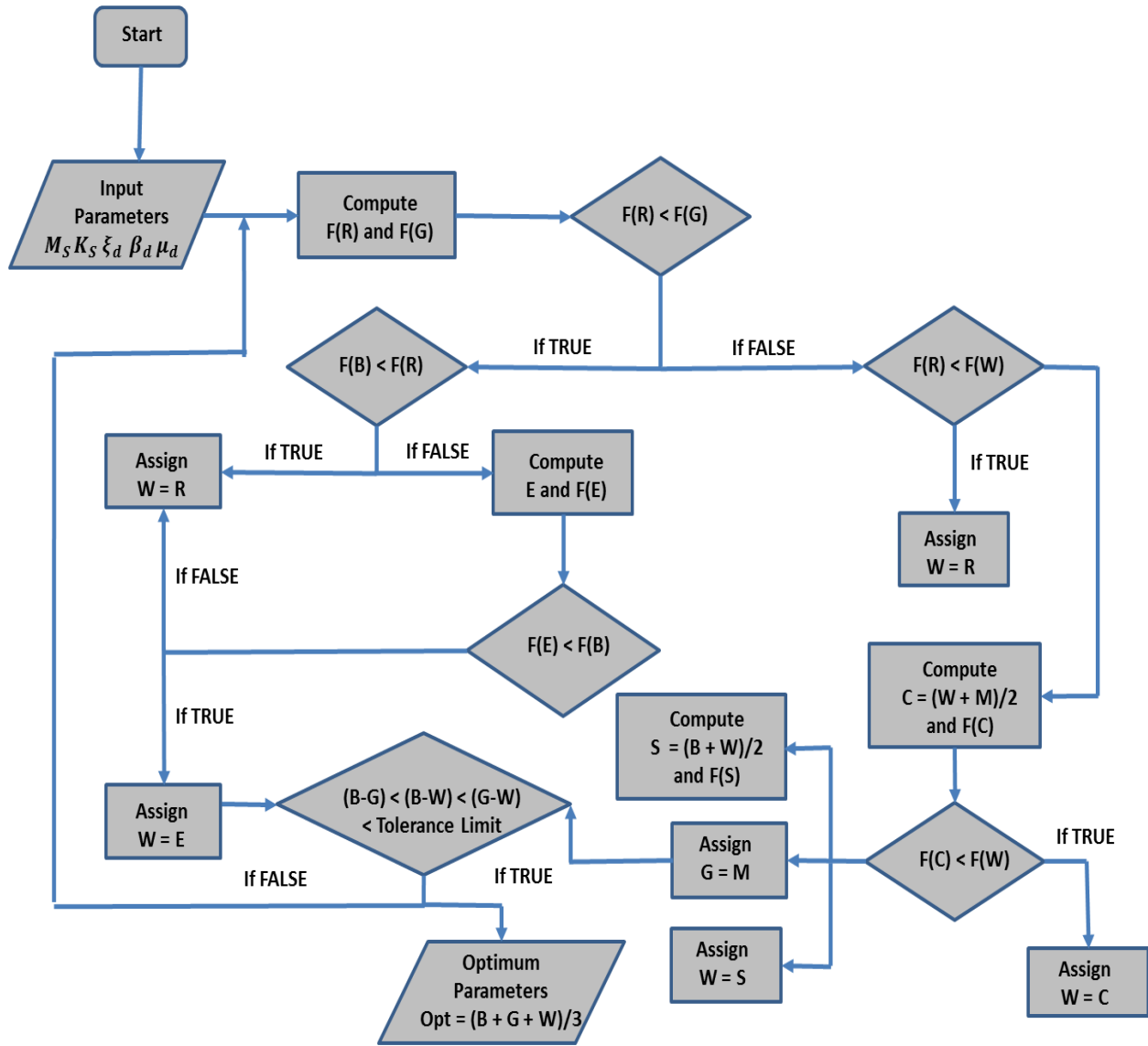


Figure 3.7 Flowchart of Nelder – Mead Algorithm

3.3.2 Covariance Matrix Adaptation Evolution Strategy (CMA-ES)

3.3.2.1 Introduction

The ‘Covariance Matrix Adaptation Evolution Strategy’ (CMA-ES) is a stochastic method of optimization for continuous non-linear, non-convex functions. Compared to other conventional optimization techniques like Genetic Algorithm, Bee Swarm, etc., CMA-ES has been found to be more flexible and efficient. Since the optimization of SS system requires 2 optimizations, time cost is an important factor to be considered.

CMA is an ‘Evolution’ optimization, similar to Genetic algorithm, which means it is based on the basic principles of evolution (i.e. the interaction between generation, selection and mutation). The overall idea behind CMA is the same as other evolution strategies except the method of generating population (‘population’ is referred to the different cases generated) method of selection and method of mutation differs. The CMA-ES algorithm exploits 2 different concepts – Maximum Likelihood Principle and Evolution Paths.

Maximum Likelihood is a popular estimation method used in the field of statistics. It is used to obtain the parameters of a statistical model. Considering an interest in finding out the heights of all the people in a state and due to time or resources constraint the height cannot be measured for everyone. In such case the principle of maximum likelihood can be used. The heights are assumed to have a particular type of distribution, say Gaussian, with unknown parameters (i.e. mean and variance). Parameters are referred to the variables used to define a particular type of distribution. The Maximum Likelihood principle calculates these parameters based on the given incomplete

data set. Thus in short, the Maximum Likelihood principle gives an estimation of the best fit to a particular incomplete set of data such that other information can be obtained from it. The question remains as to how does Maximum Likelihood come into play in CMA-ES?

The role of Maximum Likelihood is to maximize the probability of selection of correct values and search domain. Initially a test population is chosen at the beginning of the algorithm by assuming a particular distribution. After the 1st iteration the Maximum Likelihood principle is used to update the parameters of the distribution i.e. the mean and the variance, such that the likelihood of the correct values of the previous iteration tends to increase. Similarly, to increase the likelihood of the correct search domain the covariance matrix of the distribution is updated. This process of updating not just the population but also the search domain is highly beneficial and thus makes CMA-ES stand out from other evolutionary algorithms.

The second key concept is exploiting the use of Evolution or Search Paths by recording them. Evolution paths basically give an idea in which direction the favorable solutions can be found based on the results from the previous step. Thus, it gives a correlation between consecutive steps. These evolution paths are actually serving dual purpose. First, it is used in the adaptation process of the Covariance matrix instead of focusing on the variance of a single successful step. This enables a faster and a more efficient improvement in moving towards a favorable direction. The second is the use of evolution path to control the step size. The advantage of step size control is to avoid premature convergence, which is a common problem of concern in most evolutionary algorithms. Premature convergence is basically the convergence of the program on local solutions rather than the global. This takes place mainly due to lack of genetic variation among the

population generated (i.e. all the members of the population have identical properties). Figure 3.8 shows a schematic of the concept of CMA-ES in a simple manner by demonstrating how the randomly generated search points tend to move towards the optimal solution.

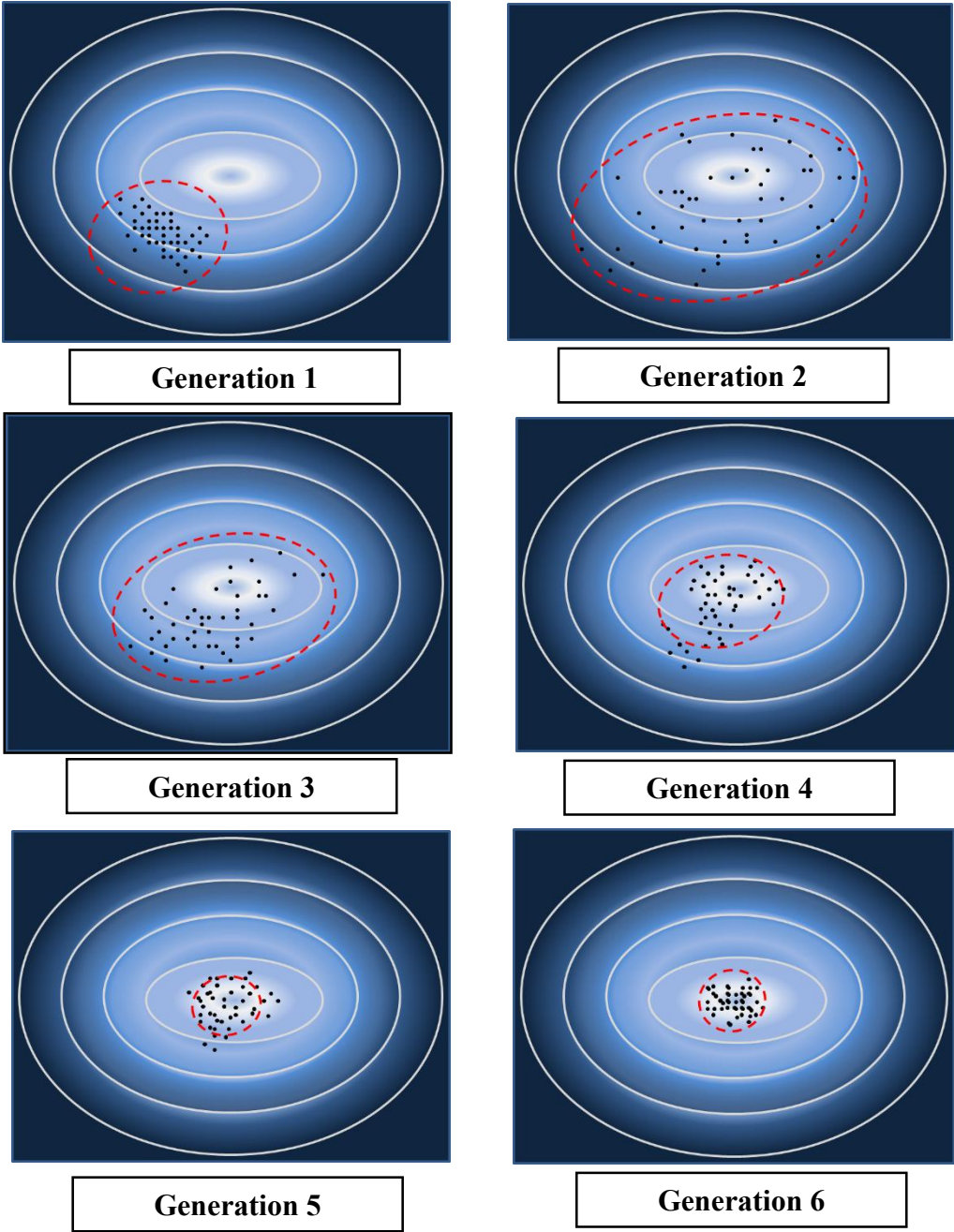


Figure 3.8 Schematic of Data Movement Pattern of CMA-ES Algorithm

3.3.2.2 Sampling

Similar to most algorithms the CMA-ES also start with generating a sample of search points. This sampling is done basically by using a multivariate normal distribution with pre-determined mean and variance for the first generation. However for subsequent generations these parameters are updated using a suitable procedure as discussed in further sections. Normally, the sampling is given by Equation (4.14)(Hansen 2011) however, the equation may vary depending on the limits on the variables. For example if the function only takes non-negative points then the above equation would not be considered suitable, in that case a new sampling function is required, which gives sampling points only in the positive domain.

In light of such requirements, research have been done to modify the sampling equations Hoshimura (2005) suggested 2 methods of sampling non-negative points – Lognormal distribution method and Projection method. In lognormal method, simply a lognormal distribution is used instead of a normal distribution. Using lognormal function forces all the sampling points to be positive. In case of the Projection method, the negative sampled points obtained are projected on the axes as shown in Figure 3.9.

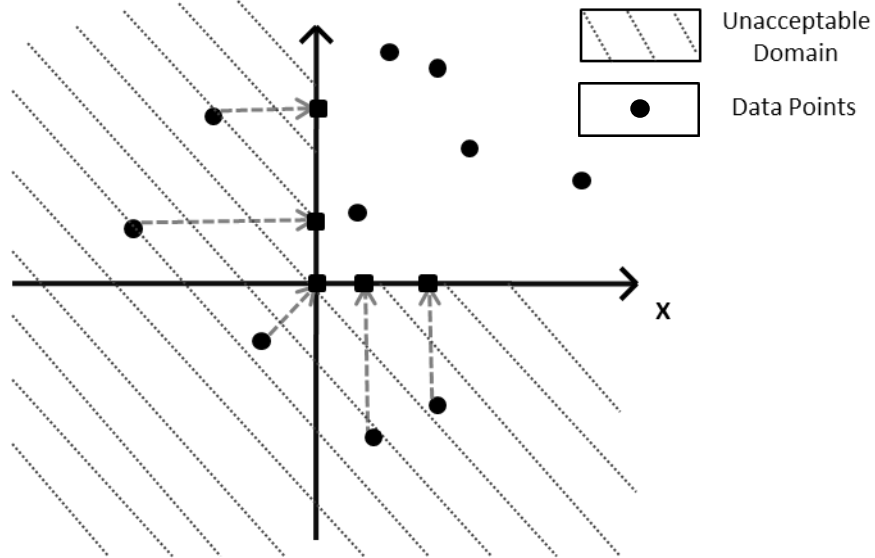


Figure 3.9 Projection Method

As mentioned previously, the variable considered for optimization is C_n , which governs the presence or absence of the Suspended slabs. This parameter is considered for each floor and take only two values – 0 or 1. Therefore, the discussed methods cannot be used for sampling in this case and thus a new equation is formed. The equation uses the same concept as discussed earlier but with a filter function that converts the generated search points into binary values. Basically, now the sampling function is divided into 2 parts, the first part (Equation 4.14) generates random sample points (x_k^{g+1}) based on a normal distribution with a mean of 0.5 and variance 0.3. Once the points are generated they are passed through the filter function (Equation 4.15) to convert into binary values.

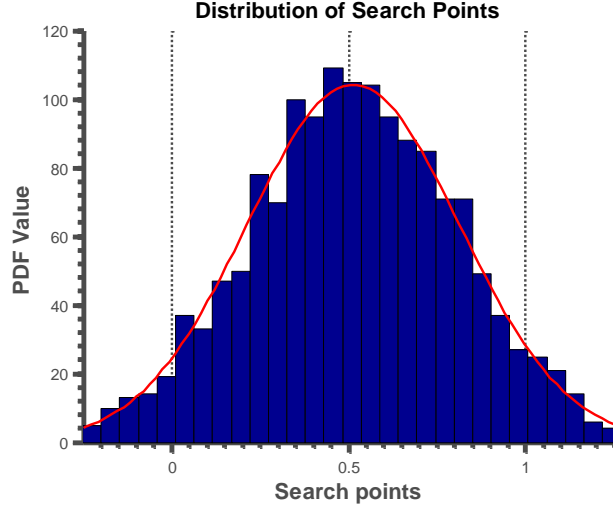


Figure 3.10 Unbiased Nature of Sampling Function

For the sampling functions to successfully work an important point to be kept in mind is that while generating the sampling points there should not be any bias. In order to ensure this in our developed function the mean (m^g) was chosen to be 0.5 and the standard deviation (σ^g) to be 0.3. For the initial assumption of the standard deviation Equation 4.13 is considered to be a good initial assumption (Hansen 2011). It would be clearer from Figure 3.10 that the probability of getting a 0 or 1 for C_n is the same initially, thus the developed sampling function is unbiased in the beginning.

$$\sigma = 0.3(b - a) \quad (4.13)$$

where, a and b are the bounds of the search domain (in this case a = 0 and b = 1)

$$x_k^{g+1} = m^g + \sigma^g N(0, C^g) \quad (4.14)$$

where, $N(0, C^g)$ is a Normal or Gaussian distribution for mean = 0 and covariance C^g

$$C_n = \begin{cases} 1 & (\text{if } x_k^g > 0.5) \\ 0 & (\text{if } x_k^g \leq 0.5) \end{cases} \quad (4.15)$$

3.3.2.3 Selection and Recombination

In each generation (or each run) a population is created which comprises a certain number of cases. The first step is to determine the size of the population (λ). Equation 4.16 (Hansen 2011) gives the population size based on the number of variables (n_{var}) being optimized. The population size is quite important for the proper execution of the algorithm. If the size is too big then the processing time would be too infeasible, and if its too small then the algorithm might get stuck on local solutions due to lack of variation. The next step is to determine parameter ' μ ', which is the number of members of the population to be selected to update the mean for the next generation. Equation 4.17 (Hansen 2011) is used to get the value of μ from the population size (λ).

Once these parameters are defined the weights are calculated by using Equations 4.18 and 4.19 (Hansen 2011). The next step is to rank the individual member sof the population. Each member of the population is assigned to the fitness function to get a respective fitness value, based on which the members of the population are given suitable ranks. Based on the ranks given to each case, weights are given to them which follow the relation (Equation 4.20) as the case with rank I should have the highest weight i.e. the mean of the distribution should shift towards this point. By shifting the mean towards the point of highest fitness, it is ensured that the chance of this value being selected in the next generation is the highest. Based on the weights the mean is modified using the relation (4.21) (Hansen 2011).

$$\lambda = 4 + \lceil 3 \ln n \rceil \quad (4.16)$$

$$\mu = \lceil \mu' \rceil \quad \text{where,} \quad \mu' = \frac{\lambda}{2} \quad (4.17)$$

$$w_i' = \ln(\mu' + 0.5) - \ln i \quad (4.18)$$

where, i is the index number of the population member and $\mu' = \text{size of population } (\lambda)/2$

$$w_i = \frac{w_i'}{\sum_{i=1}^{\mu} w_i'} \quad , \text{ such that} \quad (4.19)$$

$$w_1 \geq w_2 \geq w_3 \geq \dots \geq w_{\mu} > 0 \quad \text{and} \quad F(x_{1:\lambda}^{g+1}) \leq F(x_{2:\lambda}^{g+1}) \leq F(x_{3:\lambda}^{g+1}) \leq \dots \leq F(x_{\lambda:\lambda}^{g+1}) \quad (4.20)$$

where, w_i is the weight assigned to i^{th} member and F is the fitness function

$$m^{g+1} = \sum_{i=1}^{\mu} w_i x_{i:\lambda}^{g+1} \quad (4.21)$$

3.3.2.4 Adaptation

Estimating Covariance Matrix

Equation (4.22) gives the covariances of sampled steps. However, an improved version of this equation is generally used (Hansen, 2011) as shown in equation (4.23).

$$C_{\lambda}^{g+1} = \frac{1}{\lambda} \sum_{i=1}^{\lambda} (x_{i:\lambda}^{g+1} - m^g)(x_{i:\lambda}^{g+1} - m^g)^T \quad (4.22)$$

$$C_{\mu}^{g+1} = \sum_{i=1}^{\mu} w_i (x_{i:\lambda}^{g+1} - m^g)(x_{i:\lambda}^{g+1} - m^g)^T \quad (4.23)$$

Rank μ -update

If we want the mean of covariance matrices up to a particular generation then it would be given by equation (4.24) (Hansen 2011). From the look of this equation each generation has been given the

same weight i.e. each generation has the same amount of contribution to the covariance. However, this is not the best way to go about because from the 1st generation onwards the results keep getting refined as a result the contribution of the recent generations need to be higher. This is usually incorporated by assigning weights to each generation using an exponential smoothing, which is done as shown in equation (4.25) (Hansen 2011). This concept is known as the learning rate for updating the covariance matrix. A small value indicates that most of the information for previous generation is retained and therefore there is quite small learning. On the other hand if the value is close to 1 then no prior information is retained. Thus, the choice of value is quite important for the proper functioning of the algorithm. The relation used to obtain the value of learning rate is shown in Equation 4.26 (Hansen 2011). Important parameters and their definition have been listed in Table 4 – 1 for reference.

$$C^{g+1} = \frac{1}{g+1} \sum_{i=0}^g \left(\frac{1}{\sigma_i^2} C_{\mu}^{i+1} \right) \quad (4.24)$$

$$C^{g+1} = (1 - c_{\mu}) C^g + c_{\mu} \frac{1}{\sigma_g^2} C_{\mu}^{g+1} \quad (4.25)$$

$$c_{\mu} = \min \left(1 - c_1 \cdot \alpha_{\mu} \frac{\mu_{\text{eff}}^{-2} + \frac{1}{\mu_{\text{eff}}}}{(n+2)^2 + \alpha_{\mu} \mu_{\text{eff}} / 2a} \right) \quad (4.26)$$

Evolution Path

In the previous section selected steps were used to update the covariance matrix. Now we will introduce the concept of Evolution Path, which is the 2nd feature of CMA-ES. As discussed earlier, the CMA not only updates the distribution parameters but also the search paths. The evolution path is the direction the search pattern takes over a certain number of generations. It gives an idea of

where to search for feasible solutions. Mathematically, the evolution path is expressed as the sum of successive steps, so the same technique can be applied as the previous section. As before exponential smoothing is applied to incorporate higher weights to recent generations based on their higher importance. The relationship used to obtain the evolution path is given by Equation (4.28) (Hansen 2011), where $\sqrt{c_c(2-c_c)}$ is the normalization constant. Based on the evolution path the modified relation for updating the covariance matrix is given by Equation (4.29) (Hansen 2011).

$$\mu_{eff} = \frac{1}{\sum_{i=1}^{\mu} w_i^2} \quad (4.27)$$

$$p_c = (\mathbf{1} - c_c)p_c + \sqrt{c_c(2-c_c)} \mu_{eff} \left(\frac{m_{k+1} - m_k}{\sigma_k} \right) \quad (4.28)$$

$$C^{g+1} = (\mathbf{1} - c_1)C^g + c_1 p_c^{g+1} p_c^{g+1T} \quad (4.29)$$

$$c_1 = \frac{2}{(n + 1.3) + \mu_{eff}} \quad (4.30)$$

Combination

Combining the two approaches – ‘Rank μ ’ update and ‘Evolution Path’ we obtain Equation (4.32). The equation is the combination of both the strategies and thus utilizes the advantages of both. The rank- μ update is generally helpful in case of small populations, and the rank-one update in case of large populations.

$$c_\sigma = \frac{\left(\frac{\mu_{eff} + 2}{n + \mu_{eff} + 5} \right)}{\left(\frac{\mu_{eff} + 2}{n + \mu_{eff} + 5} \right)} \quad c_c = \frac{\left(\frac{\mu_{eff}}{n} + 4 \right)}{\left(n + 2 \left(\frac{\mu_{eff}}{n} + 4 \right) \right)} \quad (3.31)$$

$$C^{g+1} = (\mathbf{1} - c_1 - c_\mu)C^g + c_1 \left((p_c p_c^T) + (\mathbf{1} - h_\sigma) c_c (2 - c_c) C \right) + c_\mu \sum_{i=1}^{\mu} y_{i:w} w_i y_{i:w}^T \quad (4.32)$$

3.3.2.5 Step Size (σ)

In the previous sections updating the mean and covariance is addressed; however the variance or the step size is also an important parameter to be considered. Thus far no efforts has been made for optimizing the step size. Therefore, a step-size control is required. The control is achieved using the concept of evolution path (p_σ), which has been discussed in earlier sections. Based on the length of the evolution path the step size can be modified; for eg:- a short evolution path would suggest steps opposite in nature and so the step size needs to be decreased. Similarly, longer evolution paths suggest steps in similar direction and so the step size needs to be increased. The updated equation for step –length is given by Equation (4.33). The question remains as to how to decide whether the evolution path is long or short. To achieve this, the evolution path is compared to its expected length under random selection, which states that the steps are independent and uncorrelated. So, if there is bias in selection that produces a longer than expected path, then the step size is increased and vice-versa.

(NOTE: The theoretical aspects of CMA-ES have not been investigated in detail as the scope of this study is mainly the application of it.)

$$\sigma_{k+1} = \sigma_k \exp\left(\frac{c_\sigma}{d_\sigma} \left(\frac{\|p_\sigma\|}{E\|N(0,I)\|} - 1\right)\right) \quad \text{where, } E\|N(0,I)\| = \sqrt{2}\Gamma\left(\frac{n+1}{2}\right)\Gamma\left(\frac{n}{2}\right) \approx \sqrt{n}\left(1 - \frac{1}{4n+1/21n^2}\right) \quad (4.33)$$

$$d_\sigma = 1 + 2 \max\left(0, \sqrt{\frac{\mu_{eff}-1}{n+1}} - 1\right) + c_\sigma \quad (3.34)$$

$$p_\sigma = (1 - c_\sigma) + \sqrt{1 - (1 - c_\sigma)^2} \sqrt{\mu_w} C_k^{-1/2} \left(\frac{m_{k+1} - m_k}{\sigma_k}\right) \quad (4.35)$$

Table 3-1 List of important parameters for Adaptation process in CMA-ES

p_c	Evolution Path of Covariance Matrix
p_σ	Evolution Path of Step – Length
c_μ	Learning Rate for Rank – μ Update for Covariance Matrix
c_1	Learning Rate for Rank – One Update for Covariance Matrix
c_c	Inverse Backward Time Horizon of Evolution Path p_c
c_σ	Inverse Backward Time Horizon of Evolution Path p_σ
d_σ	Damping parameter
c_μ	Learning Rate for Rank – μ Update for Covariance Matrix

3.3.2.6 Process Flowchart

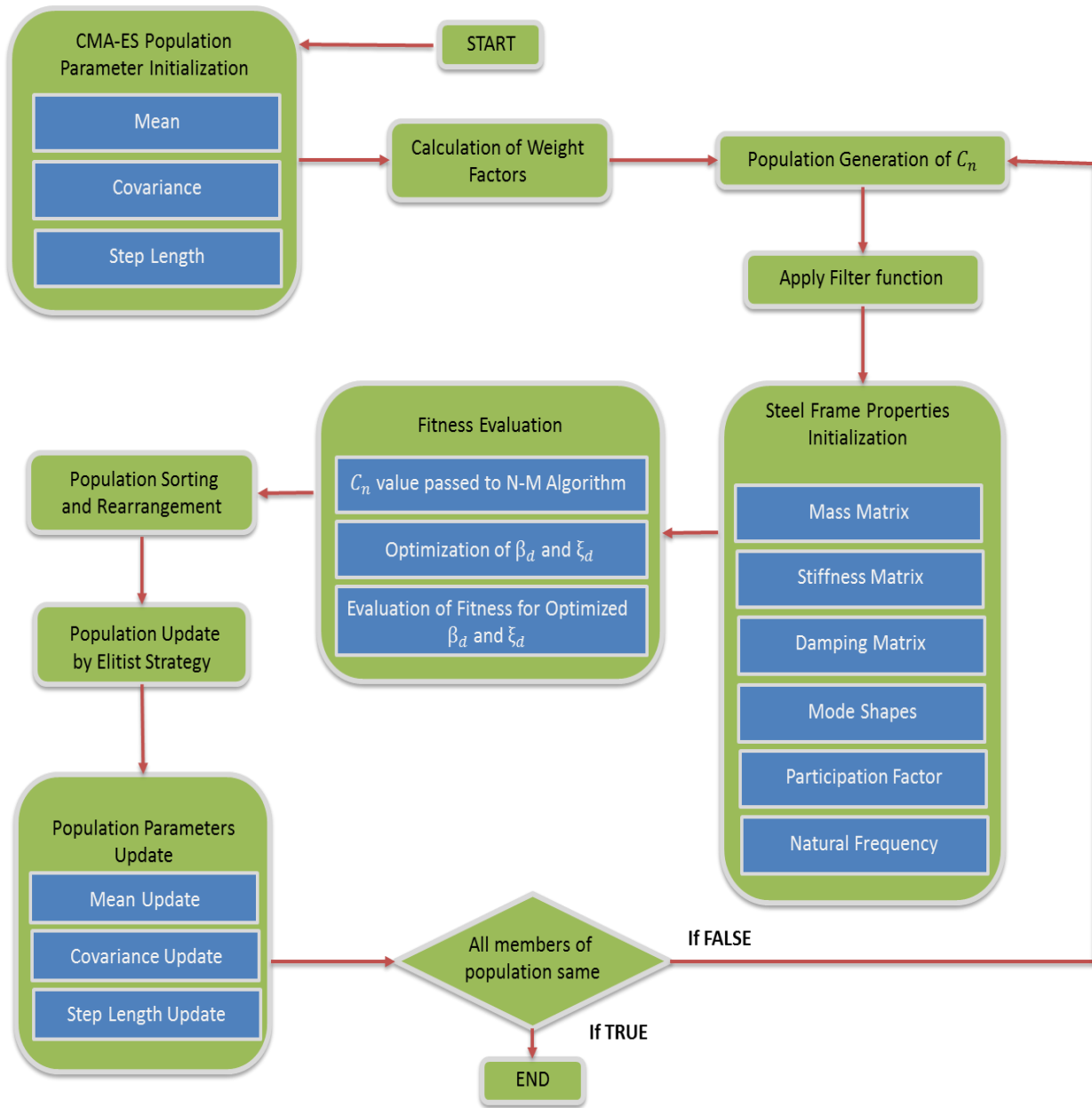


Figure 3.11 CMA – ES Procedure Flowchart

3.3.3.1 Introduction

A Numerical example is considered to see the behavior and effectiveness of the new algorithm. A 10-story 2-bay SS system is considered for analysis whose structural properties are shown in Table 3-2. Several modifications have been considered to the combinatorial algorithm, which are tested separately and their convergence is evaluated to obtain a suitable time effective optimization algorithm. First, few new concepts are introduced that are used to modify the algorithm.

Table 3-2 Structural Properties of 10 Story 2 Bay Frame

Floor No.	Mass (slugs)	Stiffness (kips/inch)
1	0.618	75.3
2	0.608	75.3
3	0.608	75.3
4	0.608	75.3
5	0.608	75.3
6	0.608	75.3
7	0.608	75.3
8	0.608	75.3
9	0.608	75.3
10	0.547	75.3

3.3.3.2 Elitist Selection (Elitism)

Elitism in reference to evolutionary algorithms is quite a popular selection approach. The Elitist Selection is a supplementary tool applied to the selection method of evolutionary algorithms to improve the chances of finding the optimal solution. The Elitist Selection basically states that in every generation the best case is always selected to be carried on to the next generation. In Evolutionary Algorithms such as Genetic Algorithm, a certain number of population is generated in every generation and out of which a few are selected based on the weights given to them.

The Elitist selection ensures that the best case is always carried on to the next generations, which ensures that the optimum point does not get lost. The CMA-ES algorithm generates the search points based on a probabilistic distribution, as a result sometimes the optimum point generated in the previous step may not be generated in the next generation. In case of the SS system the sampling function uses a filter to convert the random search points to binary values, as a result the movement of the mean and other parameters tend to occur at a faster rate than the usual. Due to this fast movement sometimes it is possible that some solutions may be overlooked or the search may get “stuck” on a local solution, so the elitist selection is highly essential in this case. To further improve efficiency of the Elitist selection, 2 modifications are made and tested separately.

The first modification (TYPE – I) states that in a particular generation the best case is identified and selected. The stored value is then compared to the best case from the next generation. In case the stored value turns out to be better, then the worst case for that generation is replaced by the stored value. The second type (TYPE – II) states that if the best case from the previous generation

turns out to be equal or worse than the best case of the next generation, then it replaces the worst case from that generation. The difference between the two cases is that in case the best solution is not better than the one from the successive generation, then TYPE – I would not come into play. However TYPE – II would still replace the worst case. Both the types have been shown in Figure 3.12 for better understanding.

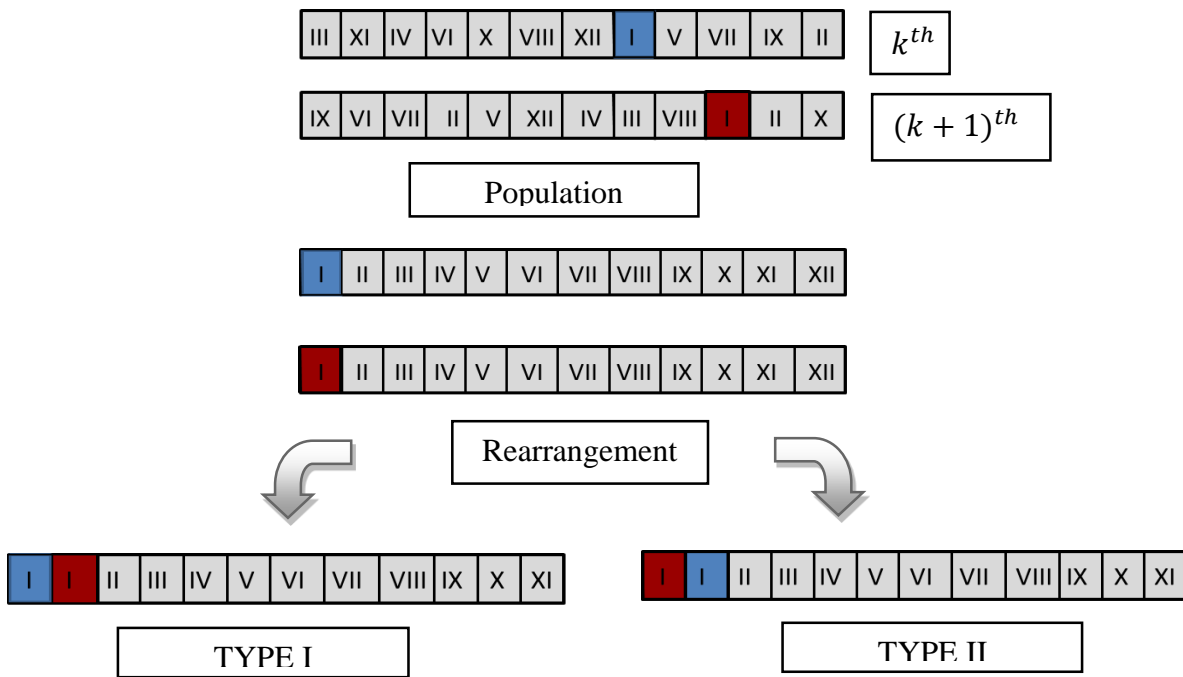


Figure 3.12 Elitist Strategy Modifications

3.3.3.3 Flatness Recovery

In CMA-ES it is seen that after certain generations all the members of the population tend to converge to a single point. If this point of convergence is the optimal solution, the algorithm works as expected, however if the point of convergence is a local solution then the program has to be terminated. In this study the chances of getting stuck on a local solution are higher and so in order to increase the efficiency of the algorithm a flatness recovery option is implemented. As CMA-ES

converges to a solution the step length tends to decrease so in order to escape from flatness the step length has to be increased by a particular factor. However increasing the step length too much may cause the algorithm to diverge so an educated estimation has to be made.

As previously mentioned, the variables take only 0 or 1, so once flatness is achieved the mean would converge to 0 or 1. In order to convert a 0 to 1 or vice-versa the standard deviation has to be chosen such that the probability of generating a number greater than 0.5 is significant. Equation 4.36 gives the Cumulative Density Function (CDF) or Cumulative distribution function value, which determines the probability of generating a number below a certain point (X). Equation 4.37 gives the probability to get a number greater than a fixed point (X). Equation 4.38 is used to transform from a standard normal distribution to a normal distribution. Table 3-3 shows the increase in probability to get a number greater than 0.5 with increase in standard deviation. It is seen that for sigma greater than 2 the increase in probability is not significant thus it is set as the maximum limit and the step length is modified according to the Equation 4.39.

$$P(Z < X) = \phi(Z) \quad (3.36)$$

$$P(Z > X) = 1 - \phi(Z) \quad (3.37)$$

$$Z = \frac{X - \mu}{\sigma} \quad (3.38)$$

$$\sigma_{k+1} = \min \left[\sigma_k \exp \left(\frac{c_\sigma}{d_\sigma} + 1 \right), 2 \right] \quad (4.39)$$

Table 3-3 Probability values for different step - lengths

S no.	μ	σ	X	Z	P (Z > X)
1	0	1	0.5	0.50	0.3085
2	0	2	0.5	0.250	0.4013
3	0	3	0.5	0.1667	0.4364
4	0	4	0.5	0.125	0.4522
5	0	5	0.5	0.10	0.4602
6	0	6	0.5	0.0830	0.4681
7	0	7	0.5	0.0714	0.4721
8	0	8	0.5	0.0625	0.4761
9	0	9	0.5	0.0566	0.4801
10	0	10	0.5	0.050	0.4801

3.3.3.4 Cases Considered

Initially, a simple combination of CMA-ES and Nelder – Mead was implemented, however it was seen that algorithm tend to get stuck on local solutions. To increase the effectiveness of the algorithm few strategies were implemented and tested out.

Case I: Nelder – Mead + CMA-ES

This case deals with a simple combination of Nelder-Mead and CMA-ES. The algorithm's effectiveness is first evaluated by plotting the best fitness value for each generation. From the perspective of time cost the algorithm performed quite well compared to the Numerical Search.

The time taken by this algorithm was about 1/10th the Numerical Search. Further, Boxplots were plotted to see the behavior of the algorithm. Boxplots are an effective way to represent a cluster of data as they indicate important distribution parameters such as mean, upper and lower quartile range (75% and 25%). The boxplots also give an understanding of the way the data is distributed.

Figure 4.13 shows that the best fitness value in each generation tends to converge to a point and remains unchanged after that. A better view of the convergence is seen from the boxplot shown below in Figure 3.13. The algorithm starts out with a wide domain and with passing generations the mean, standard deviation and covariance gets updated which forces the search space to shift towards the optimal solution, as expected. In terms of performance the algorithm converged to local solutions and missed the global optima, which tends to suggest a scope of improvement. Figure 3. shows the variation in step-length as how it first increases to expand the search space and then once the best solution is found it decreases to reduce the search space.

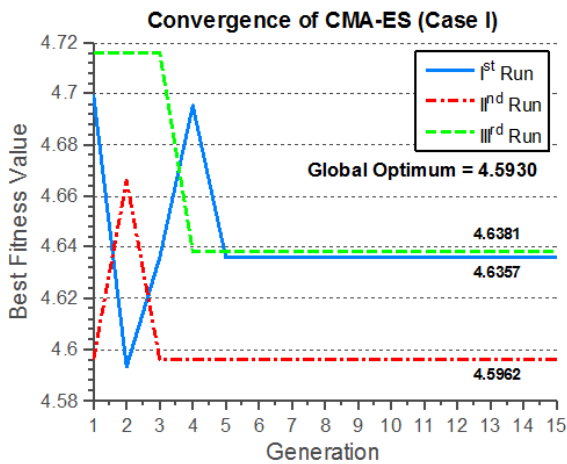


Figure 3.13 Case I Convergence and Accuracy

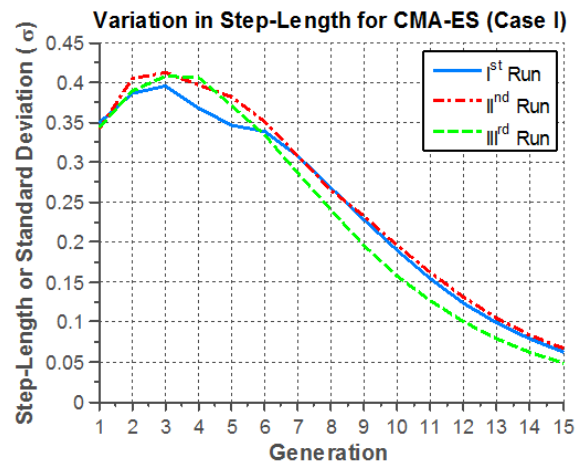


Figure 3.14 Change in Step – Length for Case I

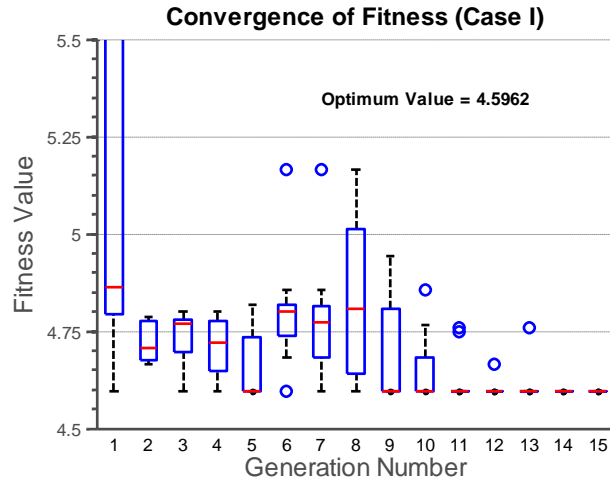


Figure 3.13 Boxplot of Case I Convergence

Case II: Nelder-Mead + CMA-ES + TYPE I Elitism

To improve the accuracy of the algorithm, principle of ‘Elitism’ is implemented. For this case only Type I Elitism is applied. The same plots, as those mentioned for the previous case, were plotted to see the accuracy and convergence. It is seen that the time and generations taken for convergence were found to be identical to the previous case. Even the accuracy was seen to be identical to the previous case, which does not necessarily mean no improvement. It only states that even with Elitism there is still need of improvement as the accuracy is not satisfactory.

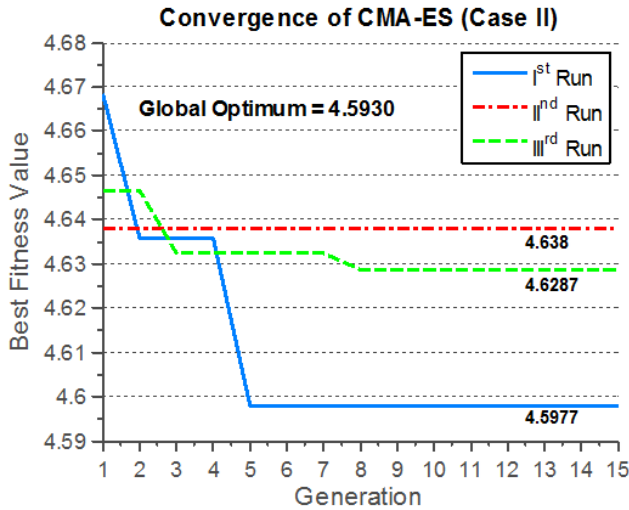


Figure 3.16 Case II Convergence and Accuracy

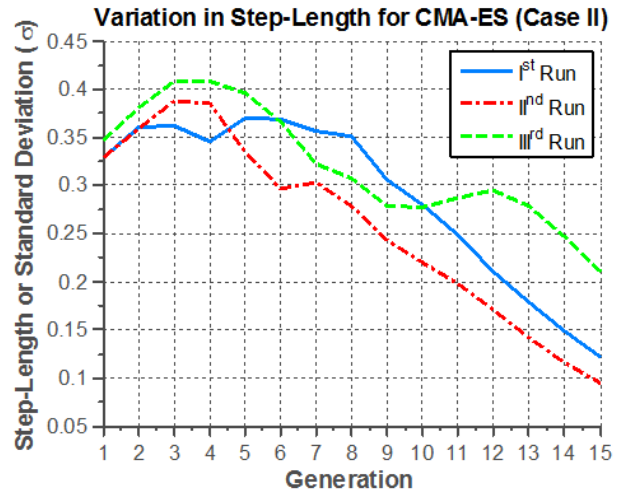


Figure 3.17 Change in Step – Length Case II

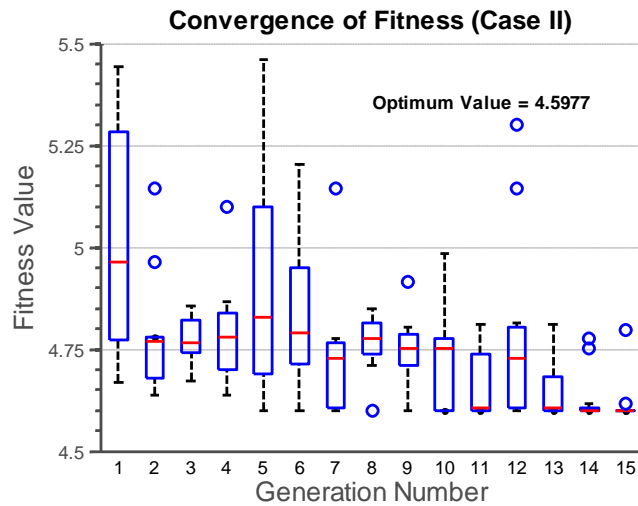


Figure 3.14 Box plot of Case II Convergence

Case III: Nelder-Mead + CMA-ES + TYPE I Elitism + TYPE II Elitism

In this case both, Type I and Type II Elitism are implemented simultaneously. Now the algorithm tends to have the benefits of the previous cases along with some additional advantage. The convergence plots are plotted same as before. For this case also the algorithm shows similar response in terms of time cost and number of generations, however this time significant

improvement in accuracy was seen. The modified algorithm tend to produce much accurate results than before. The boxplot and variation in standard deviation showed a similar pattern.

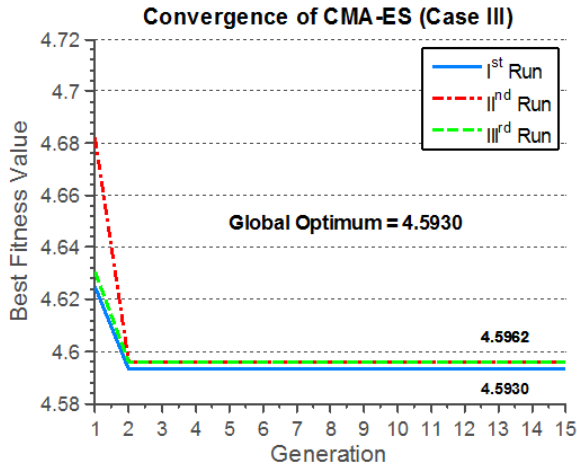


Figure 3.19 Case III Convergence and Accuracy

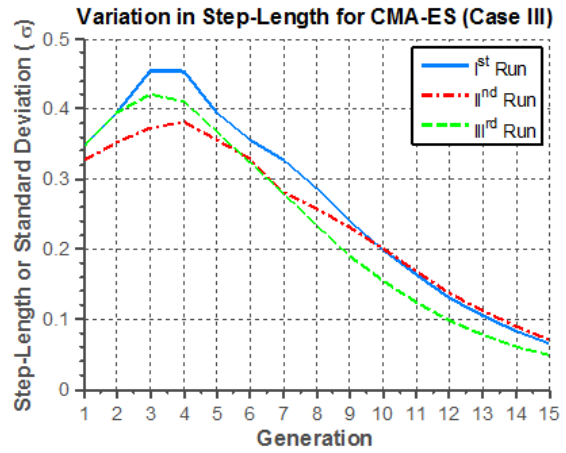


Figure 3.20 Change in Step – Length for Case III

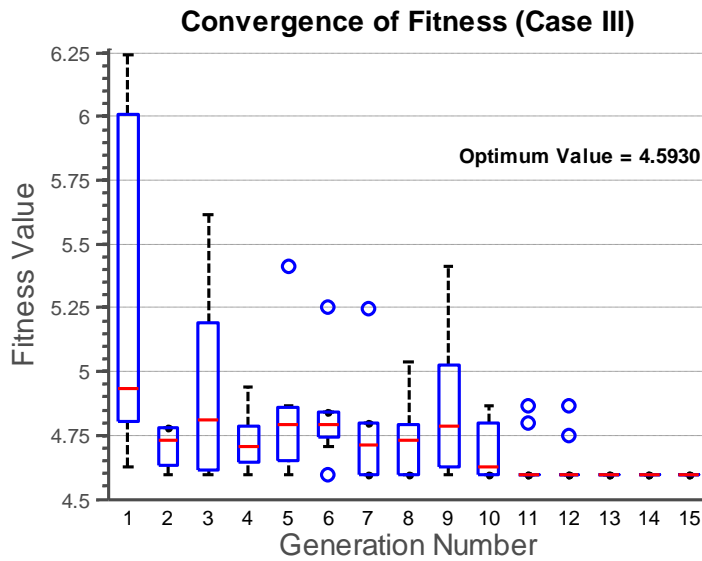


Figure 3.15 Box plot of Case III Convergence

Case IV: Nelder-Mead + CMA-ES + TYPE I Elitism + TYPE II Elitism + Flatness Recovery

Case III is considered acceptable however it still failed to pin point the exact global optima in every run. A new unprecedented approach is suggested which utilizes the concept of Elitism in combination to another approach called 'Fitness Recovery', which has been discussed earlier in detail. The concept behind this strategy is to increase the standard deviation when the search starts to reach flatness, such that the algorithm is forced to generate new search points that are outside the expected domain. This tends to cause the algorithm to diverge, however due to the inherent adaptation capability of the CMA-ES, the algorithm prevents from diverging to a failure. After a few generations of divergence the algorithm tends to move in the direction of the best value. The algorithm moves in a zig-zag pattern and fails to converge to a single point, however this is the advantage of this strategy as it prevents the search to get stuck on a local solution and instead allows a higher probability of finding the global optima. The pattern is shown in Figure 3.16 which represents the variation in the standard deviation. The purpose served by the Elitist Selection is to keep track of the best solution. This strategy fails to converge to a single point thus the Elitist selection stores the best value and makes sure that the value is not lost.

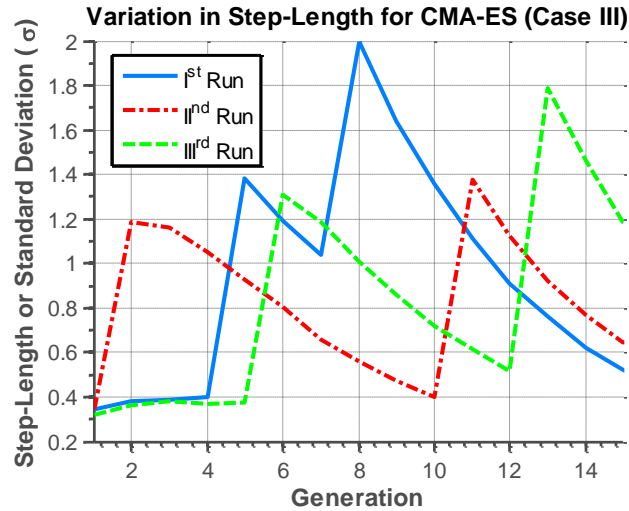


Figure 3.16 Change in Step – Length for Case IV

The convergence plots for this case have been shown below in Figure 3.17 and Figure 3.18. As opposed to other cases where the search ran till all the points converged to a single point, in this strategy the algorithm is run until a specific number of generations. From Figure 3.17 the accuracy is seen to be better than the predecessors. From Figure 3.18 it is seen that the algorithm does not converge to a unique solution however it does manage to find the optimal solution. The convergence pattern can be seen in much detail from this plot. As for the time of convergence, it is seen to be almost the same as previous cases.

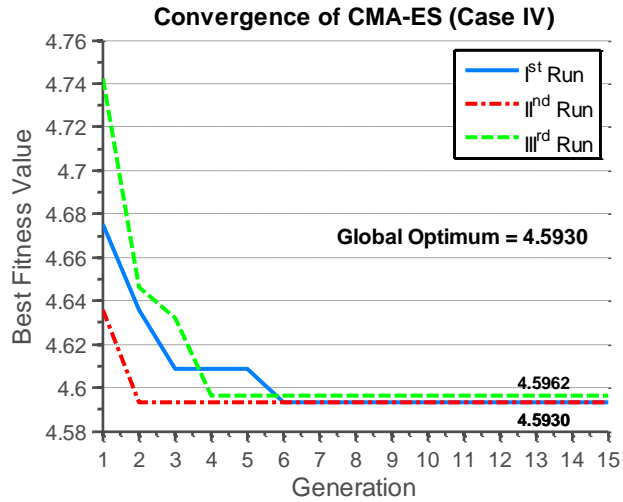


Figure 3.17 Case IV Convergence and Accuracy

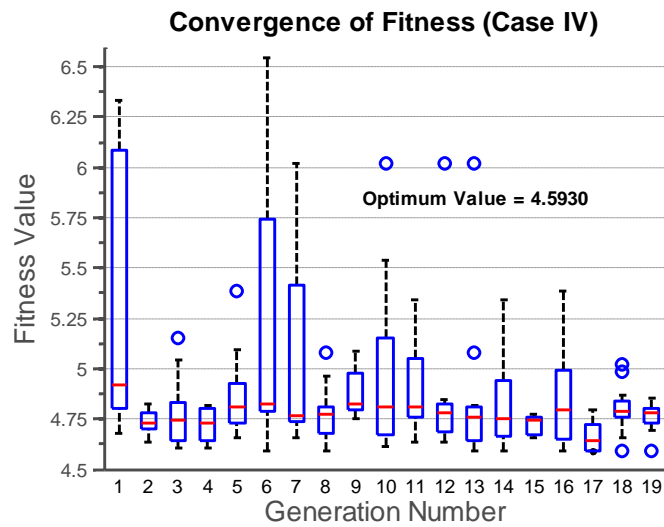


Figure 3.18 Box – Plot of Case IV Convergence

CHAPTER 4

SYSTEM RESPONSE TO GENERATED WHITE NOISE EARTHQUAKE EXCITATIONS

4.1 Stationary White Noise

A white noise is generally considered as a random signal whose data points are uncorrelated to each other and have a mean equal to zero and a finite variance. In terms of energy, a white noise has a constant power spectral density (i.e. the signal consists of equal power within any frequency band width). The white noise is considered to have a Gaussian distribution. White noise have application in a variety of fields including – music, acoustics, electrical, among many others. It is usually used to generate signals by passing through a suitable filter. Based on this concept, white noise is used in the field of earthquake engineering to simulate ground motions. Figure 4.1 shows a typical stationary white noise signal used to simulate a random ground motion excitation. In this study, the earthquake ground acceleration is modeled as a stationary white noise, which is characterized by its Power Spectral Density Function (PSDF). The PSDF is obtained using a commonly used filter developed by Kanai (1957) and Tajimi (1960), also commonly known as the Kanai-Tajimi Filter.

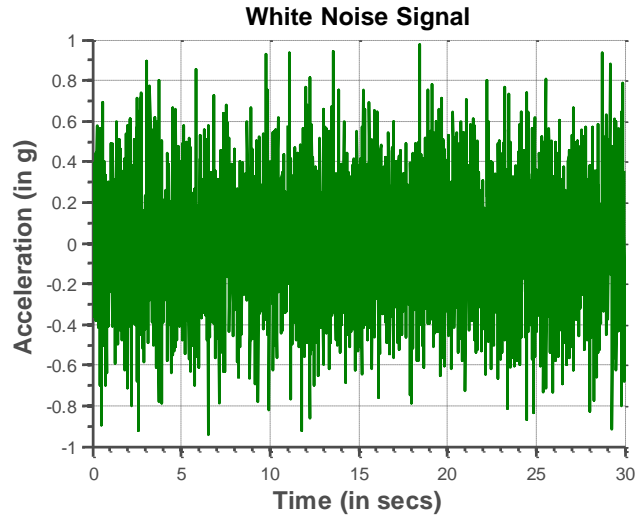


Figure 4.1 An Example of a White Noise Signal

4.2 Kanai-Tajimi Filter

The Kanai-Tajimi filter has been widely used in the analysis of structures under the influence of earthquake excitations. According to this model, the ground is assumed to be made up of soil layer over rock strata, which is quite logical. The rock and soil interaction is represented using a linear system of spring and dashpot in parallel connecting a mass, which represents the soil, to the ground, which represents the rock strata. The ground or the rock strata acceleration is assumed to be a stationary white noise, in response to which the system is solved for the response of the soil layer. The PSDF given by Kanai and Tajimi is shown in Equation (5.1).

$$\frac{S_{KT}(\omega)}{S_0} = \frac{1 + 4\xi_g^2 \left(\frac{\omega}{\omega_g}\right)^2}{\left(1 - \left(\frac{\omega}{\omega_g}\right)^2\right)^2 + \left(2\xi_g \frac{\omega}{\omega_g}\right)^2} \quad (4.1)$$

It is seen to be a function of three parameters ω_g , which represents the ground natural frequency, ξ_g , the damping ratio of ground, and S_0 , which is the ground intensity. These parameters are varied to simulate different earthquakes or even an ensemble of earthquakes. Figure 4.2 shows a typical form of the Kanai-Tajimi Spectrum. Since Kanai-Tajimi model can easily simulate earthquake excitations and is mathematically simple it is used in this study to evaluate the performance of the SS system.

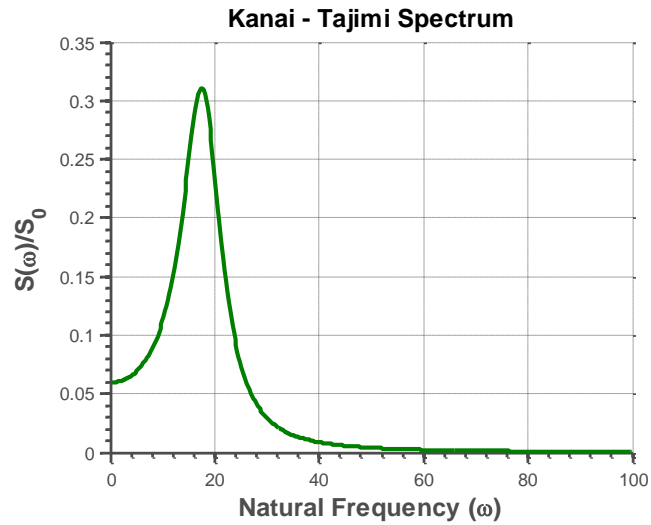


Figure 4.2 Typical Shape of Kanai – Tajimi Spectrum

4.3 Fast Fourier Transform (FFT) and Power Spectral Density Function (PSDF)

To determine the frequency content of a signal Fourier transform is used. In case of earthquakes, the fourier transform converts the earthquakes from a time domain to a frequency domain, which gives an indication of the predominant frequencies. In practice the fourier transform is obtained using an approach called the ‘Discrete Fourier Transform’, which is programmed as FFT (Fast Fourier Transform) in most mathematical software. In FFT, the Fourier synthesis of a time history is considered as a pair of Fourier Integrals in the complex domain and is given by Equation (5.3). The FFT gives the frequency content of a time history in complex quantities from which the Amplitude Spectrum is obtained by taking the magnitude of the complex quantities.

$$x(i\omega) = \int_0^T x(t) e^{-i\omega t} dt \quad (4.2)$$

where, T is the Total time period of the time history

PSDF is another way of representing the frequency content of a signal. Where as the fourier amplitude spectrum gives the frequency content of an actual ground motion of a site, the PSDF is a probabilistic measure of the frequency and is given by the Equation (5.4)

$$S_E = \frac{A^2}{\pi T} \quad (4.3)$$

where, A is the amplitude of the Fourier amplitude spectrum, and T is the total duration of the time history.

4.4 Analysis Procedure

For the purpose of this study 2 sets of earthquakes excitations are generated – Near fault earthquakes and Far fault earthquakes. According to ATC-63 the definition for Near fault earthquakes constitutes the ground motion records at stations within a distance of 10 km of the fault, and Far fault earthquakes constitute records from stations of more than 10 km distance from the fault. With respect to these classifications 19 records for Near fault and 30 records were chosen in the region of United States, with a soil type D (i.e. broad soil). These 2 sets of earthquakes are combined separately by taking the mean of earthquakes selected for the 2 respective cases to obtain the effective Power Spectral Density for each case (Equation 5.5). In order to smooth these PSDF's the Kanai – Tajimi Spectrum was used. For each case a different set of parameters for the Kanai – Tajimi spectrum are obtained to simulate the ensemble of earthquakes. Table 4-1 Parameters of Kanai – Tajimi Model for Near Fault and Far Fault Earthquakes shows the parameters obtained for the 2 sets of earthquakes. As expected, except the ground intensity, the other parameters are seen to be quite close to each other for the 2 cases. This can be attributed to the fact that both set of earthquakes were chosen on the same type of soil (Type – D soil). Figure 4.3 and Figure 4.4 show the power spectrum obtained after averaging the 2sets of earthquakes selected for near and far fault.

$$S_E = \frac{\sum_{j=0}^{\omega_0} S(\omega_j)}{Num} \quad (4.4)$$

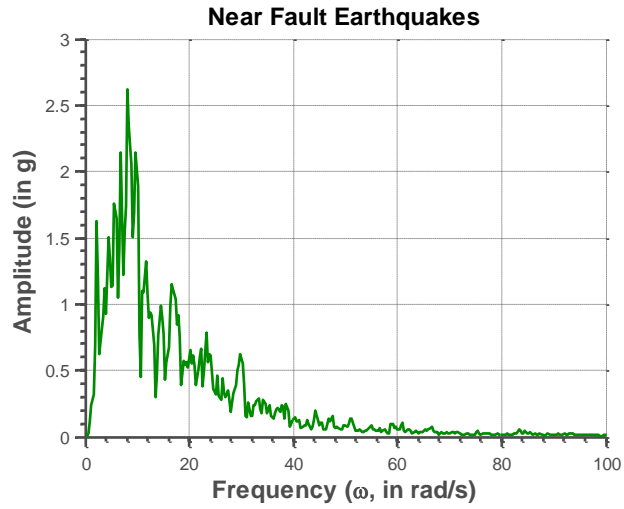


Figure 4.3 Average Power Spectrum for Near Fault Earthquakes

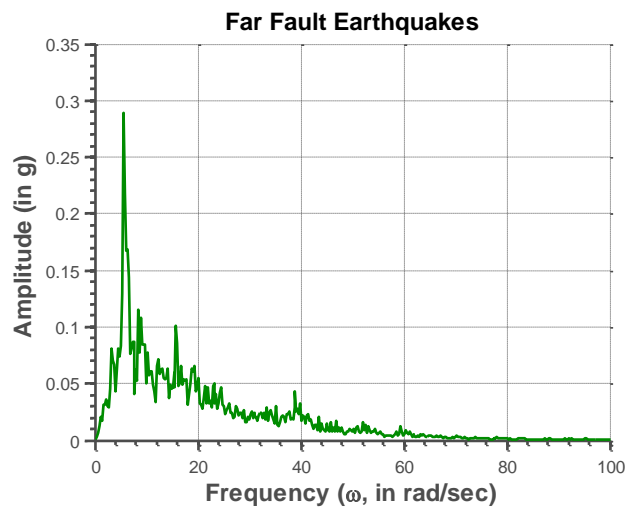


Figure 4.4 Average Power Spectrum for Far Fault Earthquakes

Table 4-1 Parameters of Kanai – Tajimi Model for Near Fault and Far Fault Earthquakes

Earthquake Type	No. of Records	ω_g	ξ_g	S_0
Near fault	19	17.77	0.30	0.978
Far fault	30	18.43	0.25	0.0596

The PSDF has 3 statistical characteristics – RMS acceleration, central frequency, and the shape factor. These 3 terms are utilized in obtaining the respective parameters of Kanai – Tajimi Spectrum by equating the 3 terms from of the PSDF obtained to the Kanai – Tajimi spectrum. The three characteristics are given by the following relations (Equations 5.6, 5.7 and 5.8), where λ_n is the n^{th} spectral moment and given by Equation (5.9). ω_0 is the maximum frequency until which the spectrum is considered, and is termed the cut-off frequency.

$$\psi = \sqrt{\lambda_0} \quad (4.5)$$

$$\omega_c = \sqrt{\frac{\lambda_2}{\lambda_0}} \quad (4.6)$$

$$\delta = \sqrt{1 - \frac{\lambda_1^2}{\lambda_0 \lambda_2}} \quad (4.7)$$

$$\lambda_n = \int_0^{\omega_0} \omega^n S(\omega) d\omega \quad (4.8)$$

The Kanai – Tanaji PSDF is used to obtain the root mean square response of the SS system and the composite frame (Equation 5.10). The mean response is considered as the performance evaluation parameter for the SS system. A thing to note is that in the previous chapters it has been discussed that the optimized values of the SS system were evaluated by minimizing the maximum response amplitudes (also known as the Mini-Max approach). However, now the approach is changed since the reference parameter has changed from response amplitude to the RMS response. The SS system is now optimized by minimizing the RMS response to the input of Kanai-Tajimi's spectrum.

$$\sqrt{\sigma^2} = \sqrt{\int_{-\infty}^{+\infty} |H_N|^2 S_{KT}(\omega) d\omega} \quad (4.9)$$

Once the optimized parameters are obtained, they are used to get the final RMS response of the SS system. To gain better insight on the performance of the SS system, a new term is introduced, which is termed Improvement Factor (I). Improvement factor basically gives the percentage improvement in performance of the SS system in comparison to a composite system considered with the same properties (Equation 5.11).

$$\text{Improvement Factor} = 1 + \frac{\text{RMS of Composite Frame} - \text{RMS of SS System}}{\text{RMS of Composite Frame}} \quad (4.10)$$

4.5 Numerical Examples

The design procedure discussed in the previous section is applied to 3 cases to see the effectiveness of the SS system with increase in size of the structure. A 4 story 2 bay, 7story 3 bay and a 10 story 5 bay structure are considered for analysis. In each case the SS system is optimized corresponding to 2 different cases:

- TYPE – I : Steel frame's top floor RMS displacement
- TYPE – II : Steel frame's top floor RMS displacement + Top floor SS RMS acceleration

In 1st case the system is just optimized to steel frame's top floor displacement, however in the second case a simultaneous optimization is carried out to try and improve the overall performance of the SS system. For both the cases the input response spectrum considered are the Near and Far fault Kanai Tajimi spectrums derived in the previous section. The Importance factors for all the

cases are plotted below to see the variation in performance of the SS system and draw conclusions from it. The structural properties of each case have been shown below.

Table 4-2 Structural Properties of 4-Story 1-Bay Frame

Floor No.	Mass (slugs)	Stiffness (kips/inch)
1	0.309	37.6
2	0.304	37.6
3	0.304	37.6
4	0.274	37.6

Table 4-3 Structural Properties of 7-Story 3-Bay Frame

Floor No.	Mass (slugs)	Stiffness (kips/inch)
1	0.8924	112.95
2	0.8979	112.95
3	0.8979	112.95
4	0.8979	112.95
5	0.8979	112.95
6	0.8979	112.95
7	0.7928	112.95

Table 4-4 Structural Properties of 10-Story 5-Bay Frame

Floor No.	Mass (slugs)	Stiffness (kips/inch)
1	1.4641	188.25
2	1.4441	188.25
3	1.4441	188.25
4	1.4441	188.25
5	1.4441	188.25
6	1.4441	188.25
7	1.4441	188.25
8	1.4441	188.25
9	1.4441	188.25
10	1.30	188.25

The performance of the three structures systems is shown in Figure 5.5 – Figure 5.10. The Figure 5.5, Figure 5.7, and Figure 5.9 show the improvement factor versus the story number for both the displacement and acceleration of the steel frame. Figure 5.6, Figure 5.8, and Figure 5.10, on the other hand, show the improvement factor for the displacement and acceleration of just the top story SS.

4.5.1 4 Story 2 Bay

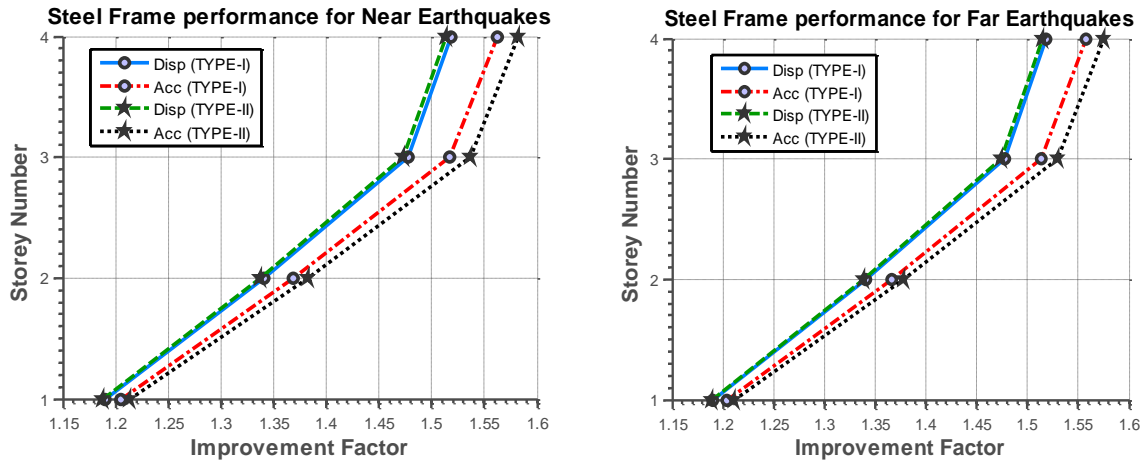


Figure 4.5 Performance of Steel Frame for Near and Far Fault Earthquakes

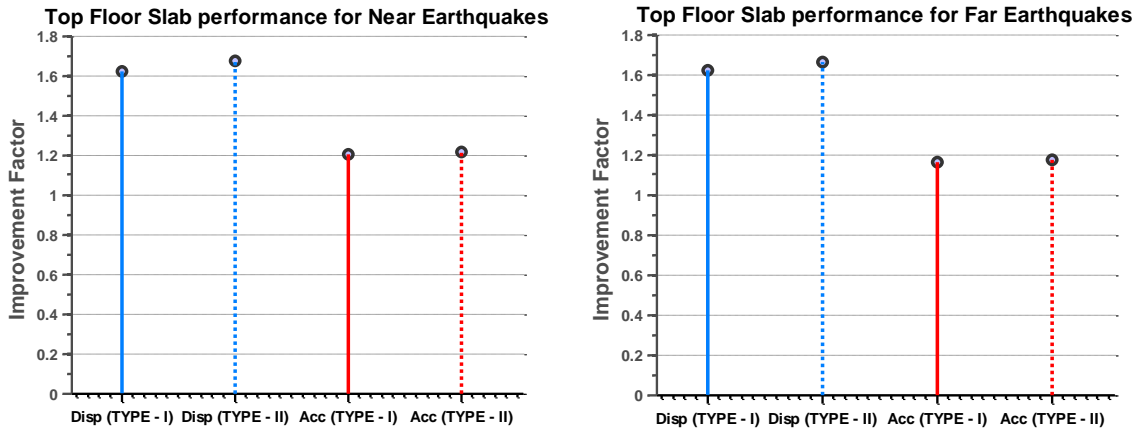


Figure 4.6 Performance of Top Floor Suspended Slab for Near and Far Fault Earthquakes

4.5.2 7 Story 3 Bay

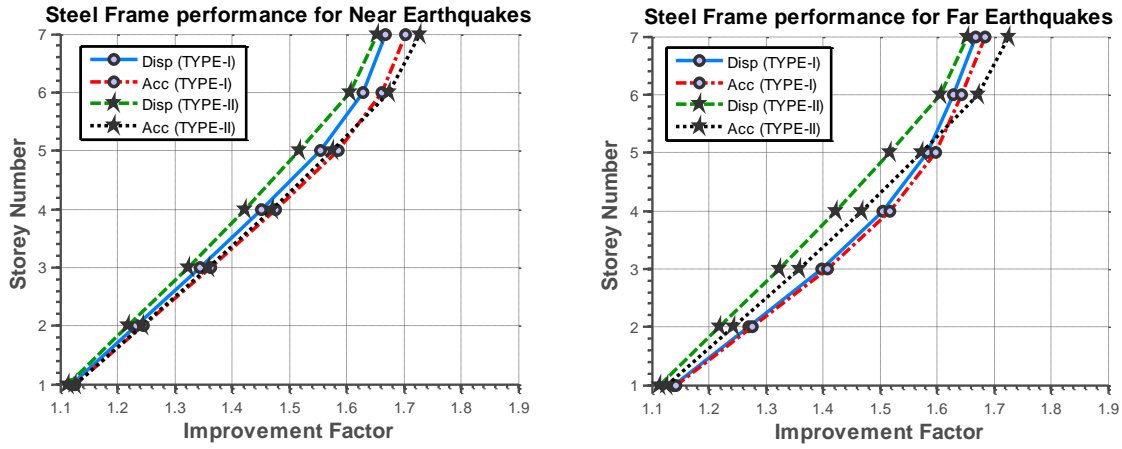


Figure 4.7 Performance of Steel Frame for Near and Far Fault Earthquakes

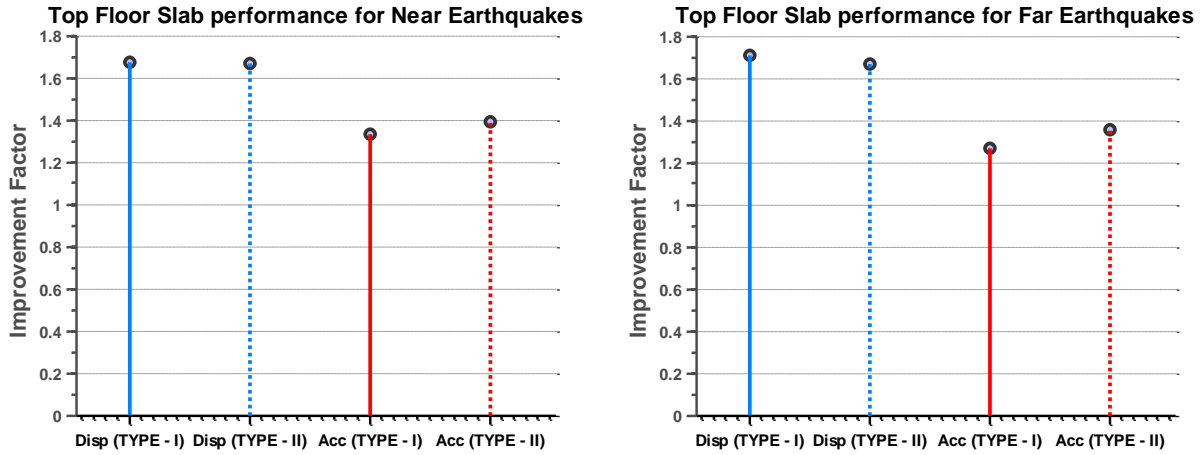


Figure 4.8 Performance of Top Floor Suspended Slab for Near and Far Fault Earthquakes

4.5.3 10 Story 5 Bay

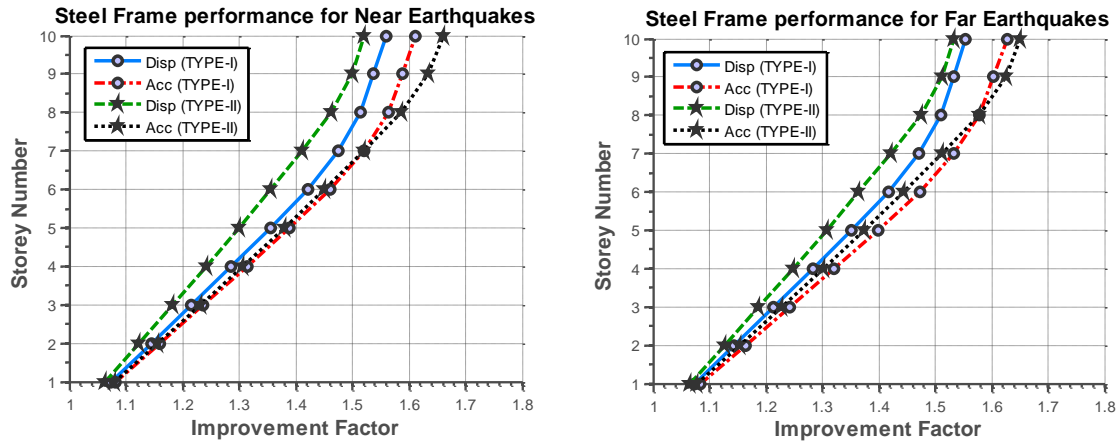


Figure 4.9 Performance of Steel Frame for Near and Far Fault Earthquakes

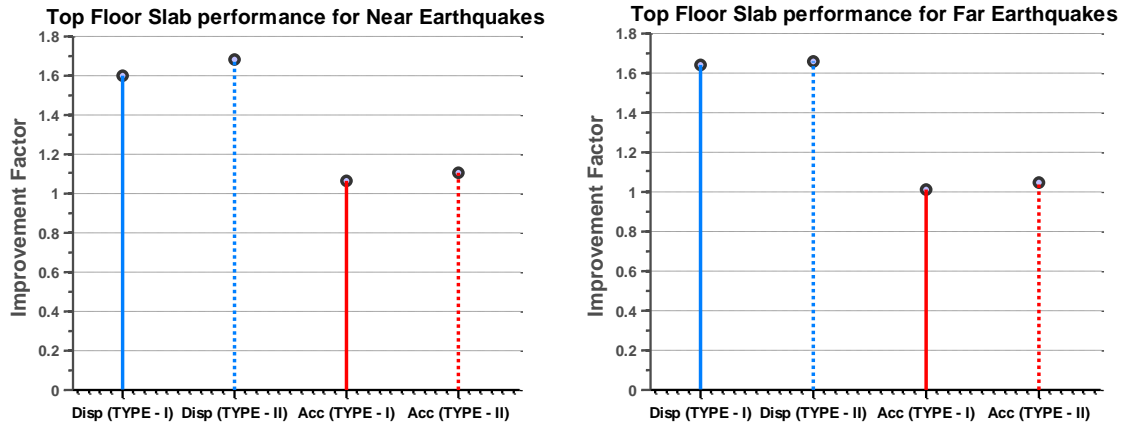


Figure 4.10 Performance of Top Floor Suspended Slab for Near and Far Fault Earthquakes

4.5.4 Results

The results from all cases have been tabulated in Table 4-5 Transfer Function Values and SS system optimized parameters for different Optimizations. The table shows the Improvement factors for all response variables of the SS system, along with the optimized parameters - β_d , ξ_d and C_n . From the results it can be clearly seen that performance difference in Near and Far Fault spectrums is not much as their ground frequencies and damping are quite close to each other. Since the Improvement factor is a relative measure of performance, the ground intensity of the 2 spectra's does not contribute to anything, hence the 'I' factors are a function of ground frequency and damping.

From the 3 structures considered a clear improvement is seen in the performance of the MSS system. For TYPE – I optimization the overall performance of the MSS system is seen to be quite satisfactory for the 1st two structures – 4-story and 7-story. However, for the 10th story the 'I' factor of SS acceleration is almost 1 for TYPE – I optimization, which means there is almost no improvement. For TYPE – II it can be seen that now the 'I' factor for SS acceleration is a little better.

Although the improvement is not that much, further improvement can be achieved if ξ_d is allowed to increase further. For the scope of this thesis the damping ratio of the SS is limited to 0.30 to keep a somewhat practical perspective. Since the design aspects of the SS system are not dealt with, it is quite difficult to quantify actual values. However, it can be shown that even higher ξ_d values can be practically applicable. Equations 5.12 are divided and the damping ratio of structure

and the SS are assumed to be the same (Equation 5.13). By rearranging the final relation between the damping coefficient of SS and the structure is shown in Equation 5.14. For the 10 story structure, $\mu_d = 0.05$ (5%) and $\beta_d = 0.60$ (60%), therefore $c_d = 0.03x C_S$ or 3% of C_S . Thus, even if the ξ_d value turns out to be high it may still be practically feasible.

$$\xi_d = \frac{c_d}{2m_d\omega_d} \text{ and } \xi_s = \frac{C_S}{2M_S\omega_S} \quad (5.12)$$

$$\frac{\xi_d}{\xi_s} = 1 \quad (5.13)$$

$$c_d = \frac{C_S \cdot (2m_d\omega_d)}{2M_S\omega_S} = C_S \cdot (\mu_d\beta_d), \text{ where } \mu_d = \frac{m_d}{M_S} \text{ and } \beta_d = \frac{\omega_d}{\omega_S} \quad (5.14)$$

Table 4-5 Transfer Function Values and SS system optimized parameters for different Optimizations

Structure	Earthquake	Optimization	I_{Fd}	I_{Fa}	I_{Sd}	I_{Sa}	β_d	ξ_d	C_n
4x2	Near – Fault	TYPE – I	1.518	1.562	1.623	1.202	0.6263	0.30	[0 1 0 1]
4x2	Near – Fault	TYPE - II	1.513	1.582	1.674	1.214	0.6822	0.30	[0 1 0 1]
4x2	Far – Fault	TYPE – I	1.518	1.558	1.623	1.164	0.6263	0.30	[0 1 0 1]
4x2	Far – Fault	TYPE - II	1.515	1.575	1.665	1.174	0.6726	0.30	[0 1 0 1]
7x3	Near – Fault	TYPE – I	1.668	1.703	1.672	1.332	0.6734	0.23	[0 1 1 1 0 0 1]
7x3	Near – Fault	TYPE - II	1.654	1.728	1.669	1.394	0.5322	0.30	[0 1 1 1 1 0 1]
7x3	Far – Fault	TYPE – I	1.669	1.685	1.711	1.270	0.6998	0.25	[0 1 0 0 0 1 1]
7x3	Far – Fault	TYPE - II	1.654	1.725	1.667	1.358	0.5304	0.30	[0 1 1 1 1 0 1]
10x5	Near – Fault	TYPE – I	1.559	1.612	1.598	1.059	0.575	0.30	[0 1 1 1 1 0 0 0 1 1]
10x5	Near – Fault	TYPE - II	1.521	1.660	1.677	1.104	0.6381	0.30	[0 1 1 1 1 1 1 0 0 1]
10x5	Far – Fault	TYPE – I	1.553	1.627	1.639	1.007	0.629	0.30	[0 1 1 1 1 0 0 0 1 1]
10x5	Far – Fault	TYPE - II	1.534	1.651	1.653	1.044	0.6046	0.30	[0 1 1 1 1 1 1 0 0 1]

CHAPTER 5

DESIGN CONSIDERATIONS

5.1 Design Considerations

The scope of this study is just the performance analysis of the SS system, however complete evaluation of this system cannot be completed without a design perspective. The most important design component of the SS system are the post – tensioned and energy dissipation links, which govern the parameters - k_d and c_d . Throughout the study the focus has been on the performance aspect of the SS system, however the purpose of studying the SS system as an analogue to a TMD system was not just to evaluate the performance but also to develop a procedure to design these links.

5.1.1 Design of Energy Dissipation Links

Once optimum values for parameters β_d and ξ_d are obtained for any particular SS system they are used to design the links. First we look at the energy dissipation links, which are designed by obtaining the damping coefficient from ξ_d by Equation (6.1). The parameters on the right hand side are known from the analysis, thus we can get the damping coefficient.

$$\xi_d = \frac{c_d}{2m_d\omega_d} \Rightarrow c_d = \frac{C_S \cdot (2m_d\omega_d)}{2M_S\omega_S} = C_S \cdot (\mu_d\beta_d) \quad (6.1)$$

where, C_S is the damping coefficient of the steel frame excluding the suspended slabs,

μ_d is the mass ratio and β_d is the frequency ratio of the suspended slabs

5.1.2 Design of Post – Tension (PT) Links

The second important design aspect is to design the post – tensioned links. The typical schematic of the post tensioned link is shown in Figure 6.1, the definition parameters used are given in Table 6.1. Once optimal value of β_d is obtained Equation 6.2 can be used to k_{total} , the total stiffness provided of the suspended slab. However, we are concerned with just the stiffness of the PT links because the inherent stiffness of the suspended slab (Equation 6.3) cannot be changed due to architectural constraints. By using Equation 6.4 we can get the stiffness due to only PT links. Once we have the separate stiffness, it is used to get the design force in each PT link using Equations 6.5, 6.6 and 6.7, since h_s , s_p and n_{PT} are pre – decided and X_{max} is obtained from the analysis procedure.

Table 5-1 List of parameters for PT links

Variable	Definition
k_{total}	Total stiffness of suspended slab
k_d	Stiffness of suspended slab only due to PT links
k_{in}	Inherent stiffness of suspended slab
X_{max}	Maximum displacement of suspended slab
h_s	Spacing between suspended slab and beam
s_p	Horizontal spacing between the two ends of a PT link
θ	Horizontal angle PT link for maximum displacement of slab
F_{PV}	Vertical force of PT link
F_{PH}	Horizontal force of PT link
F_P	Net force of PT link
n_{PT}	Number of PT links

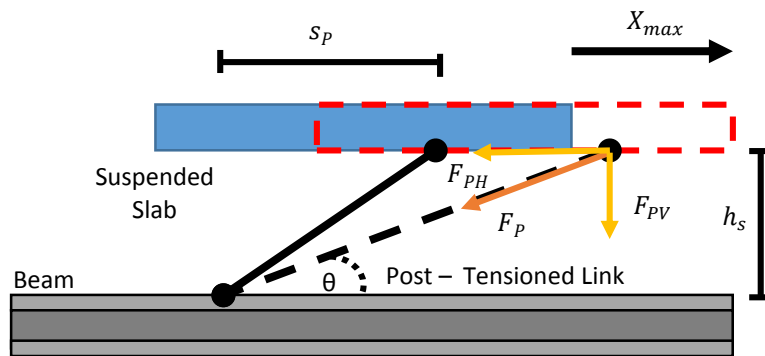


Figure 5.1 Schematic of Post – tensioned links

$$\beta_d = \frac{\omega_d}{\omega_s} = \sqrt{\frac{k_{total} M_s}{m_d K_s}} = \sqrt{\frac{k_{total}}{\mu_d K_s}} \Rightarrow k_{total} = \beta_d^2 \mu_d K_s \quad (6.2)$$

$$k_{in} = \frac{m_d g}{L} \quad (6.3)$$

$$k_d = k_{total} - k_{in} \quad (6.4)$$

$$F_{PH} = k_d \times X_{max} \quad (6.5)$$

$$\theta = \tan^{-1} \left(\frac{h_s}{X_{max} + s_p} \right) \quad (6.6)$$

$$F_p = \frac{F_{PH} \cos \theta}{n_{PT}} \quad (6.7)$$

CHAPTER 6

CONCLUSIONS AND FUTURE WORK

6.1 Conclusions

The suspended and self-centered slabs system is a novel system developed to mitigate the effects of earthquake while minimizing the requirement of repairs. The SS system works on the principle of vibration isolation and dissipation of energy in replaceable elements, which makes it a high potential system. Other earthquake mitigation systems such as – the reduced beam section and the dog – bone connection, require high repair cost due to replacement of beams after an earthquake. However, in the SS system since the energy is dissipated in the energy dissipation links attached to each slabs, thus the repair cost could be highly reduced. Also, the SS system utilizes the benefits of passive TMD system, however it does not encounter the problem of architectural constraints, as experienced by regular TMD systems. In order to implement TMD's separate space has to be reserved for them, which is not the case with the SS system.

The SS is identified to be equivalent to a MTMD system, thus optimization procedure is required to 'Tune' the system. TMD systems tend to perform best when attuned to specific conditions. The theoretical models are analyzed in congruence with 2 optimization methods - Numerical Search and Combinatorial optimization. Both methods are found to be quite accurate, however as the size of SS system increased the former got too time costly. On the other hand, the latter method showed better accuracy and reduction in processing time by almost one – tenth. Finally, to test the performance of the SS system 3 test structures were considered – 4 story 2 bay, 7 story 3 bay and

10 story 5 bay, and the Kanai – Tajimi spectrum is used to model the input earthquakes. The tests revealed about 50 – 60 % improvement in performance of the SS system over the composite frame for the 3 test structures.

6.2 Future Work

There is still need to look into the designing aspects of the SS system in detail i.e. the size of beams, design of suspension connections, etc. In addition, the analysis conducted in this study assumes a unidirectional earthquake and a symmetric structure, which neglects the feasibility of this system if torsional effects are to be considered. In case the suspended slabs are not evenly distributed then there will be some torsion produced in the system. Thus, it is necessary to investigate this aspect of the system as well. These are the analytical aspects that need to be further explored, but at the end it is quite necessary to do experimental testing or a software simulation to verify the theoretical formulation. Since the SS system is an unexplored domain, the scope for future research in regard to it is quite vast and at the same time essential due to its high potential.

REFERENCES

- Abe, M., & Igusa, T. (1995). Tuned mass dampers for structures with closely spaced natural frequencies. *Earthquake Engineering and Structural Dynamics*, (24(2)), 247–261.
- Alhan, C. and G. H. (2005). Reliability of base isolation for the protection of critical equipment from earthquake hazards. *Engineering Structures*, (27(9)), 1435–1449.
- Almazán, J. L., De la Llera, J. C., Inaudi, J. a., López-García, D., & Izquierdo, L. E. (2007). A bidirectional and homogeneous tuned mass damper: A new device for passive control of vibrations. *Engineering Structures*, 29(7), 1548–1560. doi:10.1016/j.engstruct.2006.09.005
- Ariga, T., Kanno, Y., & Takewaki, I. (2006). Resonant behaviour of baseisolated high-rise buildings under long-period ground motions. *Structural Design Tall Special Buildings*, (15), 325–338.
- Bergman, L., McFarland, D., Hall, J., Johnson, E., & Kareem, A. (1989). Optimal distribution of tuned mass dampers in wind-sensitive structures. *Proceedings of ICOSSAR '89, the 5th International Conference on Structural Safety and Reliability* (pp. 95–102).
- Chang, S. P., Makris, N., Whittaker, A. S., & Thompson, A. (2002). Experimental and analytical studies on the performance of hybrid isolation systems. *Earthquake Engineering and Structural Dynamics*, (31), 421–443.
- Chen, S. J., Yeh, C. H., & Chu, J. M. (1996). Ductile steel beam-to-column connections for seismic resistance. *Journal of Structural Engineering*, (122(11)), 1292–1299.
- Chen, G., and Wu, J. (2001). Optimal Placement of Multiple Tuned Mass Dampers for Seismic Structures. *Journal of Structural Engineering*, (127(9)), 1054–1062.
- Chey, M.H., Carr, A.J., Chase, J.G., and Mander, J. B. (2007). Design of Semi-Active Tuned Mass Damper Building Systems using Resettable Devices. *8th Pacific Conference on Earthquake Engineering*. Singapore.
- Chey, M.H., Chase, J.G., and Mander, J.B., Carr, A. J. (2010). Semi-Active Tuned Mass Damper Building Systems: Design. *Earthquake Engineering and Structural Dynamics*, (39(2)), 119–139.
- Chi, B., & Uang, C. M. (2002). Cyclic Response and Design Recommendations of Reduced Beam Section Moment Connections with Deep Column. *Journal of Structural Engineering*, (128(4)), 464–473.
- Connor, J. J. (2003). *Introduction to Structural Motion Control*. Pearson Education Inc.

- Corbi, O. (2003). Shape memory alloys and their application in structural oscillations attenuation. *Simulation Modeling Practice and Theory* (pp. 387–402).
- Deb, S. (2004). Seismic base isolation-an overview. *Curr. Sci.*, (87(10)), 1426–1430.
- Demetriades, G.F. Constantinou, M.C. Reinhorn, A. M. (1992). *Study of Wire-Rope Systems for Seismic Protection of Equipment in Buildings* (p. Technical Report NCEER–92–0012).
- Den Hartog, J. P. (1940). *Mechanical Vibrations* (2nd ed.). McGraw Hill, New York.
- Di Egidio, A., & Contento, A. (2010). Seismic response of a non-symmetric rigid block on a constrained oscillating base. *Engineering Structures*, (32), 3028– 3039.
- Dicleli, M., & Buddaram, S. (2007). Comprehensive evaluation of equivalent linear analysis method for seismic-isolated structures represented by sdof systems. *Engineering Structures*, (29), 1653–1663.
- Dolce, M., Cardone, D., & Marnetto, R. (2001). SMA re-centering devices for seismic isolation of civil structures. *Proceedings of SPIE* (p. 4330: 238–49).
- Eatherton, M. R., Hajjar, J. F., Deierlein, G. G., Krawinkler, H., Billington, S., & Ma, X. (2008). CONTROLLED ROCKING OF STEEL-FRAMED BUILDINGS WITH REPLACEABLE ENERGY-DISSIPATING FUSES. *The 14th World Conference on Earthquake Engineering*. Beijing, China.
- Engelhardt, M. D. Winneberger, T., Zekany, A. J., & Potyraj, T. J. (1998). Experimental Investigations of Dogbone Moment Connections. *Engineering Journal*, (35(4)), 128–139.
- F.Y., C., H., J., & K., L. (2008). *Smart Structures, Innovative Systems for Seismic Response Control* (p. 672). CRC Press.
- Farshidianfar, A., & Soheili, S. (2011). Bee Colony Optimization of Tuned Mass Dampers for Earthquake Vibrations of High-rise Buildings Including Soil Structure Interaction, 1–8.
- Feng, M. Q., & Mita, A. (1995). Vibration Control of Tall Buildings Using Mega SubConfiguration. *Journal of Engineering Mechanics*, 121(10), 1082–1088. doi:10.1061/(ASCE)0733-9399(1995)121:10(1082)
- Frahm, H. (1909). Device for damping vibration of bodies.
- Franklin, G. F., Powell, J. D., & Emami-Naeini, A. (2009). *Feedback Control of Dynamic Systems* (6th ed.). Prentice Hall.
- Gavin, H.P., and Zaicenco, A. (2007). Performance and reliability of semi-active equipment isolation. *Journal of Sound and Vibration*, (306, 1–2), 74–90.

- Goodno, B. (1975). *Dynamic Analysis of Suspended Floor High-Rise Building using Super-Elements* (p. Report number 13). CA.
- H.C., T., & Lin G.C. (1993). Optimum tuned mass dampers for minimizing steady state reponse of support excited and damped systems. *Earthquake Engineering and Structural Dynamics*, (31), 897–919.
- Hansen, N. (2011). *The CMA Evolution Strategy: A Tutorial*.
- Hartog, D., Although, I., & Namara, M.-. (1998). OPTIMUM DESIGN OF ABSORBER FOR MDOF STRUCTURES By Muhammad N. S. RadiI and Yoyong Arfiadi 2, 1272–1280.
- Hong, W., & Kim, H. (2004). Performance of a multi-story structure with a resilient-friction base isolation system. *Comput. Struct.*, (82), 2271– 2283.
- Hoshimura, K. (2005). *Covariance Matrix Adaptation Evolution Strategy for Constrained Optimization Problem*. University of Kyoto.
- Igusa, T., and Xu, K. (1994). Vibration Control Using Multiple Tuned Mass Dampers. *Journal of Sound and Vibrations*, (175(4)), 491–503.
- Islam, A., & Ahmad, S. (2010). Isolation System Design for Buildings in Dhaka: Its Feasibility and Economic Implication. *Proceedings of the International Conference on Engineering Research, Innovation and Education*. (pp. 99–104). Bangladesh, Sylhet.
- Kanai, K. (1957). Semi-empirical formula for the seismic characteristics of the ground motion. *Bulletin of the Earthquake Research Institute*. Tokyo.
- Kaneko, M., Yasui, Y., and Okuda, Y. (1995). *Simultaneous horizontal and vertical vibration tests of three-dimensional floor isolation system* (pp. 186–190).
- Kareem, A., Kijewski, T., & Tamura, Y. (2007). Mitigation of Motion of Tall Buildings with Specific Examples of Recent Applications. *Wind and Structures*, (2(3)), 201–251.
- Kareem, A., & Klein, S. (1995). Performance of multiple mass dampers under random loading. *Journal of Structural Engineering*, (121(2)), 348–361.
- Kelly, J. M., Leitmann, G., & Soldatos, A. G. (1987). Robust control of base-isolated structures under earthquake excitation. *Journal of Optimization Theory and Applications*, (53), 159–180.
- Khan, M. M., & Lagoudas, D. (2002). Modeling of shape memory alloy pseudo-elastic spring elements using Preisach model for passive vibration isolation. *Proceedings of SPIE* (pp. 4693:336–47).

- Kilar, V., & Koren, D. (2009). Seismic behaviour of asymmetric base isolated structures with various distributions of isolators. *Engineering Structures*, (31), 910–921.
- Komodromos, P. (2008). Simulation of the earthquake-induced pounding of seismically isolated buildings. *Comput. Struct.*, (86), 618–626.
- Komodromos, P., Polycarpou, P., Papaloizou, L., & Phocas, M. (2007). Response of seismically isolated buildings considering poundings. *Earthquake Engineering and Structural Dynamics*, (36), 1605–1622.
- Lambrou, V. and Constantinou, M. C. (1994). *Study of Seismic Isolation Systems for Computer Floors* (p. Technical Report NCEER-94-0020). University at Buffalo.
- Li, C. (2000). Performance of multiple tuned mass dampers for attenuating undesirable oscillations of structures under the ground acceleration. *Earthquake Engineering and Structural Dynamics*, (9(9)), 1405–1421.
- Lin, C.C., Lin, G.L., and Wang, J. F. (2010). Protection of Seismic Structures Using Semi-Active Friction TMD. *Earthquake Engineering and Structural Dynamics*, (39(6)), 635–659.
- Lin, Y.Y., and Cheng, C. M. (2001). Performance of Multiple Tuned Mass Dampers for Suppressing Buffeting Response and Increasing Flutter Speed of Long-Span Bridges. *Journal of the Chinese Institute of Engineers*, (24(3)), 273–266.
- Lourenco, R. (2011). Design , Construction and Testing of an Adaptive Pendulum Tuned Mass Damper By.
- Lu, L.-Y., & Lin, G.-L. (2008). Predictive control of smart isolation system for precision equipment subjected to near-fault earthquakes. *Engineering Structures*, (30), 3045–3064.
- Maldonado-mercado, J. C. (1995). *Passive and Active Control of Structures*. Massachusetts Institute of Technology.
- Matsagar, V., & Jangid, R. (2004). Influence of isolator characteristics on the response of base-isolated structures. *Engineering Structures*, (26), 1735–1749.
- Mayes, J., Lagoudas, D., & BK., H. (2001). An experimental investigation of shape memory alloy pseudoelastic springs for passive vibration isolation. *AIAA space 2001 conference and exposition*.
- Mohebbi, M., Shakeri, K., Ghanbarpour, Y., & Majzoub, H. (2012). Designing optimal multiple tuned mass dampers using genetic algorithms (GAs) for mitigating the seismic response of structures. *Journal of Vibration and Control*, 19(4), 605–625.
doi:10.1177/1077546311434520

- Moon, K. (2005). *Dynamic Interrelationship between Technology and Architecture in Tall Buildings*. Massachusetts Institute of Technology, Cambridge, MA.
- Nagarajaiah, S., and Sonmez, E. (2007). Structures with Semiactive Variable Stiffness Single/Multiple Tuned Mass Dampers. *Journal of Structural Engineering*, (133(1)), 67–77.
- Nagarajaiah, S., and Varadarajan, N. (2005). Short Time Fourier Transform Algorithm for Wind Response Control of Buildings with Variable Stiffness TMD. *Engineering Structures*, (27(3)), 431–441.
- Nagashima, I. (2001). Optimal Displacement Feedback Control Law for Active Tuned Mass Damper. *Earthquake Engineering and Structural Dynamics*, (30(8)), 1221–1242.
- Nelder, J. A., & Mead, R. (1965). A simplex method for function minimization. *The Computer Journal*, (7), 308–313.
- Nishimura, T., Kobori, T., Sakamoto, M., Koshika, N., Sasaki, K., & Ohru, S. (1992). Active Tuned Mass Damper. *Smart Materials and Structures*, (1(4)), 306–311.
- Olsen, A., Aagaard, B., & Heaton, T. (2008). Long-period building response to earthquakes in the San Francisco Bay Area. *Seismological Society Am.*, (98(2)), 1047–1065.
- Plumier, A. (1997). The dogbone: back to the future. *Engineering Journal*, (34(2)), 61–67.
- Pocanschi, A., & Phocas, M. (2007). Earthquake isolator with progressive nonlinear deformability. *Engineering Structures*, (29), 2586–2592.
- Ramallo, J. C., Johnson, E. A., & Spencer, B. F., J. (2002). Smart base isolation systems. *Journal of Engineering Mechanics*, (128(10)), 1088–1099.
- Randall, S. E., Taylor, D. L., & Halsted, D. M. (1981). *Optimum vibration absorbers for linear damped systems*. (J. Mech, Ed.) (pp. 908–913). ASME 103.
- Reinhorn, A. M., & Riley, M. (1994). Control of bridge vibrations with hybrid devices. *1st World Conf. on Structural Control* (pp. 50–59.). Los Angeles.
- Roffel, A. J., Lourenco, R., Narasimhan, S., & Yarusevych, S. (2011). Adaptive Compensation for Detuning in Pendulum Tuned Mass Dampers. *Journal of Structural Engineering*, (137(2)), 242–251.
- Setareh, M. (2002). Floor Vibration Control Using Semi-Active Tuned Mass Dampers. *Canadian Journal of Civil Engineering*, (29(1)), 76–84.
- Setareh, M., & Hanson, R. (1992). Tuned Mass Dampers to Control Floor Vibrations from Humans, *Journal of Structural Engineering*, (118), 741–762.

- Setareh, M. Ritchey, J.K., Baxter, A.J., and Murray, T. M. (2006). Pendulum Tuned Mass Dampers for Floor Vibration Control. *Journal of Performance of Construction Facilities*, (20(1)), 64–73.
- Setareh, M. Ritchey, J.K., Murray, T.M., Koo J.H., and Ahmadian, M. (2007). Semi-Active Tune Mass Damper for Floor Vibration Control. *Journal of Structural Engineering*, (133(2)), 242–250.
- Shenlei Cui, M., M. B. and A. K. (2010). Behavior of Bidirectional Spring Unit in Isolated Floor Systems. *Journal of Structural Engineering*, 944–952.
- Spencer, B. F., & Sain, M. K. (1997). Controlling Buildings: A New Frontier in Feedback. *Control Systems Magazine*, 17(6) 19–35.
- Spyrakos, C., Koutromanos, I., & CA, M. (2009). Seismic response of base-isolated buildings including soil-structure interaction. *Soil Dynamics and Earthquake Engineering*, (29), 658–668.
- Sun, L.M., Fujino, Y., Pacheco, B.M., and Chaiser, P. (1992). Modelling of Tuned Liquid Damper. *Journal of Wind Engineering and Industrial Aerodynamics*, (41), 1883–1894.
- Symans, M. D., & M.C., C. (1997). Seismic testing of a building structure with a semi-active fluid damper control system. *Earthquake Engineering and Structural Dynamics*, (26), 759–777.
- Taghavi, S., & Miranda, E. (2003). *Response assessment of nonstructural building elements* (p. Report No. PEER 2003/05). Richmond, CA.
- Tajimi, H. (1960). A statistical method of determining the maximum response of a building structure during an earthquake. *2nd WCC*. (pp. 781 – 798).
- Tedesco, J. W., McDoughal, W. G., & Ross, C. A. (1999). *Structural Dynamics Theory and Applications* (1st ed.). Addison Wesley Longman Inc.
- Venture, S. J. (2000). *Recommended Seismic Evaluation and Upgrade Criteria for Existing Welded Steel Moment-Frame Structures* (p. Report no. FEMA–351). Washington, D.C.
- Villaverde, R. (1990). Are vibration control techniques a competitive alternative for the seismic design of structures. *In Proceedings of Seismic Engineering*. A.C.
- Warburton, G. B., & Ayorinde, E. O. (1980). Optimum absorber parameters for simple systems. *Earthquake Engineering and Structural Dynamics*, (8), 197–217.
- Whitaker, A., Gilani, A., & Bertero, V. (1998). Evaluation of Pre-Northridge Steel Moment Resisting Frame Joints. *Journal of the Structural Design of Tall Building*, (7), 263–283.

- Yamaguchi, H., & Harnpornchai, N. (1993). Fundamental characteristics of multiple tuned mass dampers for suppressing harmonically forced oscillation. *Earthquake Engineering and Structural Dynamics*, (22), 51–62.
- Yoshioka, H., Ramallo, J. C., & Spencer, B. F., J. (2002). 'Smart' base isolation strategies employing magnetorheological damper. *Journal of Structural Engineering*, (128(5)), 540–551.
- Zekioglu, A., Mozaffarian, H., Chang, K. L., & Uang, C. M. (1997). Designing after Northridge. *Modern Steel Construction*, (37(3)), 36–42.

APPENDIX A

RESPONSE EQUATIONS DERIVATION FOR MSS MODEL

$$\tilde{m}_E \ddot{u}_4 + \tilde{c}_E \dot{u}_4 + \tilde{k}_E u_4 = -a_g \left(\frac{\sum_{j=1}^4 m_j \phi_{1j}}{\phi_{14}} \right) + C_4 \sum_{j=1}^2 \left[k_{d4j} u_{d4j} + c_{d4j} \dot{u}_{d4j} \right] + \sum_{n=1}^3 \left[C_n \frac{\phi_{1n}}{\phi_{14}} \left[\sum_{j=1}^2 \left(k_{dnj} u_{dnj} + c_{dnj} \dot{u}_{dnj} \right) \right] \right] \quad (\text{A. 1})$$

$$m_{d4j} \ddot{u}_{d4j} + c_{d4j} \dot{u}_{d4j} + k_{d4j} u_{d4j} + m_{d4j} \ddot{u}_4 = -m_{d4j} a_g \quad (\text{A. 2})$$

$$m_{dnj} \ddot{u}_{dnj} + c_{dnj} \dot{u}_{dnj} + k_{dnj} u_{dnj} + m_{dnj} \ddot{u}_n = -m_{dnj} a_g, \text{ where } n = 1 - 3 \text{ and } j = 1 - 2 \quad (\text{A. 3})$$

Steel Frame Displacement Amplitude Derivation (H_4)

Equation A.1 – A.3 represents the equations of motion of the steel frame, j^{th} SS of top floor and j^{th} SS of floors 1st – 3rd. First, the displacement amplitudes are derived by substituting the assumptions (Equation A.4) in Equation A.1 and dividing this equation by ω_S^2 and \tilde{m}_E to get complex form Equation A.7, where ‘i’ represents the complex root $\sqrt{-1}$. Similarly, the relations (A.2) and (A.3) are divided by $(m_{d4j} \cdot \omega_S^2)$ and $(m_{dnj} \cdot \omega_S^2)$, and Equations A.5 and A.6 are substituted to obtain the complex form Equations A.8 and A.9.

$$u_4 = H_4 e^{-i\alpha t} \quad (\text{A. 4})$$

$$u_{d4j} = H_{d4j} e^{-i\alpha t} \quad (\text{A. 5})$$

$$u_{dnj} = H_{dnj} e^{-i\alpha t}, \text{ for } n \in [1, 3] \text{ and } j \in [1, 2] \quad (\text{A. 6})$$

$$\left(-\alpha^2 + i2\xi_s \alpha + 1\right)H_4 = -\frac{\Gamma_e a_g}{\omega_s^2} + C_4 \sum_{j=1}^2 \left[\mu_{d4j} \left(i2\xi_{d4j} \beta_{d4j} \alpha + \beta_{d4j}^2 \right) H_{d4j} \right] + \sum_{n=1}^3 \left[C_n q_n \left[\sum_{j=1}^2 \left(\mu_{dnj} \left(i2\xi_{dnj} \beta_{dnj} \alpha + \beta_{dnj}^2 \right) H_{dnj} \right) \right] \right] \quad (\text{A. 7})$$

$$\left(-\alpha^2 + i2\xi_{d4j} \beta_{d4j} \alpha + \beta_{d4j}^2\right)H_{d4j} = \alpha^2 H_4 - \frac{a_g}{\omega_s} \quad (\text{A. 8})$$

$$\left(-\alpha^2 + i2\xi_{dnj} \beta_{dnj} \alpha + \beta_{dnj}^2\right)H_{dnj} = \alpha^2 q_n H_4 - \frac{a_g}{\omega_s} \quad (\text{A. 9})$$

Equations A.8 and A.9 are rearranged to obtain relations for H_{d4j} and H_{dnj} in terms of H_4 , and these are substituted in Equation A.7 to obtain a relation in terms of single variable U_4 . After the substitution the equation is rearranged to get the relation for steel frame displacement amplitude as shown below (Equation A.10).

$$H_4 = -\frac{a_g \left[\Gamma_e + \sum_{n=1}^3 \left[C_n q_n \sum_{j=1}^2 \left[H_{dnj} S_{dnj} \mu_{dnj} \right] \right] + C_4 \sum_{j=1}^2 \left[H_{d4j} S_{d4j} \mu_{d4j} \right] \right]}{\omega_s^2 \left[H_S^{-1} - \sum_{n=1}^3 \left[C_n q_n^2 \sum_{j=1}^2 \left[H_{dnj} S_{dnj} \mu_{dnj} \alpha^2 \right] \right] - C_4 \sum_{j=1}^2 \left[H_{d4j} S_{d4j} \mu_{d4j} \alpha^2 \right] \right]} \quad (\text{A. 10})$$

$$H_{dnj} S_{dnj} = \frac{\left(\beta_{dnj}^2 - i2\xi_{dnj} \beta_{dnj} \alpha \right)}{\left(-\alpha_{dnj}^2 - i2\xi_{dnj} \beta_{dnj} \alpha + \beta_{dnj}^2 \right)} = \frac{\left(\beta_{dnj}^2 - i2\xi_{dnj} \beta_{dnj} \alpha \right) \left(-\alpha_{dnj}^2 + i2\xi_{dnj} \beta_{dnj} \alpha + \beta_{dnj}^2 \right)}{\left(-\alpha_{dnj}^2 - i2\xi_{dnj} \beta_{dnj} \alpha + \beta_{dnj}^2 \right) \left(-\alpha_{dnj}^2 + i2\xi_{dnj} \beta_{dnj} \alpha + \beta_{dnj}^2 \right)} = \text{Re}_{H_{dnj}} + i \text{Im}_{H_{dnj}} \quad (\text{A. 11})$$

$$H_{d4j} S_{d4j} = \frac{\left(\beta_{d4j}^2 - i2\xi_{d4j} \beta_{d4j} \alpha \right)}{\left(-\alpha^2 - i2\xi_{d4j} \beta_{d4j} \alpha + \beta_{d4j}^2 \right)} = \frac{\left(\beta_{d4j}^2 - i2\xi_{d4j} \beta_{d4j} \alpha \right) \left(-\alpha_{d4j}^2 + i2\xi_{d4j} \beta_{d4j} \alpha + \beta_{d4j}^2 \right)}{\left(-\alpha^2 - i2\xi_{d4j} \beta_{d4j} \alpha + \beta_{d4j}^2 \right) \left(-\alpha_{d4j}^2 + i2\xi_{d4j} \beta_{d4j} \alpha + \beta_{d4j}^2 \right)} = \text{Re}_{H_{d4j}} + i \text{Im}_{H_{d4j}} \quad (\text{A. 12})$$

$$H_S^{-1} = \text{Re}_{H_S^{-1}} + i \text{Im}_{H_S^{-1}} \quad (\text{A. 13})$$

The Equations A.11 – A.13 show how the components of equation A.10 are divided into real and imaginary parts. These parts are solved separately to break into real and imaginary components, which are clearly shown in Equations A.14 – A.29. Equation A.20 shows a much clearer picture of the complex nature of the main equation.

$$\text{Re}_{H_S} = 1 - \alpha^2 \quad (\text{A. 14})$$

$$\text{Re}_{H_{dnj}} = \frac{\beta_{dnj}^2 (\beta_{dnj}^2 - \alpha^2) + 4 (\xi_{dnj} \beta_{dnj} \alpha)^2}{(\beta_{dnj}^2 - \alpha^2)^2 + 4 (\xi_{dnj} \beta_{dnj} \alpha)^2} \quad (\text{A. 15})$$

$$\text{Re}_{H_{d4j}} = \frac{\beta_{d4j}^2 (\beta_{d4j}^2 - \alpha^2) + 4 (\xi_{d4j} \beta_{d4j} \alpha)^2}{(\beta_{d4j}^2 - \alpha^2)^2 + 4 (\xi_{d4j} \beta_{d4j} \alpha)^2} \quad (\text{A. 16})$$

$$\text{Im}_{H_{dnj}} = \frac{2 \xi_{dnj} \beta_{dnj} \alpha^3}{(\beta_{dnj}^2 - \alpha^2)^2 + 4 (\xi_{dnj} \beta_{dnj} \alpha)^2} \quad (\text{A. 17})$$

$$\text{Im}_{H_{d4j}} = \frac{2 \xi_{d4j} \beta_{d4j} \alpha^3}{(\beta_{d4j}^2 - \alpha^2)^2 + 4 (\xi_{d4j} \beta_{d4j} \alpha)^2} \quad (\text{A. 18})$$

$$\text{Re}_{H_S} = -2 \xi_S \alpha^2 \quad (\text{A. 19})$$

$$H_4 = \frac{\left[\Gamma_e + \sum_{n=1}^3 \left[C_n q_n \sum_{j=1}^2 \left[(\text{Re}_{H_{dnj}} + i \text{Im}_{H_{dnj}}) \mu_{dnj} \right] \right] + C_4 \sum_{j=1}^2 \left[(\text{Re}_{H_{d4j}} + i \text{Im}_{H_{d4j}}) \mu_{d4j} \right] \right]}{\left[(\text{Re}_{H_S} + i \text{Im}_{H_S}) - \sum_{n=1}^3 \left[C_n q_n^2 \sum_{j=1}^2 \left[(\text{Re}_{H_{dnj}} + i \text{Im}_{H_{dnj}}) \mu_{dnj} \alpha^2 \right] \right] - C_4 \sum_{j=1}^2 \left[(\text{Re}_{H_{d4j}} + i \text{Im}_{H_{d4j}}) \mu_{d4j} \alpha^2 \right] \right]} \quad (\text{A. 20})$$

The real terms of Equation A.20 are coupled together in the numerator and the denominator. Similarly, the complex terms are also collected and the equation is converted to the form of

Equation A.25, from which the actual response amplitude is obtained by taking the modulus (Equation A.26). Equations A.21 – A.24 represent the real and imaginary terms of the numerator and the denominator.

$$NUM_{R4} = \left[\Gamma_e + \sum_{n=1}^3 \left[C_n q_n \sum_{j=1}^2 \left[(\text{Re}_{Hdnj}) \mu_{dnj} \right] \right] + C_4 \sum_{j=1}^2 \left[(\text{Re}_{Hd4j}) \mu_{d4j} \right] \right] \quad (\text{A. 21})$$

$$NUM_{I4} = \left[\sum_{n=1}^3 \left[C_n q_n \sum_{j=1}^2 \left[(\text{Im}_{Hdnj}) \mu_{dnj} \right] \right] + C_4 \sum_{j=1}^2 \left[(\text{Im}_{Hd4j}) \mu_{d4j} \right] \right] \quad (\text{A. 22})$$

$$DEN_{R4} = \left[(\text{Re}_{Hs}) - \sum_{n=1}^3 \left[C_n q_n^2 \sum_{j=1}^2 \left[(\text{Re}_{Hdnj}) \mu_{dnj} \alpha^2 \right] \right] - C_4 \sum_{j=1}^2 \left[(\text{Re}_{Hd4j}) \mu_{d4j} \alpha^2 \right] \right] \quad (\text{A. 23})$$

$$DEN_{I4} = \left[(\text{Im}_{Hs}) - \sum_{n=1}^3 \left[C_n q_n^2 \sum_{j=1}^2 \left[(\text{Im}_{Hdnj}) \mu_{dnj} \alpha^2 \right] \right] - C_4 \sum_{j=1}^2 \left[(\text{Im}_{Hd4j}) \mu_{d4j} \alpha^2 \right] \right] \quad (\text{A. 24})$$

$$H_4 = \left(\frac{NUM_{R4} + i NUM_{I4}}{DEN_{R4} + i DEN_{I4}} \right) \quad (\text{A. 25})$$

$$|H_4| = \frac{\sqrt{(NUM_{R4})^2 + (NUM_{I4})^2}}{\sqrt{(DEN_{R4})^2 + (DEN_{I4})^2}} \quad (\text{A. 26})$$

Suspended Slab Displacement Amplitude Derivation ($|H_{d4j}|$)

Equation A.10 is a function of H_4 and H_{d4j} , so by substituting Equation A.25 in A.10 the SS displacement amplitude can be easily obtained. After substituting the equation is rearranged to collect the real and imaginary parts separately such that it can be represented by Equation A.31.

The amplitude is given by equation A.32.

$$\left(-\alpha^2 - i2\xi_{d4j}\beta_{d4j}\alpha + \beta_{d4j}^2\right)H_{d4j} = \left[\alpha^2\left(\frac{NUM_{R4} + iNUM_{I4}}{DEN_{R4} + iDEN_{I4}}\right) + 1\right] \quad (\text{A. 27})$$

$$\left(-\alpha^2 - i2\xi_{d4j}\beta_{d4j}\alpha + \beta_{d4j}^2\right)H_{d4j} = \left[\frac{\alpha^2(NUM_{R4} + iNUM_{I4}) + (DEN_{R4} + iDEN_{I4})}{DEN_{R4} + iDEN_{I4}}\right] \quad (\text{A. 28})$$

$$H_{d4j} = \left[\frac{\alpha^2(NUM_{R4} + iNUM_{I4}) + (DEN_{R4} + iDEN_{I4})}{(DEN_{R4} + iDEN_{I4})(\text{Re}_{H_{d4}} + i\text{Im}_{H_{d4}})}\right] \quad (\text{A. 29})$$

$$H_{d4j} = \left[\frac{\left(\alpha^2 \cdot NUM_{R4} + DEN_{R4}\right) + i\left(\alpha^2 \cdot NUM_{I4} + DEN_{I4}\right)}{\left(DEN_{R4} \cdot \text{Re}_{H_{d4}} - DEN_{I4} \cdot \text{Im}_{H_{d4}}\right) + i\left(\text{Re}_{H_{d4}} \cdot DEN_{I4} + \text{Im}_{H_{d4}} \cdot DEN_{R4}\right)}\right] \quad (\text{A. 30})$$

$$H_{d4j} = \left(\frac{NUM_{Rd4j} + iNUM_{Id4j}}{DEN_{Rd4j} + iDEN_{Id4j}}\right) \quad (\text{A. 31})$$

$$|H_{d4j}| = \frac{\sqrt{(NUM_{Rd4j})^2 + (NUM_{Id4j})^2}}{\sqrt{(DEN_{Rd4j})^2 + (DEN_{Id4j})^2}} \quad (\text{A. 32})$$

where,

$$NUM_{Rd4j} = \alpha^2 \cdot NUM_{R4} + DEN_{R4} \quad (\text{A. 33})$$

$$NUM_{Id4j} = \alpha^2 \cdot NUM_{I4} + DEN_{I4} \quad (\text{A. 34})$$

$$DEN_{Rd4j} = DEN_{R4} \cdot \text{Re}_{Hd4} - DEN_{I4} \cdot \text{Im}_{Hd4} \quad (\text{A. 35})$$

$$DEN_{Rd4j} = \text{Re}_{Hd4} \cdot DEN_{I4} + \text{Im}_{Hd4} \cdot DEN_{R4} \quad (\text{A. 36})$$

Top Story Steel Frame and SS Acceleration Amplitudes Derivation ($|A_4|$ and $|A_{d4j}|$)

The acceleration amplitude for steel frame top floor is obtained by using Equation A.37. Equation A.4 is differentiated twice and substituted in A.37 to obtain relation A.40, which relates A_4 to H_4 . Thus by simply substituting A.25 in A.40 and rearranging we get Equation A.43, from which the acceleration amplitude is obtained (Equation A.44). Similarly for SS acceleration amplitude,

Equation A.5 is differentiated twice and substituted in A.38, which is rearranged and solved to get the acceleration amplitude as given by Equation A.45.

$$\ddot{u}_4 + a_g = A_4 e^{-i\alpha t} \quad (\text{A. 37})$$

$$\ddot{u}_{d4j} + a_g = A_{d4j} e^{-i\alpha t} \quad (\text{A. 38})$$

$$\ddot{u}_4 = -\omega^2 H_4 e^{-i\alpha t} \quad (\text{A. 39})$$

$$A_4 = a_g - \omega^2 H_4 \quad (\text{A. 40})$$

$$A_4 = \left(1 + \alpha^2 \left[\frac{NUM_{R4} + i NUM_{I4}}{DEN_{R4} + i DEN_{I4}} \right] \right) \quad (\text{A. 41})$$

$$A_4 = \left[\frac{(DEN_{R4} + i DEN_{I4}) + \alpha^2 (NUM_{R4} + i NUM_{I4})}{DEN_{R4} + i DEN_{I4}} \right] \quad (\text{A. 42})$$

$$A_4 = \left[\frac{(DEN_{R4} + i DEN_{I4}) + \alpha^2 (NUM_{R4} + i NUM_{I4})}{DEN_{R4} + i DEN_{I4}} \right] \quad (\text{A. 43})$$

$$|A_4| = \frac{\sqrt{(DEN_{R4} + \alpha^2 NUM_{R4})^2 + (DEN_{I4} + \alpha^2 NUM_{I4})^2}}{\sqrt{(DEN_{R4})^2 + (DEN_{I4})^2}} \quad (\text{A. 44})$$

$$|A_{d4j}| = \frac{\sqrt{(DEN_{Rd4j} + \alpha^2 NUM_{Rd4j})^2 + (DEN_{Id4j} + \alpha^2 NUM_{Id4j})^2}}{\sqrt{(DEN_{Rd4j})^2 + (DEN_{Id4j})^2}} \quad (\text{A. 45})$$